THE EFFECT OF TEMPORALLY VARIABLE ENVIRONMENTS ON MOLECULAR CHANGES IN HUMAN CELLS

By
ALEXANDER THIEMICKE

Dissertation
Submitted to the Faculty of the
Graduate School of Vanderbilt University
in partial fulfillment of the requirements
for the degree of
DOCTOR OF PHILOSOPHY
in
Chemical and Physical Biology
December 12, 2020
Nashville, Tennessee

Approved:
Ken Lau, PhD
Tony Capra, PhD
David Harrison, MD
Jens Titze, MD
Gregor Neuert, PhD

ACKNOWLEDGEMENTS

First, I have to thank my thesis advisor, Dr. Gregor Neuert, for taking me into his lab, his continuous support and for entrusting me with the work on this fundamental biological question.

I also want to thank my thesis committee members, Drs. Ken Lau, Jens Titze, David Harrison and Tony Capra for their support, efforts and suggestions during my committee meetings. Especially, I would like to thank Dr. Jens Titze for honoring his commitment to attend my committee meetings and for all the very valuable suggestions to the project, even after he already left Vanderbilt University. I also thank the past and present members of the Neuert laboratory for always being available to help, reviewing grants or manuscripts and for contributing to a productive work environment. Next, I want to express my gratitude to everyone at Vanderbilt University who has provided feedback on the project or a manuscript. Especially, I want to thank Dr. Meena Madhur, Dr. Annet Kirabo and Dr. David Harrison for being available for discussions and providing feedback on the project many times throughout the duration of the project. Having had the opportunity to mentor other students was a great experience and I thank Robert Markowitz, Yelena Perevalova, and Minh Tran for their work on my project during their lab rotations, as well as Arunabh Singh for his work during his assistantship.

I also want to acknowledge the resources provided by Vanderbilt University, especially the VUMC Flow Cytometry Core that substantially facilitated the work on my project. I am grateful for the support from the American Heart Association under grant number 18PRE34050016 that benefitted this project immensely. In addition, I want to acknowledge the support from the NIH under grant DP2 GM11484901 to our lab and the support from the Vanderbilt Institute for Clinical and Translational Research to the project. The data analysis of my project heavily relied on the open source programming language R and several software packages made available free of charge which I want to acknowledge here as well.

Finally, I am deeply grateful for my very supportive family.

LIST OF PUBLICATIONS

[1] **Thiemicke A**, Jashnsaz H, Li G, Neuert G. Generating kinetic environments to study dynamic cellular processes in single cells. Sci Rep. 2019 Jul 12;9(1):10129

[2] Kesler B, Li G, **Thiemicke A**, Venkat R, Neuert G. Automated cell boundary and 3D nuclear segmentation of cells in suspension. Sci Rep. 2019 Jul 15;9(1):10237

[3] Johnson A, Li G, Jashnsaz H, **Thiemicke A**, Kesler B, Rogers D, Neuert G. A rate threshold mechanism regulates MAPK stress signaling and survival. 2020 [in 2nd review for PNAS]

[4] **Thiemicke A**, Neuert G. Kinetics of osmotic stress regulate a cell fate switch of cell survival. 2020 [in resubmission for Science Advances]

[5] **Thiemicke A** and Neuert G. FCBapp: An interactive application to automatically debarcode multiplexed flow cytometry datasets. 2020 [in preparation]

[6] **Thiemicke A** and Neuert G. 2020 A comprehensive time-course flow cytometry data set on stress response in human cells for 35+ cellular markers. [in preparation]

[7] **Thiemicke A** and Neuert G. 2020 The relevance of Ramp inputs in human physiology. [in preparation]

TABLE OF CONTENTS

ACKNOWLEDGEMENTS iii

LIST OF PUBLICATIONS iv

LIST OF FIGURES vii

LIST OF TABLES x

1. Introduction 1

1.1 Using temporally-variable changes in the environment as a systems biology method to study cell biology **1**
1.1.1 Systems biology as an approach to understand biology 1
1.1.2 Understanding the cell as a black box system 3
1.1.3 Perception of temporally variable changes, fold change vs. absolute change detection 4
1.1.4 Pathway network configurations in linear and adaptive pathways 4
1.1.5 Applying Ramp-like temporal changes to stimulate cells 6
1.1.6 Current approaches and methods for kinetic stimulation 6

1.2 The relevance of temporally-variable changes in human physiology **7**
1.2.1 Temporal dynamics of morphogens during development 7
1.2.2 Temporal dynamics of Glucose and Insulin in the body 7
1.2.3 Temporal dynamics of stressors in the cellular environment 8

1.3 The effect of hyperosmotic stress on mammalian cells **9**
1.3.1 Hyperosmotic stress response in eukaryotes 9
1.3.2 Hypertonic Stress activated protein pathways 15
1.3.3 Cell death in hyperosmotic stress 18
1.3.4 Hyperosmolarity in human physiology and disease 19

1.4 Goals of this Thesis **23**

2 Generating kinetic environments to study dynamic cellular processes in single cells 24

2.1 Abstract **24**

2.2 Introduction **25**

2.3 Results **28**
2.3.1 Proof of feasibility using cell lines 28
2.3.2 Computational pipeline to generate the pump profiles 30
2.3.3 Algorithm to compute pump profiles 30
2.3.4 Experimental validation of pump profiles 34
2.3.5 Time Point (TP) Measurements for cell population and single cell experiments 35
2.3.6 Time Series (TS) Measurements in single cell time-lapse microscopy experiments 36
2.3.7 Application of kinetic cell perturbation to study dynamic cell shape, cell signaling and gene regulation in single and populations of cells 38

2.4 Discussion **40**

2.5 Conclusion **41**

2.6 Methods **41**

3 Kinetics of osmotic stress regulates a cell fate switch of cell survival 47

3.1 Abstract **47**

3.2 Introduction **47**

3.3 Results **49**

3.3.1 The rate of environmental change regulates cellular phenotype. 49

3.3.2 A functional temporal screen identifies regulators of cell viability in step and ramp conditions. 55

3.3.3 Caspases differentially regulate step and ramp conditions. 65

3.3.4 Caspase signaling is the main contributor to cell death in step conditions. 66

3.3.5 Intracellular proline levels improve viability in ramp stress conditions 75

3.4 Discussion **82**

3.5 Methods **86**

4 FCBapp: An interactive application to automatically debarcode multiplexed flow cytometry datasets 93

4.1 Abstract **93**

4.2 Introduction **93**

4.3 Implementation and Results 95

4.4 Discussion **102**

5 Conclusions and Future directions 103

5.1 Conclusions **103**

5.2 Future directions **104**

5.2.1 Morphological changes and Protein aggregation in hypertonic stress in step and ramp 104

5.2.2 Redefining the role and significance of proline in evolution, metabolism and disease 106

References 111

APPENDIX 157

LIST OF FIGURES

Figure 1.1: Cell volume and osmolyte changes in hypertonicity 13

Figure 2.1: Kinetic cell culture environments mimic physiologically relevant cell environments. 27

Figure 2.2: Experimental setup to generate kinetic environmental profiles in the laboratory. 29

Figure 2.3: Calculated and experimentally verified pump profiles. 34

Figure 2.4: Application of different pump profiles and quantitative assays. 38

Figure 3.1: Human cell fate decisions are regulated differently upon step or ramp treatment conditions. 51

Figure 3.2: Kinetic environment input profiles applied for different step and ramp treatments. 52

Figure 3.3: Viability improvement in hypertonic stress during a ramp vs. a step is a general cell biological feature independent of the cell line or osmolyte. 53

Figure 3.4: Viability in hypertonic stress during a ramp vs. a step in PBMCs. 55

Figure 3.5: Temporal functional flow cytometry screen identifies differential regulation of stress and caspase signaling during step and ramp hyperosmotic stress conditions. .. 58

Figure 3.6: Markers for stress signaling..... 59

Figure 3.7: Markers for growth and proliferation. 60

Figure 3.8: Markers for DNA damage. 61

Figure 3.9: Differential caspase signaling regulates cell viability. 63

Figure 3.10: Differential caspase signaling regulates cell viability. 64

Figure 3.11: Activated Caspase 8 or 9 are not initiating apoptosis in hyperosmotic stress..... 69

Figure 3.12: Inhibtion of other cell death pathways. 70

Figure 3.13: Caspases and p38 mediate γH2AX phosphorylation during hyperosmotic stress..... 71

Figure 3.14: Contribution of p38 to apoptosis in hypertonic stress is minimal. 73

Figure 3.15: Phosphorylation of p38 is correlated with PARP cleavage. 74

Figure 3.16: cPARP+/p-p38+ fraction precedes appearance of cPARP+/p-p38- fraction 75

Figure 3.17: Intracellular proline protects human cells during ramp stress conditions. . 77

..... 79

Figure 3.18: Metabolite distribution changes in hypertonic stress. 80

Figure 3.19: External proline and glutamine improve viability in step treated cells similarly to ramp treated cells without external proline or glutamine in comparison to established osmolytes. 81

Figure 3.20: Gene expression changes in MEFs is indicative of proline accumulation. 82

Figure 4.1: Workflow of FCBapp..... 96

Figure 4.2: Gating using the FCBapp. 97

Figure 4.3: Debarcoding of fluorescently labeled cells using the FCBapp. 98

Figure 4.4: The debarcoded populations are assigned to the conditions used in the experiment. 99

Figure 4.5: Vizualizing the distributions of the debarcoded fractions. 100

Figure 4.6: Sample data from the Flowrepository debarcoded by the FCBapp. 101

Figure 4.7: Assigning conditions to the Sample data from the Flowrepository. 101

Figure 5.1: Response of proteins with and without posttranslational modifications..... 104

Figure 5.3: Proline supply affects tumor growth in the microenvironment..... 109

Figure A1: A diagram illustration of algorithm to compute the pump profiles. 158

Figure A2: Calculated pump profiles for increasing linear and nonlinear gradient kinetics 159

Figure A3: Calculated pump profiles for decreasing linear and nonlinear gradient kinetics 160

LIST OF TABLES

Table 3.1: Antibodies used in this study. 90

Table 3.2: Inhibitors used in this study. 91

Table A1: Calculation results for TS experiment profile generation. 162

Table A2. Calculation results for TP experiment profile generation. 164

1. Introduction

1.1 Using temporally-variable changes in the environment as a systems biology method to study cell biology

1.1.1 Systems biology as an approach to understand biology

Biology is very complex and despite the fact that we are constantly aiming to improve our understanding about how cells work, biological responses are yet mostly unpredictable. Systems biology is a field in biology that seeks to combine data analysis with principles of engineering, computer science and other quantitative fields to understand biological function (Kitano 2002a; Lim, Meyer, and Pawson 2014). These influences are a natural development furthered by the increase in computing speed and capacities, the accumulation of data and the advancement of high-throughput technologies (Kitano 2002b). While biochemical and molecular biological approaches seek to reduce complexity to understand each component of a living system, systems biology, leverages complexity of big data sets and interdisciplinary approaches to generate new perspectives on living systems. Systems biology aims to look at the cell or a biological system as a whole and aims to quantify new properties about this system to characterize and understand it (Kitano 2001).

To understand a biological system, it is particularly important to characterize its responses dynamically over time as opposed to assume a constant static state. Changes in the environment can control life and death of a cell (Alberts et al. 2015). Correctly sensing and interpreting changes in the environment is critical for the survival of the cell. To improve our understanding of biological systems it is necessary to carefully consider the impact of each aspect of an environmental change. There are three aspects of environmental change: (1) type of and composition of the environmental stimulus, (2) concentration of the stimulus and (3) concentration change over time of stimulus composition and concentration. The effect of the stimulus type and of its concentration

are extensively studied for many possible environments (Alberts et al. 2015; Voet and Voet 2011), but how concentrations change over time is understudied.

Making biological behavior predictable is a core aim of systems biology (Kitano 2001). It is therefore important to obtain a quantitative understanding of cell decision changes in the environment over time and of how this translates to changes in cellular behavior. By precisely controlling these temporal changes we can improve our understanding of cellular behavior. Changes in a stimulus can occur slowly or acutely over time. Naturally, a cell needs to be prepared for both instances and mount adequate responses. Cells in the human body are usually protected from large acute changes of most exogenous stimuli by buffers and homeostatic processes (Cannon 1932). Most physiologic changes in the human body are slow and minor. However, under certain physiological and pathological conditions these changes can become more severe. Local concentrations of cytokines, morphogens, osmolytes or drugs can change rapidly and differentially affect cellular behavior. Such changes can manifest themselves in the body through spatial gradients or temporal patterns, such spatial zonation in the kidney and temporal changes of osmolyte concentrations over time during diuresis. Another physiological example is the development of an embryo, during which spatial gradients of morphogens are used to differentiate the embryonal stem cells into different organs. During an inflammation or injury there are local spikes in cytokines and osmolytes causing a challenge to the local tissue. In addition, immune cells invade these tissues and are exposed to these stimuli at various profiles over time.

It is important to consider how the changes in the environment are a) used by the body to control cellular fate and b) how temporal changes can be used to manipulate cells.
Once such an understanding is obtained, this paves the way for predictive models of cell behavior. Currently, *in vitro* cell line-based studies are often performed under the assumption that exposing cells instantly to final concentrations of a stimulus represents true physiology. Unfortunately, this may not be the case as temporal changes of the stimulus can affect how cells respond to a stimulus. Therefore, the conclusion of results should be cautiously considered.

1.1.2 Understanding the cell as a black box system

A cell can be seen as enclosed system whose inputs can be controlled and whose outputs can be measured. This perspective allows to modulate and use inputs to study the system while being momentarily ignorant of the mechanisms inside of the system. In particular to obtain predictive mathematical models of biology, biological science has employed tools of control theory. Control theory, a subdiscipline in engineering, seeks to use simple engineering principles to construct a model of a dynamically changing system. (Baetica, Westbrook, and El-Samad 2019). With the help of these tools, scientists can determine thresholds of activation and response frequencies of a system. Therefore, control theory is well suited to be applied to pathway signal transduction and to sensory systems.

A way to perturb a system is to use oscillatory signals. These perturbations are characterized by defined wave inputs. By modulating the frequency of these waves, the dynamics of a biological system can be characterized. For example, by applying this approach to the osmostress response in yeast, it was found that there are two kinds of negative feedback that operate at different speeds (Mettetal et al. 2008; Hersen et al. 2008). Other studies used this approach to characterize the differences in the metabolic gene regulation in different yeast species (Bennett et al. 2008) or to understand bacterial chemotaxis (Shimizu, Tu, and Berg 2010). Perturbing cells with different input patterns governed by engineering principles opens up the possibility of exploiting the pathway topologies to encode new information. Using these approaches extends classical perturbation approaches such as mutations, or over- or underexpression of pathway components. Different stimuli and the temporal patterns through which they are delivered to a cell can function as a code, that results in specific cellular responses (P. Li and Elowitz 2019).

1.1.3 Perception of temporally variable changes, fold change vs. absolute change detection

The way we sense our environment follows physical laws. One of these laws involves the perception of signal strength. Signal strength and our ability to sense this strength and its change depend on how strong this signal is relative to baseline or background signal. Therefore, how we sense our environment depends not only on the strength of a stimulus but also on how it changes. For instance, a constant noise will cause adaptation, a rapidly pulsing noise will cause alertness. Distinguishing between lifting a weight of 100 lbs. vs. 105 lbs., is not as easy as to distinguish the difference between a weight of 5 lbs. vs.10 lbs. These examples show on an organismal level that the way a stimulus is applied matters. There have been theoretical laws formulated that try to explain these phenomena. One is the Weber-Fechner law which states that a system senses the fold change of a stimulus and not the absolute change in the stimulus (Weber 1850; Fechner 1860). Psychophysics is a field in psychology that tries to describe and understand these relationships on the level of sensory physiology (Kandel 2013). On a cellular level fold-change detection has been proposed to underlie observations of signaling dynamics (Adler and Alon 2018; Ferrell 2009). Because the sensed change in stimulus intensity is proportional to the logarithm of the stimulus, these systems are described as log sensing.

1.1.4 Pathway network configurations in linear and adaptive pathways

Signaling pathways are believed to be the main conductors of information from sensors of the environment to the execution of a response in the cell. Signaling pathways usually consist of multiple proteins or second messengers that function in a functional cascade.
A linear or analogue pathway is a signaling pathway that transduces information from a sensation to a response in direct correlation with the stimulus strength (Behar et al. 2008). The stronger the input signal, the stronger is the output signal. This relationship is only limited by a detection limit and by saturation of the transmission potential of the pathway components (saturation). Between these limits such a hypothetical pathway responds linearly.

An adaptive pathway, on the other hand, is activated upon a stimulus signal and adapts to a level of activity below the maximum activation, even if the stimulus is still present. Many pathways that control homeostatic processes have evolved to be adaptive. If the mechanisms that ensure adaptiveness break, the underlying response that is regulated by the pathway can get out of control. Cancer cells, for example, integrate growth signals differently than healthy cells. Instead of arresting growth when a setpoint is reached, they pass this setpoint and keep growing. Underlying these changes are commonly alterations in growth signaling pathways that prevent the deactivation of a pathway component by a mutation in this component.

Perfect adaptation, is the property of a system to return to its baseline level after stimulation and often observed in adaptive pathways (Ferrell 2016). A study in 2009 tried to understand what the minimal network topology for perfect adaptation is (W. Ma et al. 2009). They found that there are only two general network configurations that can achieve perfect adaptation, the negative feedback loop (NFL) and the incoherent feedforward loop (IFFL). The NFL is characterized by a node in the network that gets activated upon stimulation of the network and then suppresses the activation of the network output by inhibiting an upstream component in the network. The IFFL is characterized by a forward activating and suppressing transmission after activation, hence the name 'incoherent' (Goentoro et al. 2009).

One of the first and best studied examples of fold change detection in cell biological systems is chemotaxis in bacteria. *E. coli* are able to move in liquid media and sense the presence of nutrients. Certain nutrients, such as L-serine, function as ligands to sensors at the bacteria and trigger a signal transduction pathway that then enables the bacteria to swim towards the nutrient (Block, Segall, and Berg 1983). The response to an instant concentration change of such a nutrient results in a transient response of directed movement towards the nutrient and depends on the change of the concentration relative to the media (Shoval et al. 2010; Kalinin et al. 2009). Stimulation of Xenopus oocytes with Wnt ligand results in beta-catenin accumulation in the cells. This response follows the fold change detection principle by responding logarithmically to changes in Wnt ligand (Goentoro and Kirschner 2009). Smad3 does not respond to an absolute level of Tgf-beta

stimulation, but to the change in its concentration relative to the baseline concentration (Frick et al. 2017; Sorre et al. 2014). When HEK293 cells are exposed to carbachol, the cell responds with pulses of intracellular Ca^{2+} spikes. These responses depend on the fold change of the stimulus (Thurley, Wu, and Altschuler 2017). After stimulating HeLa cells with TNF, NF-κB RelA translocates to the nucleus in a fold change dependent manner. Upon stimulation with EGF, ERK signaling has a fold change response (Cohen-Saidon et al. 2009). The environment changes over time and can do so slowly, fast or in different patterns. It is a long-standing question, if the concentration of a compound itself is determining the response or rather the change of this compound relative to its previous concentration.

1.1.5 Applying Ramp-like temporal changes to stimulate cells

One way to query the response of a cellular system is to apply a stimulus gradually over time. A linear increase of the stimulus concentration in the environment is commonly referred to as a 'Ramp'. In this stimulation, a stimulus increases slowly at a constant rate over time. Previous studies used this approach to better understand the properties of bacterial stress signaling (Jonathan W. Young, Locke, and Elowitz 2013) and chemotaxis (Block, Segall, and Berg 1983; Shimizu, Tu, and Berg 2010) in bacteria. The speed of morphogen detection was represented by gradual increases of morphogens over time *in vitro* (Sorre et al. 2014). Glucose is known to gradually increase in the blood after a meal. Due to the importance of diabetes and the changes in glucose accumulation dynamics in this condition, some experiments have used ramps to understand the effect of slowly rising insulin concentrations on the signaling (Sano et al. 2016).

In summary, the ramp stimulation is a useful and non-invasive way to perturb a biological system and recapitulate physiology for the purpose of better characterizing its properties.

1.1.6 Current approaches and methods for kinetic stimulation

Applying temporally variable environments in a well-controlled manner is a substantial challenge in biological experiments. Applying different input profiles to cells is often equated with a change in the cell culture conditions. Previous studies on investigating the effect of temporally variable environments on cells heavily relied on microfluidic setups (Y. Zhang et al. 2013; Caen et al. 2017; Mokashi et al. 2019). While these systems offer a good control over the environment, they function at a small scale with a few cells, represent a more artificial condition relative to normal cell culture conditions, are complicated to set up and require fancy instrumentation. In addition, many common assays are not possible to be combined with these approaches. To address these issues we developed a simple and precise method to apply stimuli to cells under normal cell culture condition, as described in Chapter 2 (Thiemicke et al. 2019).

1.2 The relevance of temporally-variable changes in human physiology

1.2.1 Temporal dynamics of morphogens during development

A good example in which the temporal dynamics of the environment are important for cell fate is the development of the cell. Morphogens, molecules that determine cell differentiation decisions, are secreted to form concentration gradients that are crucial to provide an axis during polarization. Previous studies have established thresholds of morphogens critical in development and relevant for diseases of failed morphogenesis (Sorre et al. 2014; P. Li et al. 2018). For example, the Tgf/Smad pathway has been studied in the context of temporal dynamics. Another example is the Wnt pathway, in which the Wnt ligand is known to change dynamically and encode different output (Goentoro and Kirschner 2009). These signaling pathways respond to a time variable code of stimulation.

1.2.2 Temporal dynamics of Glucose and Insulin in the body

A well-known example in physiology are the dynamics of glucose and insulin. Both are known to oscillate in a negative feedback cycle. Determining these dynamics has been

easier than in other systems as the concentration of glucose and insulin can be determined from the blood of patients. In addition, diabetes, the most common associated chronic disease, is a growing epidemic that affects a substantial portion of the world population (Kharroubi 2015). In particular, the dynamical changes of insulin secretion depend on glucose application. Oral application, eating, causes a ramp like increase of insulin in blood (Rosenqvist, Licko, and Karam 1976). Intravenous application of glucose causes a step like increase in insulin (Lundbaek 1962). The different ways of increasing glucose have been shown to affect how the body responds to glucose concentrations metabolically by triggering glycolysis, gluconeogenesis or glycogenesis (Noguchi et al. 2013). Therefore, stimulating cells with ramps provided insights into the response dynamics of insulin secretion. For example it was determined that the speed by which insulin is secreted affects the expression of genes (Sano et al. 2016). Researchers also applied ramps of glucose increase to pancreatic beta cells to determine thresholds of activation for insulin secretion (C. Li et al. 2004; Lu and Li 2018). Glucose ramps are routinely used as a physiologic representation of glucose concentration dynamics to elucidate the responses of pancreatic cells in the context of drugs, mutations and disease (Bansal et al. 2019; Grespan et al. 2018; Deng et al. 2004; Jaeckle Santos et al. 2014; Douros et al. 2019). In addition, this research contributed to the development of methods and devices to apply stimulation ramps to cells such as to measure pancreatic islet function (Adewola et al. 2010).

1.2.3 Temporal dynamics of stressors in the cellular environment

There are many physiologic examples in which temporal changes of extracellular stimuli are already known to be important for cell fate decisions. One such example is the kidney which harbors one of the most extreme environments in the human body (Neuhofer and Beck 2005; Kwon, Lim, and Kwon 2009; Burg, Ferraris, and Dmitrieva 2007). Renal tissue is classified by zones (Koepsell et al. 1974). Of these the most inner zones also have regularly higher levels of osmolarity. The most inner region which has the highest osmolarity is called papillary tip. Depending on the species and the conditions, osmolarities can reach up to 9370 mosmol/l as measured in the urine of the Australian

desert mouse (MacMillen and Lee 1967) and at least 1200 mosmol/l in humans, four times the level found in plasma (Atherton, Hai, and Thomas 1968; Hai and Thomas 1969; Schmidt-Nielsen, Graves, and Roth 1983). It has been a question, how kidney cells are able to survive these extreme conditions (Neuhofer and Beck 2005). The osmolyte concentrations in the kidney change dynamically over time and follow circadian rhythms (Hara et al. 2017). If these rhythms are disrupted they can contribute to the development of several kidney pathologies (Firsov and Bonny 2018; Johnston and Pollock 2018; Hara et al. 2017), indicating that the temporal patterns of osmolyte changes may be relevant for cell survival. Surprisingly, the same cell types that are able to function properly *in vivo*, die in culture when exposed to sudden increases to the same osmolarity. A study by the Burg lab in 2002 examined the effect of slowly increasing osmolarities on cell survival (Cai et al. 2002b). The authors found that a slow increase of osmolarity drastically improves cell survival of a human kidney cell line when compared to a step increase. A follow-up study identified gene expression differences in several osmoprotective genes as the reason for the improved survival during the gradual increase (Cai, Ferraris, and Burg 2004). Kidney cells are widely recognized as cells particularly well-adapted to extreme hyperosmolar environments.

However, recent studies create an image of great cellular diversity in the kidney. Recent studies show that the inner medulla and the papillary tip are also populated by immune cells (Stewart et al. 2019; Allison 2019; Weisheit, Engel, and Kurts 2015; Van Beusecum et al. 2019). How these cells survive in this environment is not understood. It is particularly interesting that the immune cell levels are elevated in pathological conditions suggesting a role of the kidney and its particular environment in various disease contexts (Chevrier et al. 2017; Weisheit, Engel, and Kurts 2015; Wilck et al. 2019; D. N. Müller et al. 2019)

1.3 The effect of hyperosmotic stress on mammalian cells

1.3.1 Hyperosmotic stress response in eukaryotes

In order for a cell to survive and grow it needs to sense and adjust to changes in its environment. One of the most common changes any cell can be exposed to is the concentration change in the osmotically active compounds in its local environment (Else K. Hoffmann and Pedersen 2006; Else K. Hoffmann, Lambert, and Pedersen 2009). These changes can affect the osmotic pressure and subsequently the cell volume. Maintenance of the cell volume is critical for most cellular components to function correctly and for the cell to survive. Cells, therefore, had to evolve to properly sense and respond to osmotic changes to maintain their volume (Else K. Hoffmann, Lambert, and Pedersen 2009; Larsen and Hoffmann 2016; Burg, Ferraris, and Dmitrieva 2007).

The intracellular fluid is in an electrochemical equilibrium with the extracellular environment. The Gibbs-Donnan equilibrium (1.1) states that dissolved ions are in an equilibrium across a semipermeable membrane.

$$\left(C_{Na}^{i} + C_{K}^{i}\right) * C_{Cl}^{i} = (C_{Na}^{o} + C_{K}^{o}) * C_{Cl}^{o} \quad (1.1)$$

This relationship states electroneutrality which results in electrochemical gradients that dictate the flow of ions. Cells contain higher concentrations of K^+ and lower concentrations of Na^+ inside the cell. Negatively charged macromolecules, organic acids and phosphates are major components of cells. For example, 70% of all proteins have a negative net charge at physiological pH (Gianazza and Giorgio Righetti 1980) and thereby contribute to an excess of negatively charged molecules that cannot cross the cell membrane. The extracellular environment contains high levels of Cl^- and Na^+ and has only a low concentration of non-diffusible ions (Figure 1.1). Overall, electroneutrality is always maintained on both sides of the membrane.

Water and small non charged molecules can pass through the membrane. Especially due to the presence of aquaporins, water can travel across the cell membrane rather easily. This fact results in the risk for the cell to accumulate osmolytes and water and to burst. This is prevented by mechanisms described under the “pump and leak” concept (E. K. Hoffmann 2001; Ussing 1960; Leaf 1959). Under this concept, the cell maintains the equilibrium by constantly removing sodium from the cell through the activity of the Na^+/K^+ ATPase, which ensures the expulsion of sodium and the maintenance of the

electrochemical gradient. Maintaining this equilibrium is extremely energy intensive using 20-70% of the oxygen expenditure of a cell (Wheaton and Chandel 2011; Milligan and McBride 1985). Other organisms found other ways to control for osmotic pressure, such as a cell wall in plants and yeasts or the pulsatile vacuole in unicellular organisms (Allen and Naitoh 2002). The electrochemical gradient results in osmotic pressure on the cell that is defined by the Boyle-van't Hoff equation (1.2).

$$\Pi = \mathrm{RT} * \sum \mathrm{C_j} \tag{1.2}$$

The osmotic pressure (Π) depends on the gas constant R, the temperature T and the sum of the osmolyte concertation ($\sum C_j$).

Hypothermia and inhibitors of the Na^+/K^+ ATPase, such as ouabain, can disturb this process and can potentially result in osmotic lysis of the cell (Russo, van Rossum, and Galeotti 1977). Homeostatic processes control the intracellular environment to ensure the maintenance of these conditions. A change in this equilibrium on either side by osmotic alterations in the envrionment can be stressful to the cell. A resulting osmotic stress is either characterized by an increase in extracellular osmolytes (hyperosmotic stress) or a decrease in extracellular osmolytes (hypoosmotic stress). A special case of hyperosmotic stress is hypertonic stress that is characterized by an increase of osmolytes that cannot easily penetrate the cell membrane. Increasing the extracellular concentration of an osmolyte (e.g.: NaCl by 150 mM) changes the electrochemical equation substantially.

The instant effect on a cell to a step change of hypertonic addition of NaCl is an outflow of water out of the cell and a reduction in cell size. This process poses a challenge to the molecules in the cell which function best under homeostatic conditions. An early response by the cell to the shrinkage is opening K^+ channels, upon which K^+ ions enter the cell and attract water back into the cell resulting in regulatory volume increase (RVI). How long exactly each of these processes takes is difficult to determine as the cell quickly counters the outflow of water and the two processes overlap in time. Both processes have been reported to occur in the range of minutes (Else K. Hoffmann, Lambert, and Pedersen 2009). For the initial RVI, the cell opens several ion channels (Figure 1.1), such as Sodium-Potassium-Chloride-transporters (NKCC), the Sodium-hydrogen-Antiporter 1

(NHE1), Sodium-Calcium-Exchangers (NCX) and Epithelial Sodium Channels (ENaC), and other non-selective cation channels (HICC). The cell shrinkage results in several immediate consequences for the cell, as outlined below. A main consequence of cell shrinkage is molecular crowding. Cells are filled with macromolecules such as proteins and nucleic acids that are tightly packed into the cell (Katherine Luby-Phelps 1999; Kate Luby-Phelps 2013). Cell shrinkage causes molecular crowding which describes the increased concentration of these macromolecules in the cell (Miermont et al. 2013; Babazadeh et al. 2013). Recent findings indicate that molecular crowding reduces the motility of proteins (Nunes et al. 2015; Miermont et al. 2013) and diffusion (Konopka et al. 2009; Nunes et al. 2015; Mourão, Hakim, and Schnell 2014; Okumus et al. 2016) of cellular components and slows down signaling and other reactions in the cell.

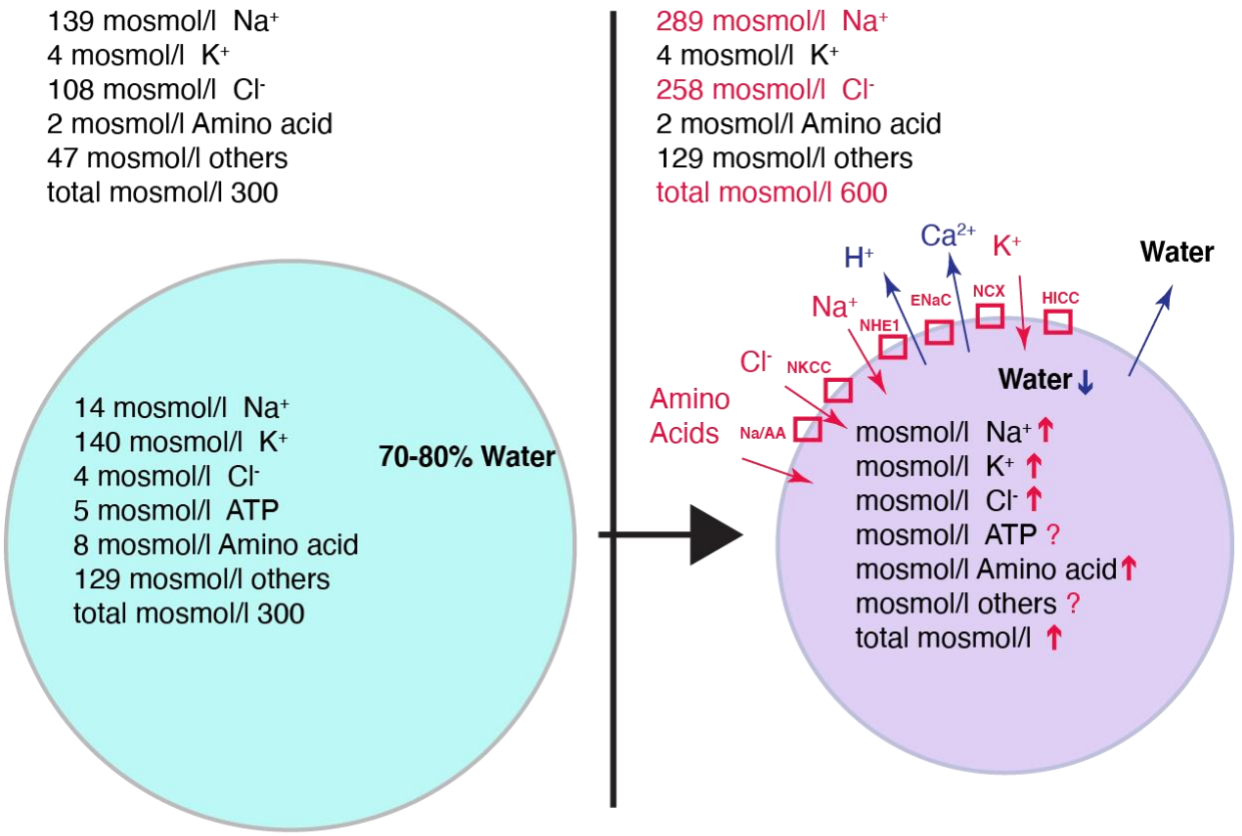

Figure 1.1: Cell volume and osmolyte changes in hypertonicity

Represented on the left is a cell in physiological isotonic conditions. The values given are osmolarities for different osmolytes inside and outside of the cell (Guyton and Hall 2000; Nguyen and Kurtz 2006). On the right side are volume relevant changes that occur after exposure to hypertonicity of additional 300 mosmol/l NaCl.

Another consequence is the increase of ionic strength in the cell (Else K. Hoffmann, Lambert, and Pedersen 2009; Orlov et al. 2018) which can have immediate effects on protein structure (Kumar et al. 2020) and metabolic functions (Yancey et al. 1982). Since the beginning of life, these changes must have occurred, and cells must have evolved to protect themselves from this stress in order to survive. Non-hypertonic hyperosmotic stress occurs when cells are in an environment that is high in compounds able to cross the cell membrane. A common example for this is urea. Urea concentrations are high in some tissues such as the kidney. Urea in the kidney microenvironment buffers the high levels of NaCl (Kwon et al. 2009), but has toxicity on its own (Z. Zhang et al. 2004; Wahiduzzaman et al. 2019). While high osmolarities by a combination of urea and NaCl

are better tolerated than each osmolyte on its own at that osmolarity, adding either one of the two does not improve viability over the other alone (Santos et al. 1998). Hypertonicity and subsequent shrinkage have profound effects on the cell. Cell shrinkage is rapid (Bustamante et al. 2003) and may have immediate effects on protein folds. Recent studies report, that some proteins are able to undergo phase separation (Jalihal et al. 2019; Alexandrov et al. 2019) and thereby functionally sense the volume change. Another study identified a sensor for sodium, Na+/Ca2+ exchanger 1 (NCX1), through which sodium enters the cell and contributes to NFAT5 activation (Neubert et al. 2020).

Hypertonic shrinkage has been reported to disrupt the electron transport chain, to cause mitochondrial failure (Lee, Chandel, and Simon 2020) and oxidative stress (Netzer et al. 2015). A conductor of the hypoxic stress response, Hif1a, is overexpressed (Farabaugh et al. 2020; Neubert et al. 2019) and functionally important in the autophagic response to NaCl (Neubert et al. 2019). How the cellular energy metabolism and the partial pressure of oxygen are dynamically affected by the direct effects of hypertonicity is yet not fully understood. Before this study it was not known how the levels ATP content change upon hypertonic stress (Figure 1.1). However, it has been found that hypertonic stress causes a shift in metabolism from oxidative phosphorylation to glycolysis (Hamraz et al. 2020). There is evidence that increased NaCl causes oxidative stress in kidney cell lines (Z. Zhang et al. 2004) and that there is oxidative stress in the kidney (Zou, Li, and Cowley 2001). Mild oxidative stress may also contribute to osmoprotection (Zhou, Ferraris, and Burg 2006).

Hypertonicity has been found to be correlated with DNA breaks in cells, even under normal physiologic conditions and in tissue such as the kidney that is commonly exposed to hypertonicity (Dietmar Kültz and Chakravarty 2001; D Kültz et al. 2001). Interestingly, cells can tolerate this damage and survive and proliferate (Dmitrieva, Cai, and Burg 2004; Dmitrieva and Burg 2004). There are factors that maintain genomic integrity (Dmitrieva et al. 2005) and DNA damage may only be repaired once cells are back in an isotonic environment (Burg, Ferraris, and Dmitrieva 2007).

Two other aspects further complicate a general understanding of the mammalian osmotic stress response. One is the fact that there are adherent cells, such as epithelial cells, that are attached to a matrix and get inputs through the contacts to that matrix about their volume and then there are suspension cells that usually do not have this potential input. Another is the fact that mammalian cells are part of an organism and different cell types may have evolved to respond differently to osmotic stress to benefit the organism as part of their tissue context.

In conclusion, there are many processes in the cell that are directly affected by the consequences of hyperosmotic stress. The cell likely responds to each of these different processes with dedicated response pathways. Unlike in bacteria (Wood 1999) and yeast (Saito and Posas 2012; J. L Brewster et al. 1993; Jay L Brewster and Gustin 2014) that have a cell wall and osmotic stress sensors in their membrane, a dedicated osmotic sensor was not found in mammalian cells (Orlov et al. 2018; Joan D. Ferraris and Burg 2006).

1.3.2 Hypertonic Stress activated protein pathways

Hypertonic stress activates several stress pathways. Often, it is not clear how exactly the abovementioned direct consequences of hypertonic shrinkage relate to signaling activation. There have been many pathways described to be activated under hypertonic stress conditions. One of the most prominent pathways that is known to be activated by hypertonic stress are Mitogen Activated Protein Kinase (MAPK) pathways (J. M. J. Kyriakis and Avruch 2012). The MAPKs p38 and c-Jun N-terminal kinase (JNK) proteins are homologs of the MAPK Hog1 in the yeast *S. cerevisiae*, one of the most studied stress response pathway proteins, and therefore are functionally and structurally conserved for over 1 billion years of evolutionary pressure (Levin-Salomon et al. 2009; Cano and Mahadevan 1995; Han et al. 1994; Saito and Posas 2012; J. M. J. Kyriakis and Avruch 2012; J. M. Kyriakis et al. 1994; Cuadrado and Nebreda 2010). MAPKs are Ser/Thr kinases and get activated by dual phosphorylation at a Tyr and a Thr residue, that is conserved to occur as a Thr-X-Tyr motif. A hallmark of MAPK pathways is a three-

component core signaling cascade of kinases that transmit a signal linearly from the MAP3K to the MAPK (J. M. J. Kyriakis and Avruch 2012). Extracellular signal-regulated kinase (ERK), another MAPK, is sometimes reported to respond to hypertonic stress (Chou et al. 2011) and sometimes reported to be downregulated (Nielsen, Christensen, and Hoffmann 2008). However, it is generally not considered a typical stress response pathway (Else K. Hoffmann, Lambert, and Pedersen 2009). There are 4 isoforms of p38 and 3 isoforms of JNK in mammalian cells that differ in their tissue specific expression and may differ in their function. In general these 7 isoforms overlap in the stimuli they are activated by, the targets they activate and the processes they control (J. M. J. Kyriakis and Avruch 2012). The most highly expressed p38 isoform, p38α, is usually referred to when no isoform is specified and gets transiently activated in instant additions of hypertonic stress by double phosphorylation (Saito and Posas 2012; J. M. J. Kyriakis and Avruch 2012). While all isoforms may be activated in hypertonic stress, they may actually carry out opposing functions (Zhou et al. 2008). P38 phosphorylates many different targets (Trempolec, Dave-Coll, and Nebreda 2013) that are important in the hyperosmotic stress response, such as sodium transport (Wang et al. 2014) and actin remodeling (Bustamante et al. 2003). Another isoform, p38δ, has been reported to contribute to apoptosis (O'Callaghan, Fanning, and Barry 2014; Gonçalves et al. 2018; Zhou et al. 2008) and thereby to counteract the protective effects of p38α in hypertonic stress (Zhou et al. 2008).

Unfortunately, almost all of these studies have been performed by stimulating cells by an instant addition of hypertonicity. As MAPKs often have a transient response dynamic, the dynamic response in tissue may be different than what has been found in these cell culture experiments.

Nuclear Factor of Activated T Cells 5 (NFAT5) or TonEBP/OREBP is one of the most important osmostress response signaling proteins in mammalian cells (Jeon et al. 2006; Dahl, Handler, and Kwon 2001; Ho 2003; Aramburu et al. 2006; Cheung and Ko 2013; Trama, Go, and Ho 2002). It belongs to the Nuclear Factor of Activated T cells transcription factor family and upon osmotic stress gets phosphorylated and translocates

to the nucleus (Dahl, Handler, and Kwon 2001; CHA et al. 2001; López-Rodríguez et al. 2001). It recognizes an osmotic response DNA sequence element (J D Ferraris et al. 1996; Burg, Kwon, and KÜltz 1997) in promoter regions of many osmoprotective genes, such as Heat shock protein 70 (HSP70), Aldose reductase (AR) and several amino acid transporters. How exactly the sensation of osmotic change is transduced to NFAT5 activation is not fully understood. A range of proteins, such as p38 (Dahl, Handler, and Kwon 2001) and Fyn (Ko et al. 2002) have been suggested to contribute to NFAT5 activation (Zhou 2015). NFAT5 is also activated by membrane stretch (Scherer et al. 2014). Recent results indicate that NFAT5 activation may be mediated by structural changes induced by intracellular ionic strength (Kumar et al. 2020). This complex upstream regulation suggests that the cell can modulate the activation of NFAT5 very finely and ensure the transcription of its downstream gene targets under different stress conditions.

Other pathways that have been found to be relevant in hypertonic stress are the NFκ-B, COX2, FAK, Rac/Rho and PI3K pathways. In some cells NFκ-B may be activated downstream of NFAT5 (Roth et al. 2010) and contribute to inflammatory phenotypes at lower hypertonic concentrations (Farabaugh et al. 2017, 2020). Accumulation of osmolytes in the kidney has been found to be cyclooxygenase 2 (COX2) dependent (Moeckel et al. 2003). Hypertonicity has effects on the cytoskeleton (Bustamante et al. 2003; Ciano-Oliveira et al. 2003; Mountian and Van Driessche 1997; Ciano et al. 2002) that result in activation of associated pathways. For example, it is known that hypertonicity causes rapid reorganization of actin likely to counteract the strong mechanical forces due to the cell shrinkage after water loss. Actin usually forms a cortical ring along the cell membrane. In hypertonic stress, this cortical ring is depolymerized and repolymerized into a diffuse network of actin bundles. This structural change improves the cells changes to counteract the strong physical forces of the hypertonicity induced water loss induced cell shrinkage. The outflow of water also shifts the equilibrium from globular actin to polymerized actin (Fuller and Rand 1999). Rac/Rho, two G proteins, are attached to the cytoskeleton and can instantly signal changes in cytoskeletal reorganization (Ciano et al. 2002; Lunn and Rozengurt 2004). A special case are cells that are attached to the

extracellular matrix through integrins. Integrins are linked to the cytoskeleton via focal adhesions (FA) and there is evidence that the changes in volume can be detected through these structural elements (Lunn and Rozengurt 2004). Focal adhesion kinase (FAK) and Src are recruited to FAs upon integrin stimulation and subsequently phosphorylated (Rasmussen et al. 2015). In particular in adherent cells, the phosphatidylinositol 3-kinase (Pi3K) plays a role in osmoregulation and gets activated upon interaction with integrins (Low and Taylor 1998).

In conclusion, there are several different pathways that have been reported to respond to hypertonic stress. While most of the components likely have been identified, their activation dynamics, crosstalk and relative importance across different cells is not fully understood. In comparison to simple unicellular organisms, cells in multicellular organisms had to evolve under two evolutional pressures, their own cellular survival to the stress and the benefit of the organism.

1.3.3 Cell death in hyperosmotic stress

Cell Death is defined as the moment when a cell ceases to function. It is generally classified into regulated and unregulated cell death (Galluzzi et al. 2018). The predominant regulated cell death pathway is apoptosis (Galluzzi et al. 2018). The main signaling conductors of apoptotic signals are pathways involving the cleavage of caspases (McIlwain, Berger, and Mak 2013; Lamkanfi et al. 2007). Caspases are cysteine proteases that exist as zymogens and have to be cleaved to become active (Lamkanfi et al. 2002). They are grouped into initiator caspases (caspase 2, 8, 9, 10) and effector caspases (3, 6, 7). The “extrinsic apoptosis” pathway involves the activation of caspase 8 and 10 and the “intrinsic apoptosis” pathway that involves caspase 9 (Ramirez and Salvesen 2018). Initiator caspases proteolytically cleave executioner caspases to activate them, amplify the apoptotic signal and to commit the cell to apoptosis (Kesavardhana, Malireddi, and Kanneganti 2020).

As outlined in chapter 1.2.3, the kidney and the cells occupying this tissue experience drastic changes in osmolarity. Therefore kidney cell have been a focus in the research on cell death in hypertonic environments. Previous studies argued that cell proliferation and slow increases in osmolarity contribute to the cell survival (Cai et al. 2002b; Cai, Ferraris, and Burg 2004). While previous studies identified the activation of both the intracellular and extracellular caspase pathways in kidney cells under hypertonic stress, the temporal order and the stimulus of their activation were not clear (S. Y. Choi et al. 2013; Moeckel 2013). It is relevant to note that cell shrinkage is correlated with apoptosis (Lang and Hoffmann 2013). This process is called apoptotic volume decrease (AVD) and is considered an early marker of apoptosis (Maeno et al. 2000; Lang et al. 1999; Okada et al. 2001).

In conclusion, there is a lot known about different cellular components and pathways that play a role in hypertonicity induced cell death. However, the processes are not yet fully understood and their physiologic relevance in different tissues has not been elucidated. Especially dynamical aspects are underexplored. In addition, the cell death field is continuing to expand with the discovery and characterization of new cell death pathways (Gudipaty et al. 2018; Galluzzi et al. 2018).

1.3.4 Hyperosmolarity in human physiology and disease

An important question underlying this dissertation is how physiologically relevant elevated NaCl concentrations and hypertonic environments are in human tissues. What are the maximum concentrations of NaCl in tissue? In which tissues do they occur? How long do they persist and what are the temporal profiles by which these concentrations change?

A long-held assumption was that homeostasis ensures that hypertonicity does not persist in the human body (Bernard 1859; Ludwig 1861) and that consumed sodium is quickly excreted by the kidney through the production of urine in proportionate levels to its consumption. This sodium retention was long believed to require retention of adequate

amounts of water for the sodium to be osmotically inactive or neutral. Only since about 20 years, the view on sodium retention has shifted.

After initial findings in a small number of humans (Heer et al. 2000, 1993), studies on astronauts simulating a flight to mars on a terrestrial space station enabled the precise analysis of intake and output of sodium in the human body for an extended period (Titze, Maillet, et al. 2002; Rakova et al. 2017). It was revealed that sodium excretion is not perfectly correlated with sodium intake at any given day. Instead, it was found that sodium is retained in the body for longer periods depending on hormone levels in the body. Most interestingly, the sodium retention occurred absent water retention and weight increase, which was a surprising finding, shifting physiological paradigms. It was further surprising that the kidney for centuries the sole focus of fluid and sodium balance regulation of the human body, was not the organ in which excess sodium was retained and not the only organ controlling the sodium levels. It followed a search for the organ(s) in which sodium was retained. Initially, a focus for the sodium retention was the bone, which functions as a sodium reservoir (Titze, Krause, et al. 2002). While there was anecdotal evidence that sodium can be stored in the skin (Ivanova, Archibassova, and Sterental 1978), it is only since the development of ^{23}Na-magnetic resonance imaging (Sodium MRI) that sodium contents in the human body can be determined in a reproducible and non-invasive fashion. The development and application of Sodium MRI in human patients (Kopp, Linz, Hammon, et al. 2012; Kopp, Linz, Wachsmuth, et al. 2012) has revealed that sodium accumulates in the body during disease (Kopp et al. 2013a, 2016; Kopp, Linz, Hammon, et al. 2012) and during aging (Kopp et al. 2013a). These findings show that several organs, in particular the muscle and the skin (Wiig et al. 2013; Nikpey et al. 2017) and to a smaller extent the brain (Inglese et al. 2010) and other interstitial spaces (Helge Wiig, Friedrich C Luft 2017) are responsible for sodium retention. A recent study suggests that increased sodium levels could also be explained by the occurrence of edema with high extracellular volume (rich in sodium), a loss in cellularity and a subsequent isotonic shift from K^+ (high in cells) to Na^+ (Rossitto et al. 2020). However, this study does not explain why there would be a reduction in cellularity in tissues which would be necessary to explain an isotonic shift to Na^+ in their model. The study also does not determine K^+

excretion which would have to occur to comply with their model of isotonic sodium accumulation.

In parallel to these fascinating studies, other groups discovered that NaCl can stimulate and activate human immune cells. Hypertonic levels of sodium have been found to be able to activate and stimulate innate (Chou et al. 2011; Shapiro and Dinarello 1995; S. Müller et al. 2013; Schatz et al. 2016; Berry et al. 2017; Jantsch et al. 2015; Barbaro et al. 2017) and adaptive immune cells (D. N. Müller et al. 2019; Kleinewietfeld et al. 2013; Haase et al. 2018; Jörg et al. 2016; Norlander et al. 2017; Wu et al. 2013). High sodium may be functionally important to strengthen the antimicrobial defense in the skin (Jantsch et al. 2015) and in the kidney (Berry et al. 2017).

A positive correlation of sodium consumption and high blood pressure has been observed since thousands of years. In the 1960s, it was observed that the immune system may play a role in hypertension (White and Grollman 1964; Okuda and Grollman 1967). In 2007, Guzik *et al*. discovered that mice lacking adaptive immune cells (Rag-/-) have blunted hypertension when injected with Angiotensin II or fed a high salt diet and that transfer of T cells, but not B cells can restore the hypertension phenotype as seen in wildtype mice (Guzik et al. 2007). While recent reports may indicate these mice have changed their characteristics (Seniuk et al. 2020; Madhur et al. 2020; Ji et al. 2017), a substantial body of literature has now manifested the hypothesis that T cells are critical in causing hypertension (Foss, Kirabo, and Harrison 2016; Madhur et al. 2020). It was found that NaCl can activate monocytes and contribute to their differentiation to dendritic cells, which are then able to activate T cells (Barbaro et al. 2017; Kirabo et al. 2016; Loperena et al. 2016). A critical role in this process is held by isoketal-adducted proteins that accumulate in dendritic cells upon oxidative stress (Kirabo et al. 2014, 2016). Other studies have shown, that a sodium rich diet causes an increase in circulating monocytes (Yi et al. 2015) contributing to inflammatory phenotypes. Another recent study suggests that B cells may be initially activated by NaCl and then dampened in their response (Cvetkovic et al. 2019).

An organ in which the existence of a hypertonic environment is a well-established fact since a long time, are cerebral discs and cartilage tissue (Finan and Guilak 2009; Erickson, Alexopoulos, and Guilak 2001). These tissues constantly have to cope with excessive pressure (Urban 1994). When lifting weights or other strenuous use of joints, pressure compresses these cells resulting in dispelling of water from tissues and cells and extreme osmolarities (Urban, Hall, and Gehl 1993; Urban 1994). The base osmolarity in cartilage tissue is about twice the homeostatic concentration of 140 mM NaCl in serum and on other organs (Finan and Guilak 2009). If these cells are transferred to and cultured at normal osmolarities, they die (Bush et al. 2005). It is notable that these tissues have the highest concentration of collagen (proline) in the body and that collagen is degraded by enzymes secreted from the cells in the tissue upon high pressure. Rheumatoid arthritis is a common and hard to treat disease of this tissue that is characterized by chronic inflammation (Scrivo et al. 2017; Mocholi et al. 2018). A mediator of inflammation, p38, has been a key therapy target (Genovese 2009; Jones et al. 2018; Hammaker and Firestein 2010). The low tolerance of these therapies might be explained by the additional function of p38 in activating NFAT5 and osmoprotection, potentially critical in the joint microenvironment.

Pressure is an important determinant for hyperosmolarity and another example in which pressure plays a role are solid tumors. Cancers are characterized by unregulated growth. This rapid growth poses the threat of pressure in their microenvironment which is accompanied by hypoxia and metabolic changes (Hamraz et al. 2020). Interstitial fluid pressure is increased in tumors (Heldin et al. 2004). Adipocytes may even dedifferentiate and redifferentiate into myocytes in the hypertonicity caused by tumor induced pressure (Y. Li et al. 2020). Tumor tissue has been found to have high sodium levels (Barrett et al. 2018; Deen et al. 2019; Leslie et al. 2019). However, it is not fully clear, if the high sodium that has been observed is due to an increased extracellular space or if there is constant NaCl hypertonicity (Barrett et al. 2018; Deen et al. 2019).

Other tissues that have reported to be at least for some time periods hypertonic are the eye (Lemp et al. 2007; Mathers 2004), the intestine (Overduin et al. 2014), the mouth

(Yang et al. 2020) and the brain (Niswander and Dokas 2007, 2006). Several diseases are a direct or indirect result of increased hypertonicity induced immune cell activation, such as dry eye disease (Lemp et al. 2011), diabetes (Stookey, Pieper, and Cohen 2004), inflammatory bowel disease (Monteleone et al. 2016).

In conclusion, recent findings were able to demonstrate the relevance of hypertonic environments in physiologic contexts. Especially increased NaCl levels, can modulate the function of innate and adaptive immune cells and manifest chronic diseases. While there has been great progress on the determination of sodium levels in different tissues, these values only represent averages and only for a given timepoint. How different conditions change local concentrations and how fast sodium concentrations change over time is not sufficiently understood. What role potential hypertonicity may have in many physiological processes and in various different diseases is still investigated.

1.4 Goals of this Thesis

The aims of this dissertation were to understand the effect of hypertonicity in the context of the speed of addition of hypertonicity to cells on the level of molecular and metabolic changes in the cells. In particular, it has been an aim to expose cells to physiologically relevant profiles of hypertonicity and translate these temporal (kinetic) inputs to phenotypic changes, such as cell viability. To better understand the molecular mechanisms that cells undergo during these kinetic inputs, we also aimed to capture the dynamic changes of signaling molecules and the effects on cellular metabolism. To achieve this, we aimed to develop our own experimental setup and our own data analysis software.

2 Generating kinetic environments to study dynamic cellular processes in single cells

Adapted from:
Thiemicke A, Jashnsaz H, Li G, Neuert G. Generating kinetic environments to study dynamic cellular processes in single cells. *Sci Rep*. 2019;9(1):10129. Published 2019 Jul 12. doi:10.1038/s41598-019-46438-8

2.1 Abstract

Cells of any organism are consistently exposed to changes over time in their environment. The kinetics by which these changes occur are critical for the cellular response and fate decision. It is therefore important to control the temporal changes of extracellular stimuli precisely to understand biological mechanisms in a quantitative manner. Most current cell culture and biochemical studies focus on instant changes in the environment and therefore neglect the importance of kinetic environments. To address these shortcomings, we developed two experimental methodologies to precisely control the environment of single cells. These methodologies are compatible with standard biochemistry, molecular, cell and quantitative biology assays. We demonstrate applicability by obtaining time series and time point measurements in both live and fixed cells. We demonstrate the feasibility of the methodology in yeast and mammalian cell culture in combination with widely used assays such as flow cytometry, time-lapse microscopy and single-molecule RNA Fluorescent in-situ Hybridization (smFISH). Our experimental methodologies are easy to implement in most laboratory settings and allows the study of kinetic environments in a wide range of assays and different cell culture conditions.

2.2 Introduction

In a human body, cells are constantly exposed to diverse physiological environments that change over time and space. For example, it has long been known that external or internal stressors (Hai and Thomas 1969; Muzzey et al. 2009; Fujita et al. 2010; Cai, Ferraris, and Burg 2004), morphogen concentrations (Sorre et al. 2014; Cao et al. 2016), drugs (pharmacokinetics) or hormone concentrations (Norstedt and Palmiter 1984; Steiner, Bremner, and Clifton 1982; Hegemann et al. 2015) change over time (Figure 2.1a, b). Therefore, cells must have developed mechanisms to integrate kinetic changes as well as spatial gradients in the environment and respond to these in a manner benefitting the organism.

Precisely how a single cell integrates kinetic changes in the environment is often not understood. Many previous and current biomedical studies have focused on how cells are affected by sudden or instant kinetic changes of the environment (Figure 2.1b). The underlying assumption made in these types of experiments is that rapid changes in the environment serve as an adequate representation of a given physiologic or pathophysiologic cellular environment (Figure 2.1b). For example, physiologic changes in concentrations over time of stresses (Hai and Thomas 1969; Muzzey et al. 2009; Fujita et al. 2010; Cai, Ferraris, and Burg 2004), drugs or hormone levels (Norstedt and Palmiter 1984; Steiner, Bremner, and Clifton 1982; Hegemann et al. 2015) may be drastically different from instant changes and may result in a different cellular response (Figure 2.1b).

Recent pioneering studies have provided insights into how molecular processes differ in kinetic environments in comparison to instant changes in the environment (Fujita et al. 2010; Cai, Ferraris, and Burg 2004; Purvis and Lahav 2012; Goulev et al. 2017; Jonathan W Young, Locke, and Elowitz 2013; Cai et al. 2002b; Mitchell, Wei, and Lim 2015; Rahi et al. 2017; Sorre et al. 2014; Muzzey et al. 2009). These studies have often relied on two main approaches to deliver the desired kinetic perturbations on the cells. One is the use of specialized, small-scale and custom designed microfluidic setups (Shin et al. 2012; Caen et al. 2017; Crane et al. 2014; Rafael Gómez-Sjöberg et al. 2007; Bunge, Driesche,

and Vellekoop 2017). But fabricating these devices is often complex, may require specialized equipment to produce, may take significant time to set up and are limited in the compatibility with and application of many common biological assays (Shin et al. 2012; Caen et al. 2017; Crane et al. 2014; Rafael Gómez-Sjöberg et al. 2007). On the other hand, simpler approaches implemented the use of syringe pumps and flow chambers that avoid the complexity of microfluidics (Mettetal et al. 2008). Although these are state of the art methods to observe single cells in small volumes under the microscope, these methods are not compatible with standard molecular and cell biology assays. Furthermore, currently published methods generate only an approximate kinetic perturbation while they lack in validation and detailed description in how to generate kinetic environments when concentration and volumes changes over time. Therefore, a simple and precise methodology of generating a variety of kinetic environments in regular and microfluidic cell culture do not exit.

Here we provide a simple, precise and versatile methodology to generate a variety of kinetic perturbations for many common bulk and single cell assays by avoiding the complexity of common microfluidic devices. To the best of our knowledge there is no other method yet that enables the study of cells with many biological assays after exposure to a kinetic environment. We describe two methodologies to generate gradually changing environments that are compatible with standard molecular biology and cell culture conditions (Figures 2.1-2.3). We demonstrate our methodologies in yeast and a human cell line and demonstrate its applicability in combination with standard laboratory assays of signal transduction and gene regulation in population or single cell experiments (Figures 2.1d, 2.4). We believe our simple yet general methodology to precisely control the environment will enable new biological insights in how single cells respond to kinetic changes in the environment.

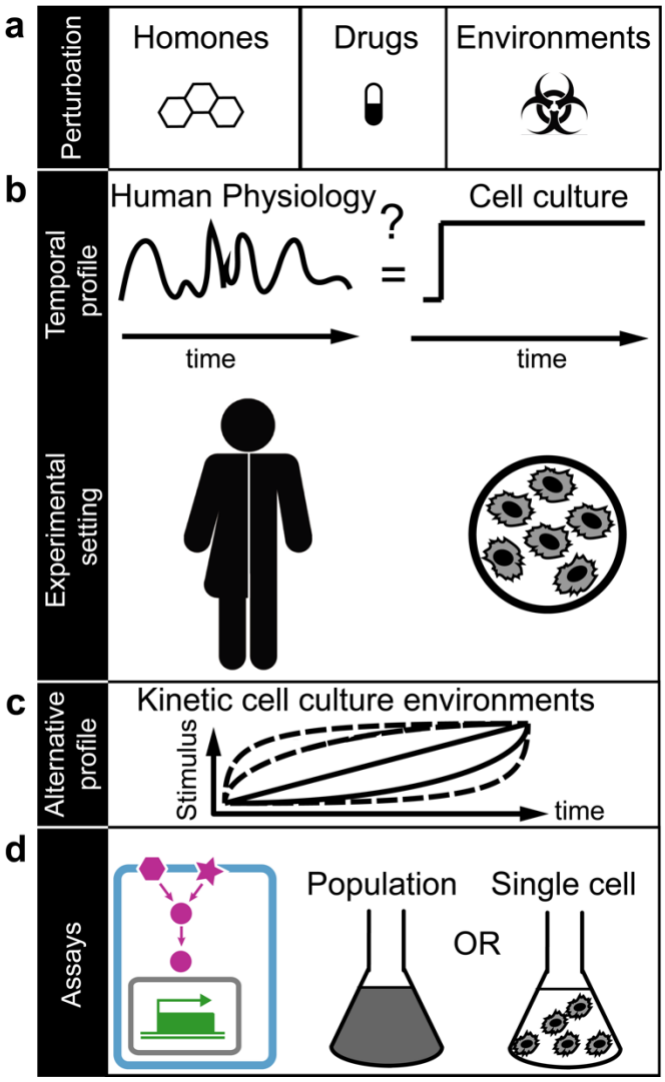

Figure 2.1: Kinetic cell culture environments mimic physiologically relevant cell environments.

(a) Examples of different types of cellular environmental perturbations. (b) Temporal profile of physiological relevant environment that may fluctuate over time as experienced by cells in humans (left). In contrast, the majority of cell culture-based experiments are performed in constant environments over time and may neglect physiologically relevant conditions (right). (c) We propose alternative profiles to study cells in precisely controlled kinetic cell culture environments. (d) The power of this approach is demonstrated on measurements of single cell volume changes (cyan), changes in signal transduction (magenta) and gene regulation (green) in cell population (middle) and single cell experiments (right) in yeast and human cells.

2.3 Results

2.3.1 Proof of feasibility using cell lines

To demonstrate our approach, we compare rapidly changing environments to gradually changing environments of increasing concentrations of a stimulus (Figures 2.1c, 2.2a). We use osmotic stress to activate the high osmolarity glycerol (HOG) Mitogen Activated Protein Kinase (MAPK) pathway in *S. cerevisiae* yeast cells and the c-Jun N-terminal kinase (JNK) MAPK pathway in a human monocytic cell line. We chose different NaCl concentrations to represent a change in the cellular environment. NaCl is a well-studied stressor in yeast cells and is relevant in human cells in the context of immune cell activation (Kleinewietfeld et al. 2013; Wu et al. 2013; Barbaro et al. 2017; Brocker, Thompson, and Vasiliou 2012; Tropini et al. 2018) and cell death(Cai et al. 2002b). We have developed two cell culture methodologies for time point (TP) measurements from continuously growing cells (Figure 2.2b) or time series (TS) measurements on the same cells over time in a simple microfluidic chamber (Figure 2.2c). Both methodologies require the use of syringe pumps. We have developed software to accurately compute the pump profiles for a desired experimental design and validated these profiles experimentally (Figure 2.3). Finally, we demonstrate the feasibility of our methodology on live-cell time-lapse microscopy experiments of cell volume change over time (Figure 2.4b), dynamic changes in signal transduction in single cells over time (Figures 2.2d (left), 2.4c), dynamic changes in protein phosphorylation in human cells using phospho-specific flow cytometry (Figure 2.4d) and single-molecule RNA fluorescent in-situ hybridization quantification of transcription in single cells (Figures 2.2d (right), 2.4e).

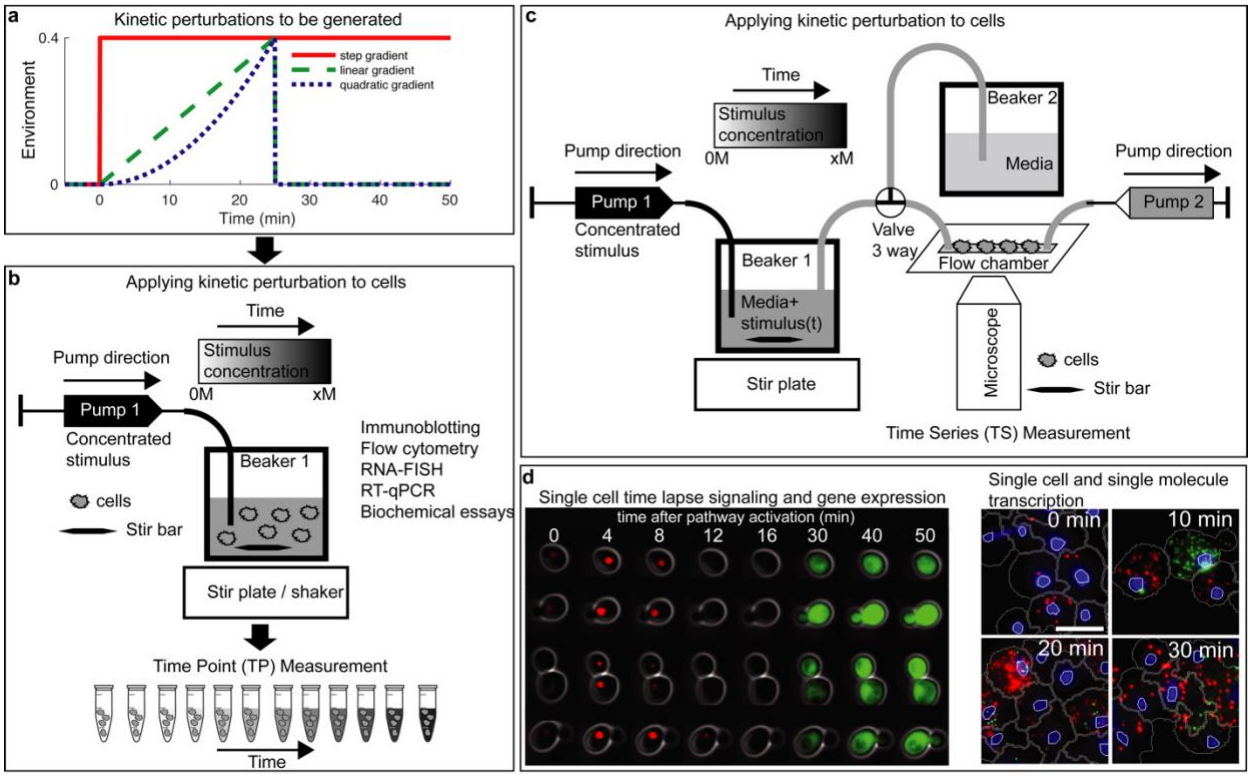

Figure 2.2: Experimental setup to generate kinetic environmental profiles in the laboratory.

(a) Three possible kinetic environmental profiles: Step (red), linear gradient (green) and quadratic gradient (blue). (b) Experimental setup to generate temporal gradients and measure cells at specific time points. A high concentration of stimulus is added through Pump 1 at constant stirring condition and samples are collected at predefined time points and sample volumes (Time Point (TP) data collection). (c) Experimental setup to follow single cells over time in a microfluidic flow chamber on a microscope. Cells are exposed to normal media (Beaker 2) or to a temporal gradient generated in Beaker 1. Pump 1 adds a concentrated substance to Beaker 1 at constant stirring. Pump 2 allows to adjust the flow rate. Time series (TS) data collection is done by tracking cells in the flow chamber using bright field and fluorescent microscopy. (d) Application images of single cell signal transduction and gene regulation measured over time using the Time Series (TS) data collection protocol (left) and of single cell transcription snapshots measured using the Time Point (TP) data collection protocol (right).

2.3.2 Computational pipeline to generate the pump profiles

Concentrated stimulus is added over time to a flask containing media and samples are taken out of the flask for time point (TP) measurements or media is removed in time series (TS) experiments resulting in changes over time of the concentration and volumes in the mixing flask. These changes need to be considered to accurately compute the desired pump profile and failure to do so can result in significant error in the pump profile as plotted in Figure 2.3.

The desired concentration profile consists of a maximum number of discrete time points set by the programmable pump. We construct any arbitrarily concentration profile by combining several short segments with linear concentration profiles. From the beginning of each interval to the end of that interval we increase the concentration linearly with a fixed rate dr_i as shown in Figure A1. However, the rate from each phase to the next could be changed to produce any arbitrary profile over the whole treatment time ($dr_i \neq dr_{i+1}$). During each interval, stimulus over time is delivered continually by adding appropriate amount (dv_i) of concentrated stimulus (C_{max}) to the total volume of growth media in a flask. The pump profile is then computed using the following considerations:

1) During each time interval, a defined volume of concentrated stimulus is being added to the total flask volume using Pump 1.
2) At each time intervals, a fixed volume is taken out of the flask. In the case of TP experiment, we sample a fixed volume of cells (Figure 2.2b) or in case of TS experiments Pump 2 delivers media with a defined stimulus concentration to cells in a flow chamber (Figure 2.2c).

Removing volume and adding stimulus to the flask result in a concentration change that needs to be accounted for in the pump profile calculation, which is not done by any other published method. In Figure 2.3 we demonstrate that not taking these considerations into account result in large errors specifically at high stimulus concentrations.

2.3.3 Algorithm to compute pump profiles

We calculate the stimulus concentration profile for discrete time points as depicted in Figure A1. First, we calculate the theoretical values of any given stimulus concentration profile, $m(t)$, at a fixed number of time points, $[t_1, t_2, t_3, \ldots\ t_N]$, with time intervals $[dt_1, dt_2, dt_3, \ldots\ dt_N]$. The time intervals could be chosen either uniformly or variable. We increase the stimulus concentration m_{i-1} linearly from the beginning of the i^{th} interval at t_{i-1} to m_i at the end of the i^{th} interval at t_i. Pump 1 adds fixed volume dv_i of concentrated stimulus to the mixing Beaker1 during interval dt_i at a fixed pump rate of $k_i = dv_i/dt_i$. The beaker has an initial volume of V_0 and an initial stimulus concentration of $m_0 = 0$ at $t = 0$. The stimulus concentration profile at any given time point (m_i) is then calculated by equation (2.1)

$$m_i = m_{i-1} + \frac{C_{max} dv_i - \bar{m}(du_i + dw_i)}{V_i + dv_i - (du_i + dw_i)} \tag{2.1}$$

where C_{max} is the concentrated stimulus (in mM), $\bar{m}$ is the average of m_i and m_{i-1} (in mM), and dv_i (in mL) is the dispensed volume of concentrated stimulus during the time interval dt_i. du_i (in mL) is the volume taken out by Pump2 (in TS experiment), and dw_i (in mL) is the volume taken out due to sampling (in TP experiments), both during the interval dt_i. Finally, V_i is the total flask volume (in mL) at t_i. Once we computed dv_i, then we compute the pump rate as $k_i = 1000 * dv_i/dt_i$ in µL/min. We operate Pump2 at a fixed rate of $\bar{k}$, therefore $du_i = \bar{k} * dt_i$, for TS experiments, while we don't need Pump2 for TP experiment and $du_i = 0$. We round the calculated values of dv_i in the specified unit to 3 digits after the decimal which is the functional value for the syringe pumps. This calculation is what we refer to setup2 in Figure 2.3. In setup1, the desired profiles are calculated by setting Pump2 rate equal to that of Pump1 over the treatment duration, which results even in larger errors in the generated profiles. Examples of corrected and uncorrected concentration profiles are shown in Figure 2.3. Our methodology, once corrected for the volume and concentration changes properly, generates stimulus profiles within 1% error of the theoretical desired profiles (Figure 2.3).

The profiles are generated under the following conditions:

a) The concentrated stimulus concentration $C_{max} = 4\ M$.
b) The total flask volume $V_0 = 50\ mL$ at $t = 0$.
c) Pump2 rate was set to $\bar{k} = 0.1\ mL/min$ for TS and $\bar{k} = 0$ for TP experiment.
d) Samples taken out at the fixed volumes of $dw_i = 1\ mL$ at the time points [1,2,4,6,8,10,15,20,25,30,35,40,45,50] minutes for TP, while no sampling done for TS.
e) Both TP and TS profiles are generated over 50 minutes. TS in 40 intervals and TP profile in 34 intervals set optimally by the programmable syringe pump.

The calculation results are shown in Tables A1 and A2 for TS and TP profiles.

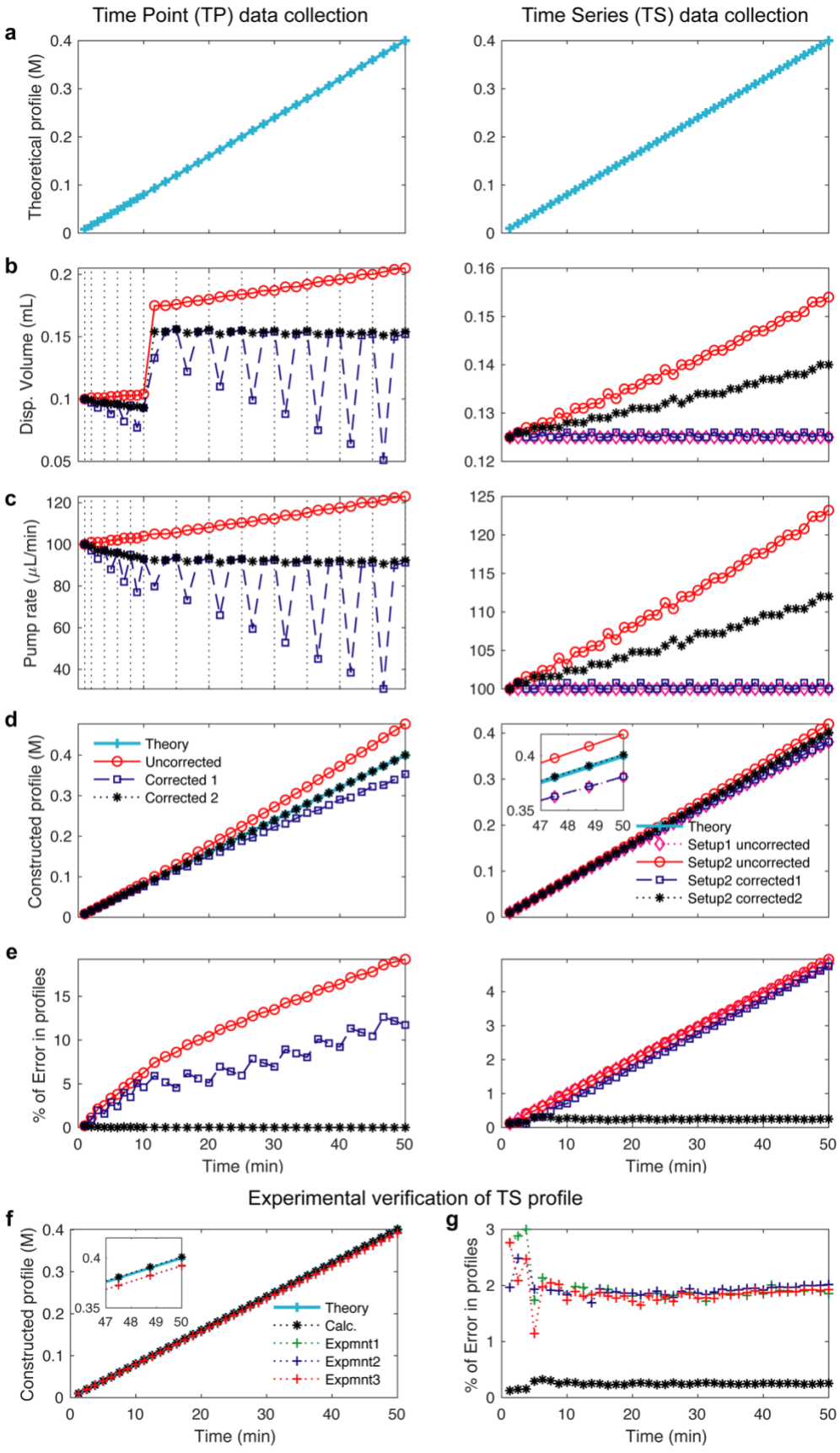
Time Point (TP) data collection
Time Series (TS) data collection
a
Theoretical profile (M)
b
Disp. Volume (mL)
c
Pump rate (μL/min)
d
Constructed profile (M)
Theory
Uncorrected
Corrected 1
Corrected 2
Setup1 uncorrected
Setup2 uncorrected
Setup2 corrected1
Setup2 corrected2
e
% of Error in profiles
Time (min)
Experimental verification of TS profile
f
Constructed profile (M)
Theory
Calc.
Expmnt1
Expmnt2
Expmnt3
Time (min)
g
% of Error in profiles
Time (min)

Figure 2.3: Calculated and experimentally verified pump profiles.

(a-e) Calculation of pump profile generation for Time Point (TP, left) and Time series (TS, right) data collection. In the TP experiment (left), pump profiles are uncorrected (red), corrected for volume removal during sampling (blue), corrected for volume removal and therefore change in stimulus concentration (black). In the TS experiment (right), two pumps are used. In Setup 1 mixing flask volume (V0) is kept constant by setting Pump 2 rate equal to that of Pump 1 (magenta). In Setup 2, the pump rate for Pump 1 is uncorrected and the pump rate for Pump 2 is kept constant (red). In Setup 2 - correction 1, the pump profile is corrected for volume taken out by Pump 2 (blue). In Setup2 - correction2, the pump profile is corrected for volume removal and therefore change in stimulus concentration (black). (a) Proposed linear pump concentration profile of 0.4 M NaCl. (b) Computed and instrument adapted syringe dispense volume. (c) Computed pump rate profile over time. (d) Computed concentration profiles over time. (e) Error comparisons between pump profiles. (f-g) Experimentally verified pump profiles. (f) The delivered molarities constructed from cumulative dispensed volume measurements via Pump 1 using the setup in Figure 2.1c in three experiments (red, green, blue) compared to the calculations (black) and theory (cyan). Insert comparing different profiles. (g) The corresponding errors from experiments and the calculations compared to the theory.

2.3.4 Experimental validation of pump profiles

We experimentally verify the specific profile presented in Figure 2.3 (right, linear gradient of 0.4 M over 50 min for TS experiment). In order to illustrate the high accuracy and precision of the profiles applied to the cells, we experimentally instrument-proof our calculations. We measure the total dispense volume via Pump 1 delivered using the setup in Figure 2.1c by measuring the weight of the Beaker 1 over the treatment time on a digital balance. As shown in Figure 2.3f, we calculate the molarity profiles resulting from these measurements and compare them to our calculation and theoretical profiles. In Figure 2.3g, we show the corresponding errors from experiments and the calculations compared to the theory. These results (errors within 2% of the theoretical values and standard deviation out of 3 experiments is below 1%) show that our setup applies the

calculated profiles to the cells with high accuracy and precision. Importantly, these corrections ensure that the pump profiles are accurate over the full-time courses correcting for any nonlinear artefacts as validated experimentally (Figure 2.3e).

2.3.5 Time Point (TP) Measurements for cell population and single cell experiments

In the Time Point (TP) Measurement setup, cells are grown in cell culture flasks in a cell culture incubator (Figure 2.2b). The concentrated stimulus is pumped into the flask through the computer programmable syringe Pump 1 (Figure 2.2b). In case of the experiments with microbial cultures, cells are mixed with a magnetic stir bar. The mixing speed is optimized to ensure fast mixing of the continuously added concentrated stimulus and at the same time cause little perturbation to the cells. In case of the human cell experiments and some of the yeast experiments, cell culture flasks sit on an orbital shaker that mixes fast enough to ensure rapid mixing but does not interfere with cell growth. At a number of predefined time points, a fixed volume of cells is removed manually with a syringe and collected for further analysis in cell population or single cell assays (Figures 2.2b, 2.4d, 2.4e). For each experiment, the dispensed volume, the number and volume of samples for each time point is defined before the experiment. Based on these experimental parameters, the pump profile is calculated, and the pump is programmed. Several considerations are important to ensure correct generation of stimulus profiles (Figure 2.3): First, the pump program must adjust for the reduction in volume in the flask during sample removal. Second, the pump rate has to decrease over time due to an increase in volume caused by continuous addition of concentrated stimulus. Figure 2.3a (left) presents an example in which cells are exposed to a linear gradient for 50 minutes to a final concentration of 0.4 M NaCl. When cells are sampled from the cell culture flask for downstream assays (dashed black lines), the cell culture volume and the total amount of NaCl in the culture changes.

To better illustrate this point, we computationally compared three possible pump profiles. These are uncorrected pump profiles (red), pump profiles corrected for volume removal during sampling (blue), and the correct pump profiles which are corrected for volume removal and therefore change in total NaCl amount in the flask (black). For each

of these cases, we compared the dispensed volume of highly concentrated NaCl solution in ml (Figure 2.3b), the pump rate in µl per minute (Figure 2.3c), the computed concentrated profiles (Figure 2.3d) and the percent of error for each condition (Figure 2.3e). Initially, the corrections are small, because cells are sampled rapidly within the first 10 minutes. But if the sampling time is not frequent, then corrections have a significant impact on the dispensed volume (Figure 2.3b) and the pump rate (Figure 2.3c). The result is that as time progresses, the corrections have a significant nonlinear effect over time on the accuracy of the pump profile (Figure 2.3d, e).

2.3.6 Time Series (TS) Measurements in single cell time-lapse microscopy experiments

In the Time Series (TS) Measurements, cells can be grown in a microfluidic flow chamber and simultaneously imaged on an inverted microscope (Figure 2.2c). This experimental setup consists of syringe Pump 1 that pumps concentrated stimulus into Beaker 1 containing growth media and a magnetic stir bar for rapid mixing (Figure 2.2c). Connected to Beaker 1 is the microfluidic flowcell and a syringe Pump 2 that pulls liquid from Beaker 1 and over the cells in the flow chamber, generating a temporal gradient of the stimulus. The cells are adhered to the concanavalin A-coated coverslip in the flow chamber, allowing for rapid media exchange over time. To better illustrate how the two pumps work in concert, we simulate the addition of a linear gradient for 50 minutes to a final concentration of 0.4 M NaCl (Figure 2.3a (right)). Because Pump 2 removes media over time, the volume and concentration changes in Beaker 1 need to be accounted for. Instead of experimentally testing these effects, we first computationally compared four possible pump profiles which are Setup1 – uncorrected in which the mixing flask volume (V0) in Beaker 1 is kept constant by setting pump rate of Pump 2 equal to that of Pump 1 (magenta). In Setup2 – uncorrected, the pump rate for Pump 1 is uncorrected and the pump rate for Pump 2 is kept constant (red). In Setup 2 - correction 1, the pump profile is corrected for volume taken out by Pump 2 (blue). In Setup2 – correction 2, the pump profile is corrected for volume removal and therefore change in stimulus concentration (black). For each setup, we compare the dispensed volume of highly concentrated NaCl

solution in ml (Figure 2.3b), the pump rate in µL per minute (Figure 2.3c), the computed concentration profiles (Figure 2.3d) and the percent of error after for each condition (Figure 2.3e). As time progresses, the corrections become more significant for the dispensed volume and the pump rate for setup 2 uncorrected and setup 2 with correction 2. These differences can be seen in the constructed profiles (Figure 2.3d). From these computational profiles, it became apparent that the corrections are important as they reduce errors in the pump profiles significantly (Figure 2.3e).

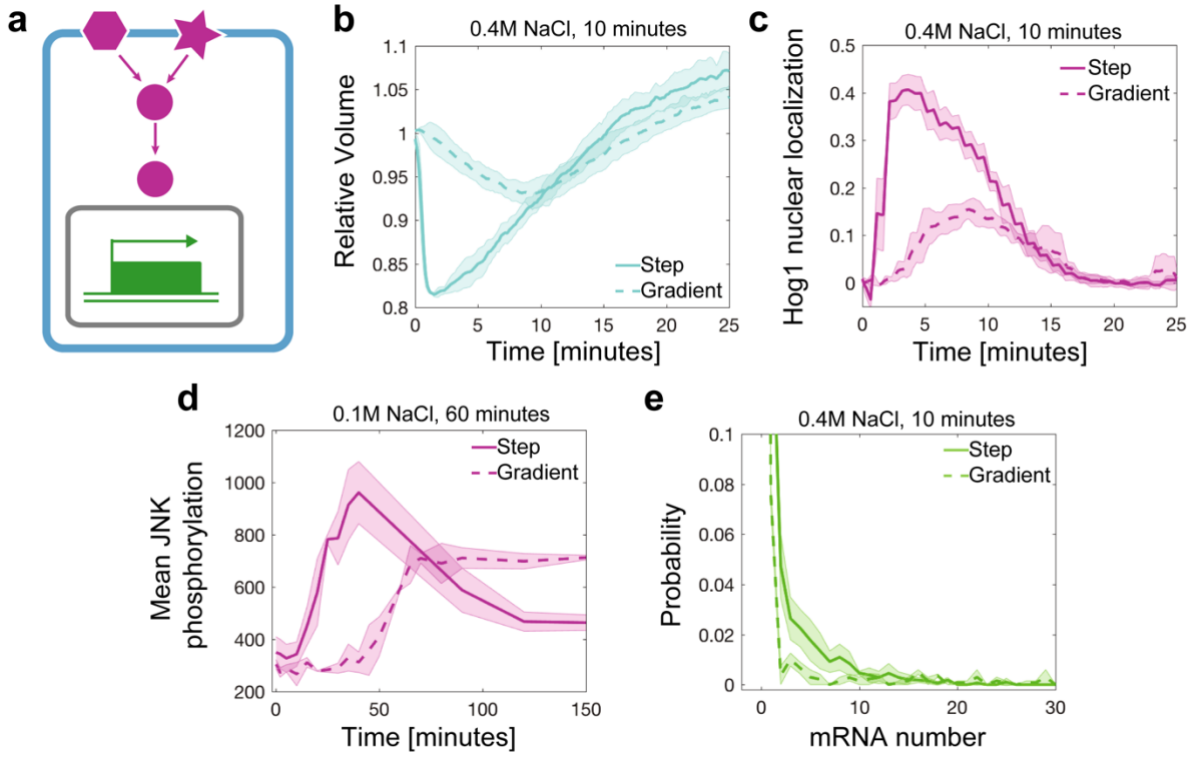

Figure 2.4: Application of different pump profiles and quantitative assays.

(a) Overview of cell processes that have been investigated in kinetic environments. (b) Quantifying volume and (c) signal transduction of Hog1 nuclear localization over time in live single S. cerevisiae yeast cells exposed to instant increase to 0.4 M NaCl (dashed line, 79 cells) or to linear gradient of 0.4 M NaCl in 10 minutes (solid line, 90 cells). (d) JNK phosphorylation over time measured with flow cytometry in human THP1 cells after exposure to instant increase to 0.1 M NaCl (solid line, 636,628 cells) or to linear gradient of 0.1 M in 60 minutes (dashed line, 1,599,923 cells). (e) Single cell distributions of single-molecule RNA FISH measurements of STL1 mRNA in S. cerevisiae yeast cells exposed to instant increase to 0.4 M NaCl (solid line, 3269 cells) or a linear gradient of 0.4 M in 10 minutes (dashed line, 2164 cells). Thick lines are the mean and shaded area are the standard deviation from two or three biological replica experiments single cells.

2.3.7 Application of kinetic cell perturbation to study dynamic cell shape, cell signaling and gene regulation in single and populations of cells

To demonstrate the power of our approach, which is the ability to precisely control the kinetic environment of a cell, we focused on three levels of cellular response: cell shape, signal transduction and gene regulation (Figures 2.1, 2.4a). As physiologically relevant environment, we chose different kinetic gradients of osmotic stress and applied these to S. cerevisiae yeast cells and the human monocytic THP1 cell line. In yeast, the High Osmolarity Glycerol (HOG) pathway belongs to the class of Mitogen Activated Protein Kinase (MAPK) that enables cells to respond to changes in external osmolarity (Hersen et al. 2008). The terminal kinase, Hog1, is evolutionary conserved between yeast and human and is a functional ortholog kinase to JNK in human cells (Galcheva-Gargova et al. 1994). In humans, JNK is involved in many pathophysiological conditions (Yarza et al. 2015; Wagner and Nebreda 2009), and JNK can rescue Hog1 function in yeast cells (Galcheva-Gargova et al. 1994). Upon osmotic stress, yeast cells are osmotically compressed resulting in significant volume decrease as measured in our time series (TS) measurements (Figure 2.4b). In comparison to instantly changing environments where volume decreases rapidly (Muzzey et al. 2009), slowly changing environments such as a linear increase to 0.4 M NaCl in 10 minutes result in slowly changing volume (Figure 2.4b). Simultaneously, we measured Hog1 nuclear localization under the same conditions resulting in maximum signaling at 8 minutes after linear osmotic stress in comparison to a maximum in Hog1 nuclear localization after 2 minutes upon an instant change in osmolarity (Figure 2.4c). Next, we tested our Time Point (TP) measurement protocol on cells that are sampled at different time points after osmotic stress. We exposed human THP1 suspension cells to instant increase of 0.1 M NaCl and a linear gradient increase of 0.1 M NaCl in 60 minutes. We sampled cells between 0 and 150 minutes in intervals of 2, 5, 10, or 30 minutes and fixed cells with formaldehyde. Cells are subsequently permeabilized and then stained with an antibody for phosphorylated form of JNK (Dreskin et al. 2001). From single cell distributions, the average JNK phosphorylation level were computed for three independent biological replica experiments (Figure 2.4d). Finally, we applied Time Point (TP) measurement protocol to S. cerevisiae yeast cells to measure mRNA expression of the osmotic stress response gene STL1 in single cells. We exposed cells to an instant increase of 0.4 M NaCl and a

linear gradient with a final concentration of 0.4 M NaCl in 10 minutes. Figure 4e depicts single cell distributions of single-molecule RNA FISH data 6 minutes after NaCl stress.

2.4 Discussion

We describe methodologies that allows the generation of physiologically relevant environmental changes in cell culture. We demonstrate in Figure 2.3 that it is critical to consider the specific sampling time, sampling volume, number of samples and volume change caused by the addition of stimulus. Because sampling changes the total number of cells in the flask, the total stimulus and the volume, these conditions need to be reflected in the programed pump profiles. Failure to do so result in wrong pump profiles with non-linear errors over time. We demonstrate in several examples that we generate gradual changes in the environment over time. Our methodology aids in the application of profiles that might more closely represent physiological conditions than rapidly changing environments (Figure 2.1). We developed two experimental methodologies to measure cells at specific time points, labeled Time Point (TP) and Time series (TS) measurements, that can be combined with standard cell population experiments and single-cell experiments (Figure 2.2). In contrast to the vast amount of microfluidic approaches that are available, our methodology allows a quick and easy setup that can be established in any biological laboratory setting. Further, because our method is scalable to large volumes of cell culture, it can be combined with microfluidic/live cell microscopy, gene expression analysis, flow cytometry and many other biological and biochemical assays. From these experiments we observe that cell volume and Hog1 signaling changes slowly if the kinetic osmolyte profiles changes rapidly. This is consistent with previous reports on Hog1 signaling during osmotic stress (Granados et al. 2017; Johnson et al. 2020). Mean JNK phosphorylation is delayed and non-adaptive in cells exposed to a gradient in comparison to a step of NaCl. This result indicates that the JNK activation dynamics respond is NaCl threshold dependent. Finally, RNA-FISH data in yeast indicate that STL1 mRNA expression is delayed if cells are exposed to gradual changing environments.

2.5 Conclusion

We developed algorithms that generate precise kinetic perturbations by accounting and correcting for the changes in cell culture volume and concentration profiles caused by the stimulus application and sample removal. We demonstrate the wide applicability of this approach to study cell response in terms of changes in cell volume, cell signaling and gene expression in cell population averages and in single cells experiments. These results demonstrate how environments that change over time can change key biological processes distinct from traditional approaches. Our results underscore the importance of experimental design to generate precise environmental perturbations that differ from rapidly changing environments. This simple yet general methodology to precisely perturb the cells will enable new understanding and insights into biological processes.

2.6 Methods

Human Cell Culture and Materials

THP1 (ATCC® TIB-202™) cells were cultured at 0.5-1x 10^6 cells/ml in RPMI 1640 media (Corning, Catalog#: 15-040-CV) containing 10% Heat inactivated FBS (Gibco, Catalog#: 16140-071), 100 U/ml Penicillin-Streptomycin (Gibco, Catalog#: 15140-122), 2 mM L-alanyl-L-glutamine dipeptide (GlutaMAX™, Gibco, Catalog#: 35050-061) and 0.05 mM 2-Mercaptoethanol (Sigma, Catalog#: M3148) at 37 °C in a 5% CO2 humidity controlled environment.

Yeast strain and cell culture

Saccharomyces cerevisiae BY4741 (MATa; his3Δ1; leu2Δ0; met15Δ0; ura3Δ0) was used for time-lapse microscopy and FISH experiments. To assay the nuclear enrichment of Hog1 in single cells over time in response to osmotic stress, a yellow-fluorescent protein (YFP) was tagged to the C-terminus of endogenous Hog1 in BY4741 cells through homologous DNA recombination. Three days before the experiment, yeast cells from a stock of cells stored at −80 °C were streaked out on a complete synthetic media plate (CSM, Formedia, UK). The day before the experiment, a single colony from the CSM

plate was picked and inoculated in 5ml CSM medium (pre-culture). After 6-12 hours, the optical density (OD) of the pre-culture was measured and diluted into new CSM medium to reach an OD of 0.5 the next morning.

Experimental procedure for human cells upon step and linear gradient stimuli application
A programmable pump (New Era Syringe Pump Systems, NE-1200) was used to apply gradually increasing (linear gradients) profiles. In brief, pumping rate and dispensed volume per interval were calculated as described in the pump profile calculation section and uploaded to the pump via a computer. A syringe pump driving a syringe (BD™, Catalog#: 309628) filled with 5 M NaCl (Corning, Catalog#: 46-032-CV) solution was connected to a needle (Jensen Global, Catalog#: JG21-1.0x) with tubing (Scientific Commodities, Catalog#: BB31695-PE/4). The tubing was inserted into a foam stopper on an autoclaved glass flask (Pyrex, Catalog#: 4980-500) holding the suspension cells. To ensure proper mixing cells were shaken at 100 rpm during the entire experiment using a CO2 resistant shaker (Thermo Fisher Scientific, Catalog#: 88881101). For step stimulation, appropriate amount of 5 M NaCl solution was added by a syringe within 5 seconds to reach the desired final concentration. 5 ml of cells were removed with a syringe (BD™, Catalog#: 309628) through autoclaved silicone tubing (Thermo Scientific, Catalog#: 8600-0020) to collect time point samples. Cell are sampled at 2, 5, 10, 15, 20, 30, 35, 40, 45, 50, 60, 65, 70, 80, 90, 120, and 150 minutes after the start of the experiment.

Flow Cytometry
Cells were fixed with 1.6% formaldehyde (Fisher, Catalog#: F79-4) in a 15 ml falcon tube. Fixation was quenched by adding 200 mM Glycine after 8 minutes. Cells were washed with PBS (Corning, Catalog#: 46-013-CM) and permeabilized with Methanol (Fisher, Catalog#: A454-4) for 15 minutes on ice. Cells were washed with PBS and blocked with 5% BSA (Rpi, Catalog#: A30075-100.0) in PBS. Cells were then washed and stained with a primary monoclonal antibody conjugated to Alexa Fluor 647 recognizing phosphorylated JNK (Cell Signaling Technologies, Cat.#: 9257) overnight at 4 °C. Flow cytometry was performed on BD LSRII (five lasers).

Flow Cytometry Analysis

Flow Cytometry data was analyzed with custom R software. The main cell population was gated on FSC-A vs. SSC-A by using the flowcore package (Meur, Hahne, and Ellis 2007). Means and standard deviations of mean fluorescent intensity were calculated for 2-3 replicates and plotted over time.

Time-lapse microscopy

1.5 ml of yeast cells (Hog1-YFP) in log-phase growth (OD=0.5) were pelleted, re-suspended in 20 µl CSM medium and loaded into a flow chamber. The flow chamber consist of an 1/8" Clear Acrylic Slide with three holes (Grace Bio-labs, 44562), a 0.17µm thick T-shape SecureSeal Adhesive spacer (Grace Bio-labs, 44560, 1L 44040, R&D), a Microscope Cover Glasse (Fisher Sci., 12545E, No 1 22 x 50 mm) and Micro medical tubing (Scientific Commodities Inc., BB31695-PE/4, 100 feet, 0.72mm ID x 1.22mm OD). The cover glass is coated with 0.1mg/ml Concanavalin dissolved in H_2O. Hyperosmotic perturbations were created using Syringe Pumps as described in the main text (TS experiments) (New Era Pump Systems). On the input of the flow chamber, a three-way valve was connected to switch between a beaker that was used to generate osmolyte concentration profiles and a beaker with media (Beakers 1 and 2, Figure 1c). A syringe pump (Pump 2) at the exit of the flow chamber was used to deliver the specific osmolye profile through the flow chamber with a constant rate. For step-like osmotic perturbation, Beaker 1 had CSM medium with a fixed concentration of 0.4 M NaCl. For the linear gradient perturbation, Beaker 1 only contained media without NaCl at time zero. Using a second syringe pump (Pump 1), profiles of increasing linear osmolyte concentration were generated through pumping 4 M NaCl CSM media into Beaker 1 under constant mixing on a magnetic stir plate (Table A1).

Image acquisition

The Micro-Manager program (Edelstein et al, 2014) was used to control the microscope (Nikon Eclipse Ti) which is equipped with perfect focus (Nikon), a 100x VC DIC lens (Nikon), a fluorescent filter for YFP (Semrock), an X-cite fluorescent light source

(Excelitas) and an Orca Flash 4v2 CMOS camera (Hamamatsu). For step input a pump rate of 0.1 ml/minute was used.

Single molecule RNA-FISH

Yeast cell culture (BY4741 WT) in log-phase growth (OD = 0.5) was concentrated 10x times (OD = 5) by a glass filter system with a 0.45 µm filter (Millipore). For osmolyte step experiments, cells are exposed to a final osmolyte concentration 0.4 M NaCl, and then fixed in 4 % formaldehyde at specific time points. For linear gradient experiments, concentrated cells are exposed to a linear osmolyte of final concentration of 0.4 M NaCl over 10 minutes, and then fixed in 4 % formaldehyde at specific time points. As described in the main text (TP experiments), a pump was used to inject 4 M NaCl into the beaker with yeast cells (Table A2). Cells are constantly shaken at 250 rpm in a 30 °C incubator to ensure homogenous mixing.

Fixation, spheroplasting and RNA-FISH probe hybridization

Cells were fixed at 0, 2, 4, 6, 8, 10, 12, 14, 16, 20 minutes after the beginning of applying a linear gradient NaCl of 0.4 M in 10 minutes. Beyond 10 minutes cells were exposed to the fixed 0.4 M NaCl osmolyte. At each time point, 5ml cells are sampled and poured into a 15 ml falcon tube containing formaldehyde resulting in cell fixation at 4% formaldehyde. Cells are fixed at RT for 30 minutes, then transferred to 4 °C and fixed overnight on a shaker. After fixation, cells are centrifuged at 500 x g for 5 minutes, and then the liquid phase was discarded. Cell pellets were resuspended in 5 ml ice-cold Buffer B (1.2 M sorbitol, 0.1 M potassium phosphate dibasic, pH 7.5) and centrifuged again. After discarding the liquid phase, yeast cells were resuspended in 1 ml buffer B, and transferred to 1.5 ml centrifugation tubes. Cells were then centrifuged again at 500 x g for 5 minutes and the pellet was resuspended in 0.5 ml Spheroplasting Buffer (Buffer B, 0.2% ß-mercaptoethanol, 10 mM Vanadyl-ribonucleoside complex). The OD of each sample was measured and the total cell number for each sample was equalized. 10 µl 2.5 mg/ml Zymolyase (US Biological) was added to each sample on a 4 °C block. Cells were incubated on a rotor for ~20-40 minutes at 30 °C until the cell wall was digested. The cells turn from an opaque to a black color, if they are digested. Cells are monitored under

the microscope every 10 minutes after addition of Zymolyase and when ~90 % of the cells turned black, cells are transferred to the 4 °C block to stop Zymolyase activity. Cells are centrifuged for 5 minutes, then the cell pellet was resuspended with 1 ml ice-cold Buffer B and spun down for 5 minutes at 500 x g. After discarding liquid phase, the pellet was gently re-suspended with 1 ml of 70 % ethanol and kept at 4 °C for at least 12 hours or stored until needed at 4 °C. Hybridization and microscopy condition were applied as previously described (Neuert et al. 2013).

Image analysis

Image segmentation was performed in a two-step process. First, the fluorescent tagged Hog1-kinase (Hog1-YFP) image was smoothed, background corrected and automatically thresholded to identify the brightest pixels for each cell. The region of brightest pixels was then used as an intracellular marker. Second, the bright field image was smoothed, background corrected and then overlaid with the previously processed YFP image. On this new image a watershed algorithm was applied to segment and label the objects. After segmentation, objects that are too small, too large or on the border of the image are removed resulting in an image with segmented cells. This process was repeated for each image. After segmentation, the centroid of each cell was computed and stored. Next, the distance between each centroid for each of the two consecutive images was compared. The cells in the two images that have the smallest distance are considered the same cell at two different time points. This whole procedure is repeated for each image resulting in single cell trajectories. For each cell the average per pixel fluorescent intensity of the whole cell (Iw) and of the top 100 brightest fluorescent pixels (It) was recorded as a function of time. In addition, fluorescent signal per pixel of the camera background (Ib) was reported. The Hog1 nuclear enrichment was then calculated as Hog1(t) = [(It(t) - Ib) / (Iw(t) - Ib)]. The single cell traces are smoothed and subtracted by the Hog1(t) signal on the beginning of the experiment. Next, each single cell trace was inspected and cells exhibiting large fluctuations are removed. Bright field images are taken every 10 s with an exposure time of 10 ms and the YFP fluorescent images are taken every 1 minute with an exposure time of 20 ms. During the time points when no fluorescent images are taken, the fluorescent signal from the previous time point was

used to segment the cell. Taking images every 10 s with an exposure time of 10 ms using bright field imaging does not result in photo bleaching of the fluorescent signal and ensures better tracking reliability because cells have not moved significantly since the previous image. For cell volume measurements, each time trace was removed of outlier points resulted from segmentation uncertainties. Volume change relative to the volume at the beginning of the experiment was calculated to compare cells of different volumes. For both, the single cell volume and Hog1(t) fluorescent traces, the median and the average median distance were computed to put less weight on sporadic outliers due to the image segmentation process.

3 Kinetics of osmotic stress regulates a cell fate switch of cell survival

Adapted from:
Thiemicke A and Neuert G. Kinetics of osmotic stress regulate a cell fate switch of cell survival. in revision
https://www.biorxiv.org/content/10.1101/2020.07.10.197871v1

Thiemicke A and Neuert G. 2020 A comprehensive time-course flow cytometry data set on stress response in human cells for 35+ cellular markers. in preparation

3.1 Abstract

Exposure of cells to diverse types of stressful environments differentially regulate cell fate. Although many types of stresses causing this differential regulation are known, it is unknown how changes over time of the same stressor regulate cell fate. Changes in extracellular osmolarity are critically involved in physiological and pathophysiological processes in several tissues. We observe that human cells survive gradual but not acute hyperosmotic stress. We find that stress, caspase, and apoptosis signaling do not activate during gradual stress in contrast to acute treatments. Contrary to the current paradigm, we see a substantial accumulation of proline in cells treated with gradual but not acute stresses. We show that proline can protect cells from hyperosmotic stress similar to the osmoprotection in plants and bacteria. Our studies found a cell fate switch that enables cells to survive gradually changing stress environments by preventing caspase activation and protect cells through proline accumulation.

3.2 Introduction

All cells employ signal transduction pathways to respond to physiologically relevant changes in extracellular stressors, nutrient levels, hormones, and morphogens. These environments vary as functions of both concentration and time in healthy and diseased states (Lim, Meyer, and Pawson 2014). Cell signaling and cell fate responses to the

environment are commonly studied using acute concentration changes (Lim, Meyer, and Pawson 2014). Only a few pioneering studies have explored the effects of the concentration and time, which is a gradual change of stimuli as a function of time on cell signaling in microbes (J. W. Young, Locke, and Elowitz 2013; Goulev et al. 2017; Granados et al. 2017; Johnson et al. 2020) and in mammalian cells (Sorre et al. 2014; Heemskerk et al. 2019; Sasagawa et al. 2005; Fujita et al. 2010; Cai, Ferraris, and Burg 2004). Thus, the impact of the rate of environmental change on cell signaling and cell fate is a fundamental and poorly understood cell biological property (Fig. 1a). We address this lack in knowledge, by thoroughly measuring molecular changes in cells exposed to gradual environmental changes in this study.

To begin to understand how the rate of environmental change regulates human cell fate decisions, we expose cells to varying temporal profiles of increasing NaCl concentrations. NaCl is a ubiquitous osmolyte in the human body and causes cells to experience hypertonic stress at concentrations that change over time (Burg, Ferraris, and Dmitrieva 2007; Stewart et al. 2019; Wilck et al. 2019). While all tissues can experience increased NaCl concentrations in their microenvironment, measurements of osmolytes in the kidney have revealed very high physiological NaCl concentrations (Cai et al. 2002a; Hai and Thomas 1969). In the kidney, spatial gradients of different osmolytes exist that change over time under normal and pathophysiological conditions (Ullrich et al. 1963; Neuhofer and Beck 2005; Firsov and Bonny 2018). Hypertonicity changes over time are also known to occur in the intestinal system (Overduin et al. 2014; Hallbäck et al. 1991), the cerebrovascular discs (Jiang et al. 2015; Urban and Maroudas 1979), and the skin (Jantsch et al. 2015). In many of these high osmolarity tissues, resident immune cells provide basal protection or require migration upon an immune response of additional immune cells (S. Müller et al. 2013). Therefore, immune cells need to have the ability to survive such harsh high osmolarity environments that change over time. We choose immune cells as a model system to study how rapidly and slowly increasing hypertonic environments impact cell survival, signaling, and metabolism.

3.3 Results

3.3.1 The rate of environmental change regulates cellular phenotype.

We compared cell viability, cell signaling, and metabolism in cells exposed to either linear (ramp) or acute (step) concentration changes in the environments in which the final concentration and the total amount of osmotic stress (Area Under the Curve - AUC) is identical (Figure 3.1a, Figure 3.2). We identify the dynamic range of cell viability by determining the tolerance of monocytes (THP1 cell line, male, acute monocytic leukemia), T-cells (Jurkat, male, acute T cell leukemia), and cervical cells (HeLa, female, cervical adenocarcinoma (Dmitrieva and Burg 2008)) to step increases in NaCl concentrations (Figure 3.1b). In the non-stress control condition, cells grow in culture under physiological NaCl concentrations of about 280 mosmol/l NaCl to which we add the hypertonic osmolytes NaCl and mannitol. To stress the cells and mimic in vivo osmolyte changes, we add up to 400 mosmol/l NaCl to the cells (Figures 3.1, Figure 3.3). We observe that the viability decreases with an increased NaCl concentration of up to 300 mosmol/l. At and above of 300 mosmol/l NaCl, the viability is below 15% for all cell lines. Our results in the abovementioned cell lines are consistent with previous studies in HeLa cells (Figure 3.1b) (Dmitrieva and Burg 2008), indicating that different cell types respond similarly to hypertonic stress.

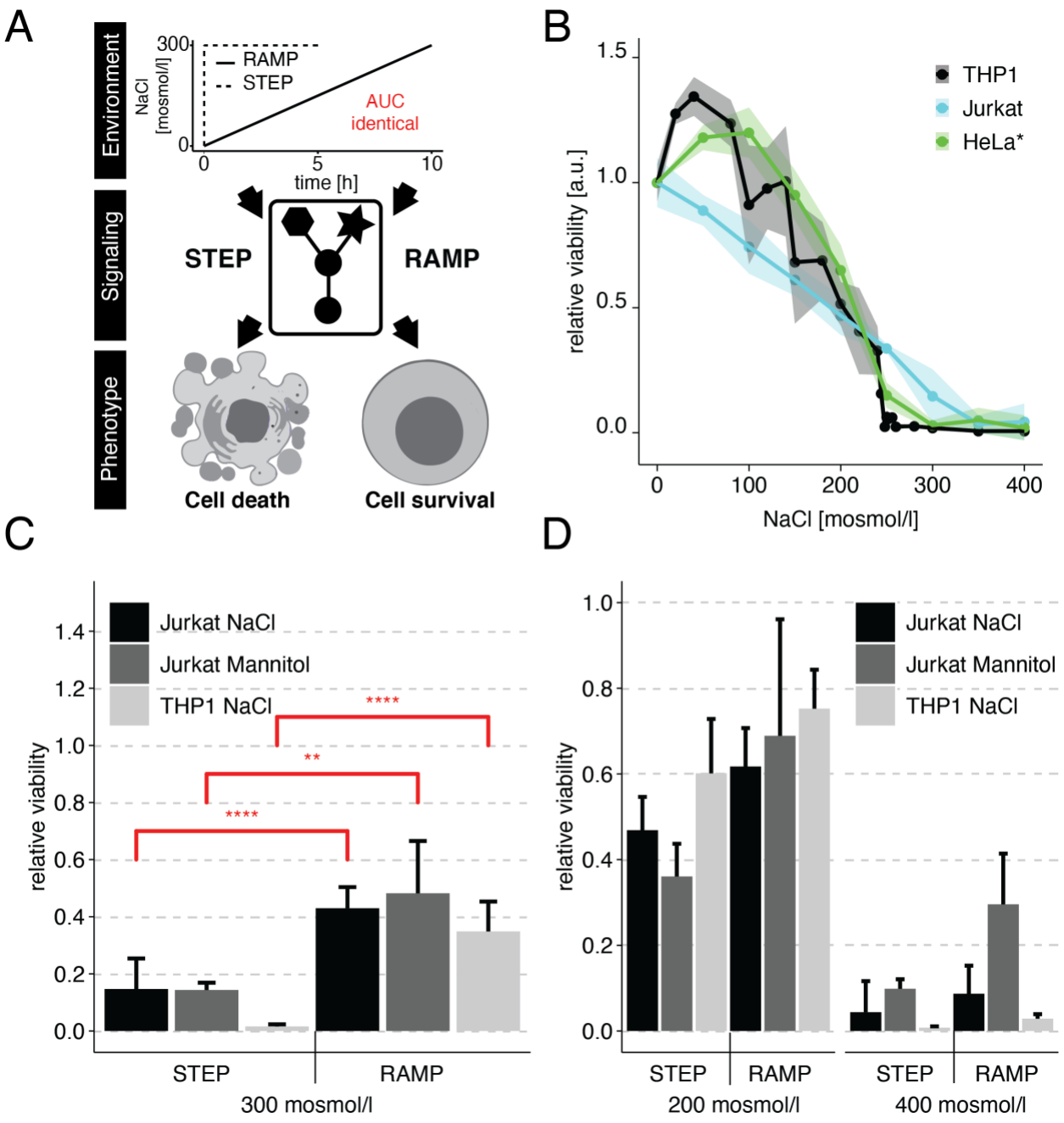
A
Environment
Signaling
Phenotype
NaCl [mosmol/l]
300
0
RAMP
STEP
AUC identical
0
5
10
time [h]
STEP
RAMP
Cell death
Cell survival
B
relative viability [a.u.]
1.5
1.0
0.5
0.0
THP1
Jurkat
HeLa*
0
100
200
300
400
NaCl [mosmol/l]
C
relative viability
Jurkat NaCl
Jurkat Mannitol
THP1 NaCl
****
**
****
STEP
RAMP
300 mosmol/l
D
relative viability
Jurkat NaCl
Jurkat Mannitol
THP1 NaCl
STEP
RAMP
200 mosmol/l
STEP
RAMP
400 mosmol/l

Figure 3.1: Human cell fate decisions are regulated differently upon step or ramp treatment conditions.

*a) Kinetic environments such as concentration ramps, as observed in different physiological relevant conditions, may differentially modulate cell signaling, cell fate, and phenotype even if the final concentration and total amount of stress are identical. Step experiments finish earlier than ramp experiments to account for the same total exposure or Area Under the Curve (AUC). b) We measured relative cell viability after exposure to instant hyperosmotic stress (NaCl for 5h for Jurkat, THP1) or 24h (HeLa cells). Cell viability was determined by measuring intracellular ATP (Jurkat, THP1) or cell counts (HeLa). The shaded area represents the standard deviation (SD) (Jurkat, THP1) or Standard Error (SE) (HeLa) (25) c,d) Relative cell viability was determined for step (c,d) and 10h ramp (d) treatment (see insert) after addition of (c) 300 mosmol/l or (d) 200 and 400 mosmol/l osmolyte. We determined viability at the end of the experiment after reaching the same cumulative exposure of additional NaCl. Bars represent data from at least 3 independent experiments for each condition. Error bars represent SD. two-sided unpaired student's t-test: **p<0.01, ***p<0.001, ****p<0.001.*

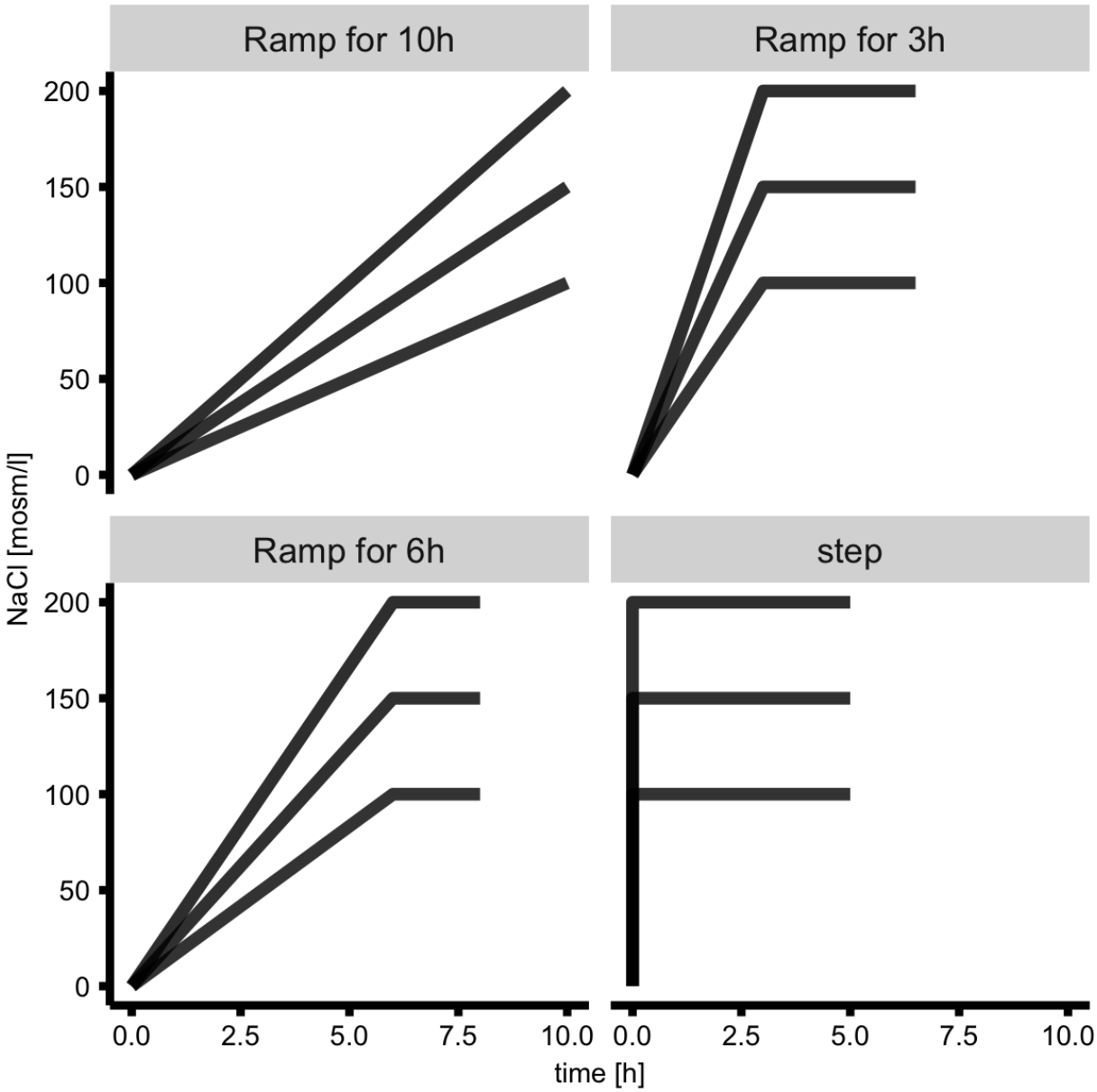

Figure 3.2: Kinetic environment input profiles applied for different step and ramp treatments.

Black lines represent the change of added NaCl osmolarity concentration over time. Cells exposed to a step or 3 and 6h ramp treatment are incubated at the final NaCl concentration until the cumulative exposure is identical between the different conditions.

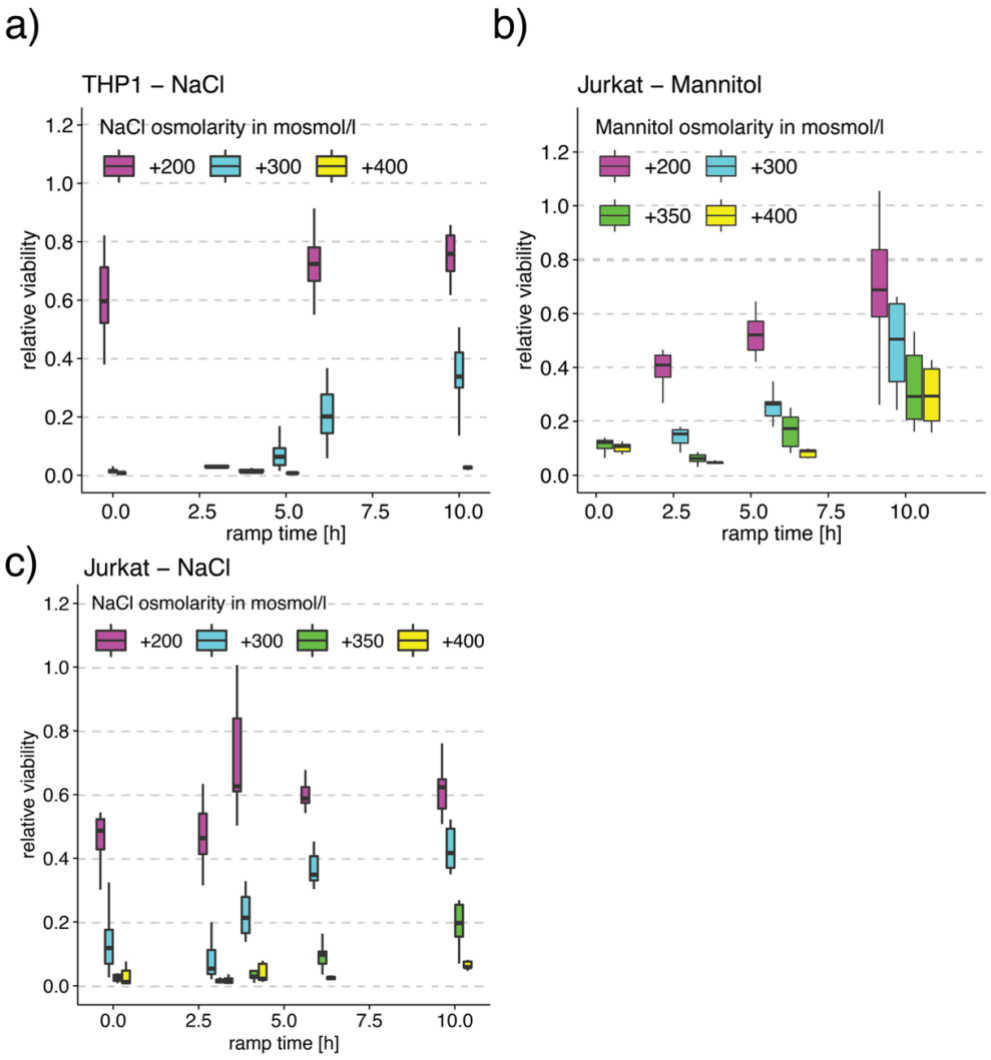

Figure 3.3: Viability improvement in hypertonic stress during a ramp vs. a step is a general cell biological feature independent of the cell line or osmolyte.

a) Viability for THP1 cells measured by intracellular ATP for step addition of NaCl (0), and ramps of 3,4,5,6,10h to indicated concentrations in mosmol/l. We determine viability at the end of the experiment at the same cumulative exposure of additional NaCl. Boxplots represent data from at least 3 independent experiments for each condition. b,c) Viability for Jurkat cells by measuring intracellular ATP for instant addition of mannitol (0), and ramps of 3,6,10h to indicated concentrations in mosmol/l for mannitol (b) and NaCl (c). We determine viability at the end of the experiment at the same cumulative exposure of additional mannitol. Boxplots represent data from at least 3 independent experiments for each condition.

We then quantified the response of different cell lines (Jurkat and THP1) to different rates and final NaCl concentrations (Figure 3.1c-d, Figure 3.3). To compare the different conditions for the same final NaCl concentration, we exposed cells to the same cumulative exposure by integrating the total amount of NaCl over the entire profile (AUC). We perform experiments for each NaCl concentration for ramp durations of up to 10h. For experiments with ramp durations of less than 10h, cells stay at the final NaCl concentration until the AUC is identical to the 10h ramp experiment (Figure 3.2). When we expose Jurkat cells to 300 mosmol/l hypertonic osmolyte, the viability improves from 15% to 40% for a ramp duration of 10h (Figures 3.1c,(black), Figure 3.3c cyan). In comparison, a step increase of 200 mosmol/l NaCl to the media for 5h reduces viability to around 50% and shows only minor improvement with increases in ramp duration (Figures 3.1d (black), Figure 3.3c, magenta). For the step condition of added 400 mosmol/l NaCl for 5 h, the viability is below 5% and shows only minor improvement with increasing ramp durations (Figures 3.1d (black), Figure 3.3, green and yellow). These observations are consistent in THP1 cells, indicating that this effect is reproducible in a different cell line and cell type (Figures 3.1c-d (light grey), 3.3a). To distinguish the effect of cell viability between NaCl toxicity and changes in external osmolarity, we repeated the experiments with mannitol in the Jurkat cell line at the same osmolar concentrations (Figures 3.1c-d (dark grey), Figure 3.3b). Mannitol is not able to easily pass through the cell membrane and is known to have low cell toxicity. When we add 300 mosmol/l Mannitol to the medium, Jurkat cells survive better during the ramp compared to the step treatment. This comparison shows no difference between cells treated with NaCl or Mannitol, indicating extracellular hypertonicity and not NaCl-specific toxicity drive these effects. These results strongly suggest that cell viability improvements, while slowly increasing NaCl concentration, are a robust cell type- and cell line-independent hypertonic stress response. We further tested our hypothesis in human primary blood mononuclear cells (PBMCs). We observe very similar levels of viability after the step and 10h ramp treatments (Figure 3.4). However, there we observe more variability between the cells of the 3 different donors we tested than there is between Jurkat and THP1 cells which could indicate a different response to NaCl hypertonicity between different donors.

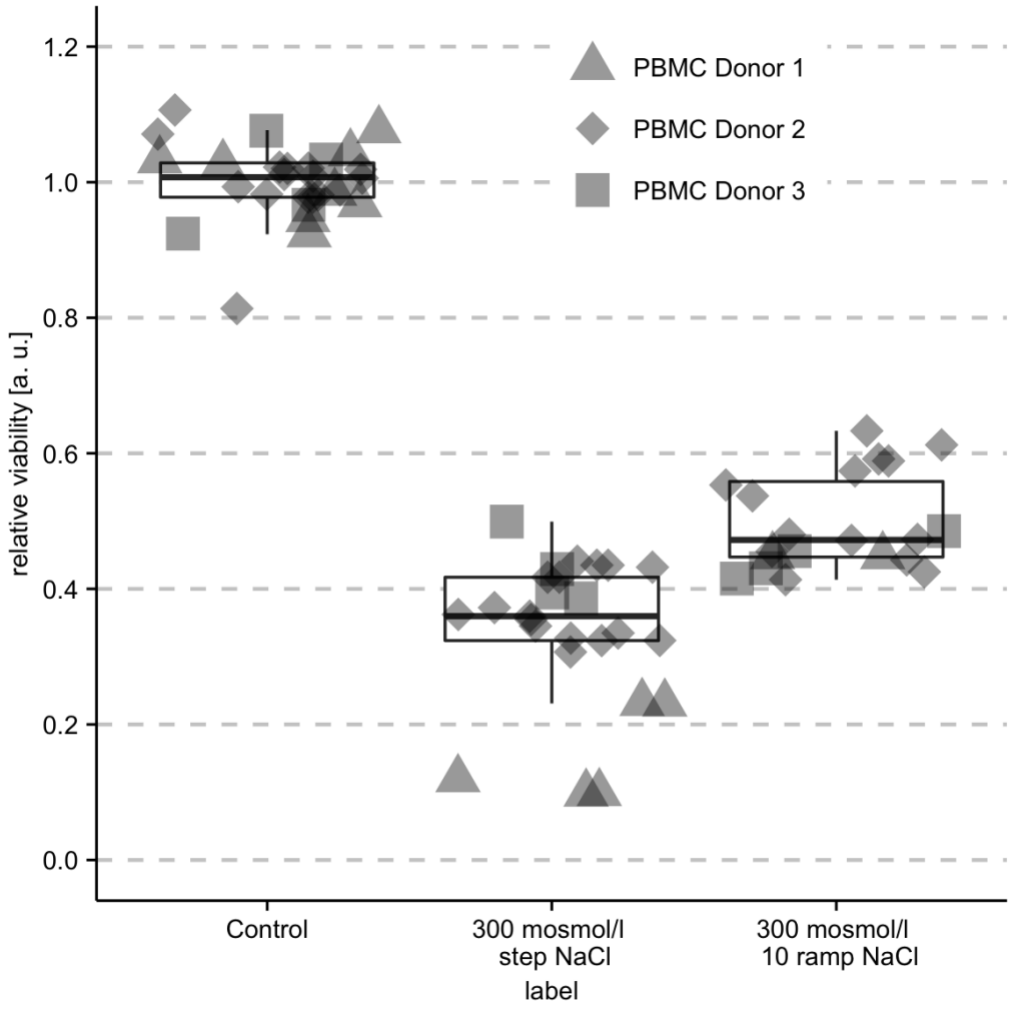

Figure 3.4: Viability in hypertonic stress during a ramp vs. a step in PBMCs.

a) Viability for THP1 cells measured by intracellular ATP for step addition of NaCl (0), and 10h ramps 300 mosmol/l. We determine viability at the end of the experiment at the same cumulative exposure of additional NaCl. Boxplots and symbols represent data from at 3 donors.

3.3.2 A functional temporal screen identifies regulators of cell viability in step and ramp conditions.

Authors of previous studies argued that upregulation of genes encoding proteins responsible for the accumulation of cell internal osmolytes such as taurine (TauT), betaine (BGT1), sorbitol (AR) and inositol (SMIT) are the cause for improved viability in kidney cells exposed to a linear increase in osmolarity (Cai, Ferraris, and Burg 2004). To address if indeed these osmolytes are increased in our experiments, we determined the change in osmolyte levels in the cells by mass spectrometry measured in 5h step and 10h ramp conditions both to a final osmolarity of additional 300 mosmol/l NaCl. We find that sorbitol, inositol, betaine, taurine, and urea do not change compared to unstimulated cells (Figure 2a).

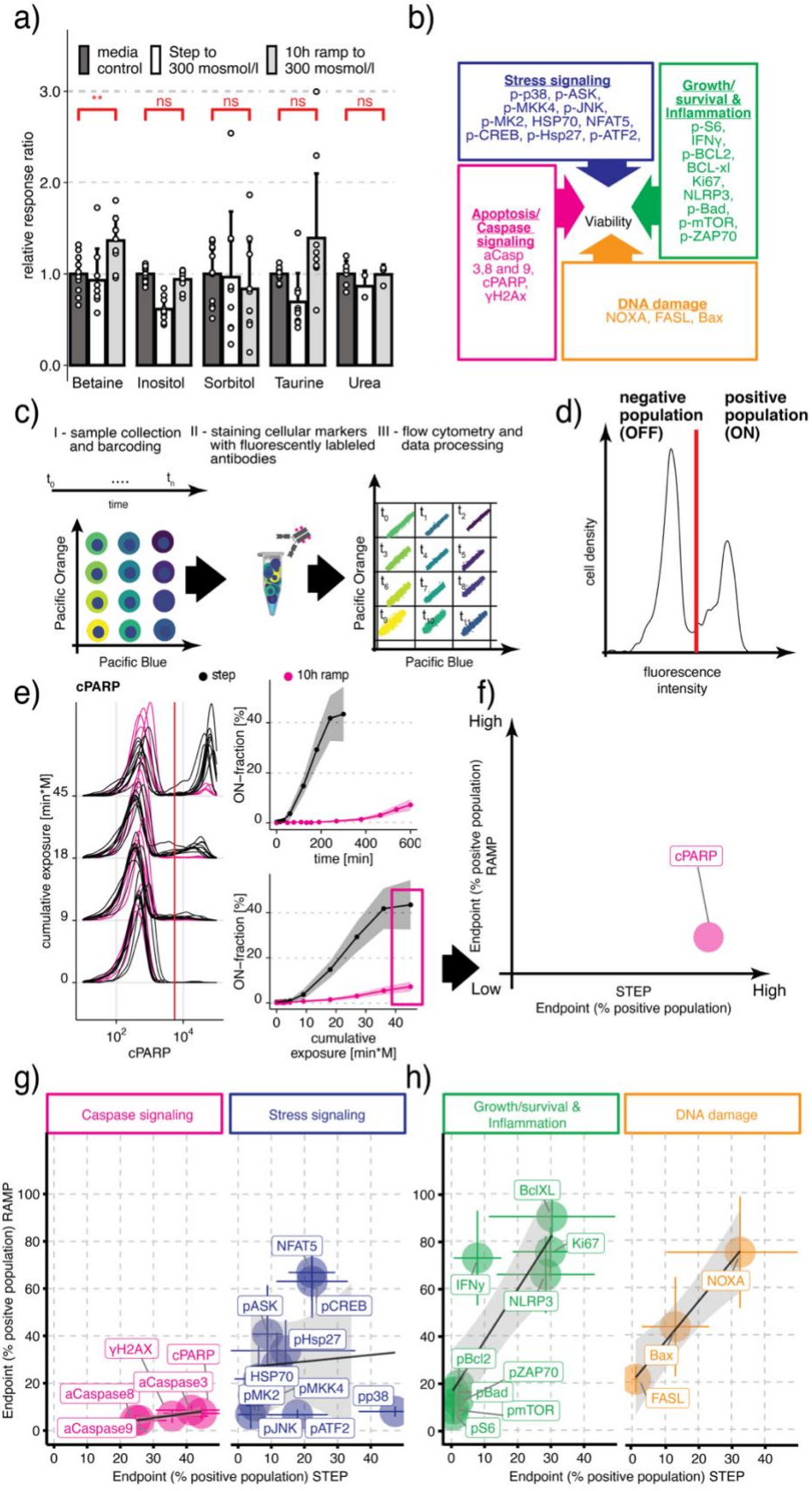
a)
media control
Step to 300 mosmol/l
10h ramp to 300 mosmol/l
relative response ratio
3.0
2.0
1.0
0.0
**
ns
ns
ns
ns
Betaine
Inositol
Sorbitol
Taurine
Urea
b)
Stress signaling
p-p38, p-ASK, p-MKK4, p-JNK, p-MK2, HSP70, NFAT5, p-CREB, p-Hsp27, p-ATF2,
Growth/ survival & Inflammation
p-S6, IFNγ, p-BCL2, BCL-xl Ki67, NLRP3, p-Bad, p-mTOR, p-ZAP70
Apoptosis/ Caspase signaling
aCasp 3,8 and 9, cPARP, γH2Ax
Viability
DNA damage
NOXA, FASL, Bax
c)
I - sample collection and barcoding
II - staining cellular markers with fluorescently labeled antibodies
III - flow cytometry and data processing
time
Pacific Orange
Pacific Blue
d)
negative population (OFF)
positive population (ON)
cell density
fluorescence intensity
e)
cPARP
step
10h ramp
cumulative exposure [min*M]
ON-fraction [%]
time [min]
cPARP
f)
High
Low
STEP
High
Endpoint (% positive population) RAMP
Endpoint (% positive population)
cPARP
g)
Caspase signaling
Stress signaling
Endpoint (% positive population) RAMP
Endpoint (% positive population) STEP
γH2AX
cPARP
aCaspase3
aCaspase8
aCaspase9
NFAT5
pASK
pCREB
pHsp27
HSP70
pMK2
pMKK4
pp38
pJNK
pATF2
h)
Growth/survival & Inflammation
DNA damage
BclXL
Ki67
IFNγ
NLRP3
pBcl2
pZAP70
pBad
pmTOR
pS6
NOXA
Bax
FASL
Endpoint (% positive population) STEP

Figure 3.5: Temporal functional flow cytometry screen identifies differential regulation of stress and caspase signaling during step and ramp hyperosmotic stress conditions.

*a) Mean response ratio of cellular osmolytes relative to media measured in Jurkat cells exposed to an additional 300 mosmol/l NaCl and determined by Mass spectrometry. Two-sided unpaired student's t-test: **p<0.01, ns=not significant. b) Overview of protein markers representing four cellular processes affecting viability. Each box lists the proteins representing each process. c) Multiplex flow cytometry workflow to quantify dynamic changes in protein activity over time: (I) Each time point is barcoded with a different combination of dyes. (II) Barcoded cells are pooled and split into different tubes for pairwise antibody staining. (III) We measured cells by flow cytometry and then computationally demultiplexed the different time points for further analysis. d) A single-cell distribution obtained by flow cytometry is threshold-gated (red line) to determine an ON-fraction. e) Representative flow cytometry single-cell distributions for cleaved PARP (cPARP) at selected time points for step (black) and 10h ramp (magenta) conditions (left). We quantified the fraction of cPARP positive cells (On-cells) as a function of time (right, top) or cumulative NaCl exposure (right, bottom). We plotted mean (solid line) and standard deviation (shaded area) of 3 – 10 biological replicas. f) We used endpoint measurement (magenta box in e) to determine ON-fraction to compare changes for step and ramp conditions. g,h) Comparison of endpoint measurement of mean ON-fraction between steps and ramps measured for individual markers of (g) caspase signaling (magenta), stress signaling (blue), and (h) DNA damage (orange), Growth/survival & Inflammation (green) in Jurkat cells in response to hypertonic stress. Circles represent the mean of 3-10 replicates per condition. ON-fraction at the final time point of cells exposed to 300 mosmol/l NaCl by a step (5h) or a 10h ramp (10h). Colored lines represent the SD. Black lines indicate linear regression fit lines. The shaded area represents 95% confidence interval.*

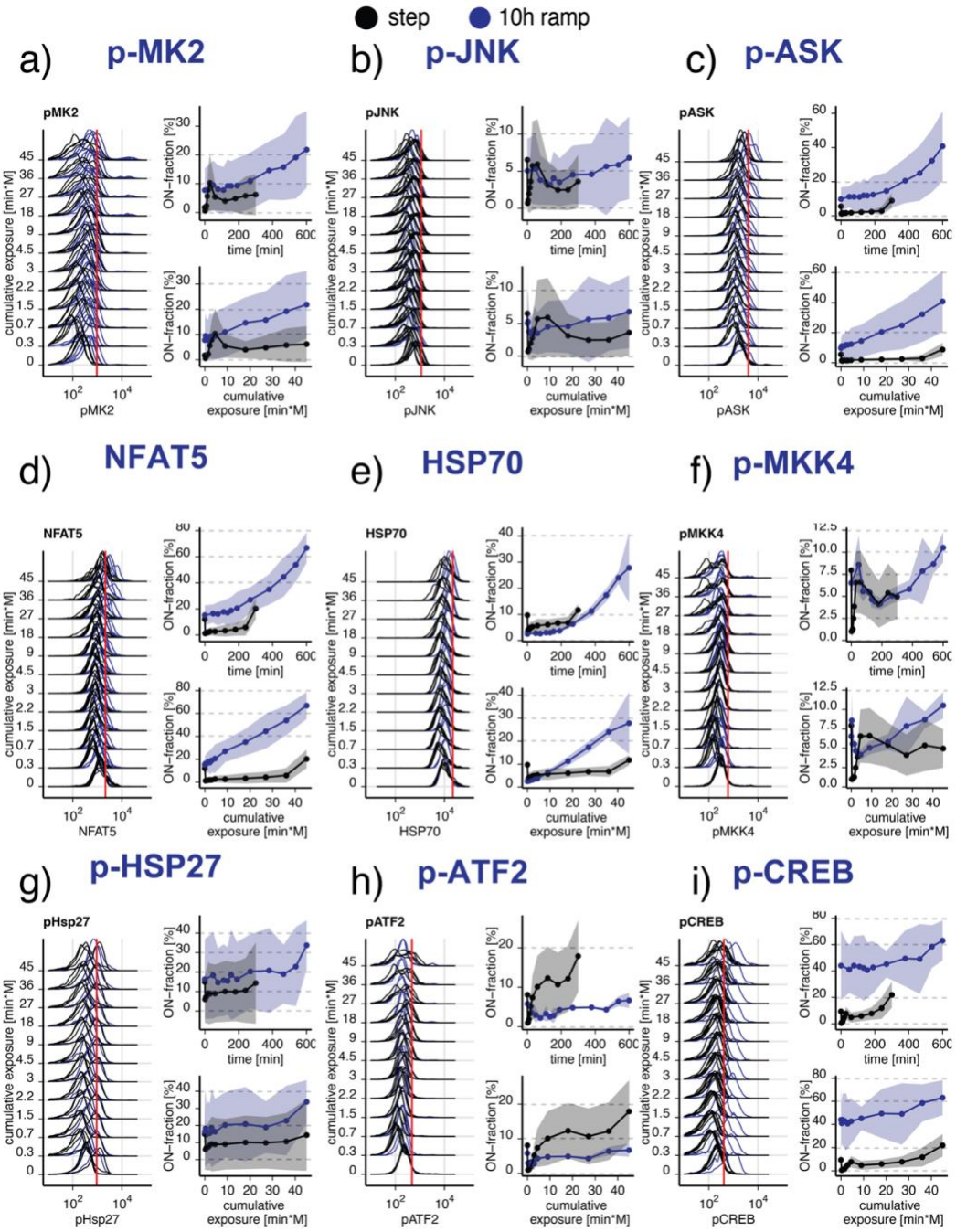

Figure 3.6: Markers for stress signaling.

a-i) Markers for stress signaling in Jurkat cells exposed to 300 mosmol/l NaCl by a step (black) or a 10h ramp (blue). The left panel shows single-cell distributions over the cumulative exposure with individual lines representing independent experiments. The Red line indicates the threshold for determining the ON-fraction. Right panels represent the mean and standard deviation of 3-10 independent experiments over time (top panel)

and cumulative exposure (lower panel).

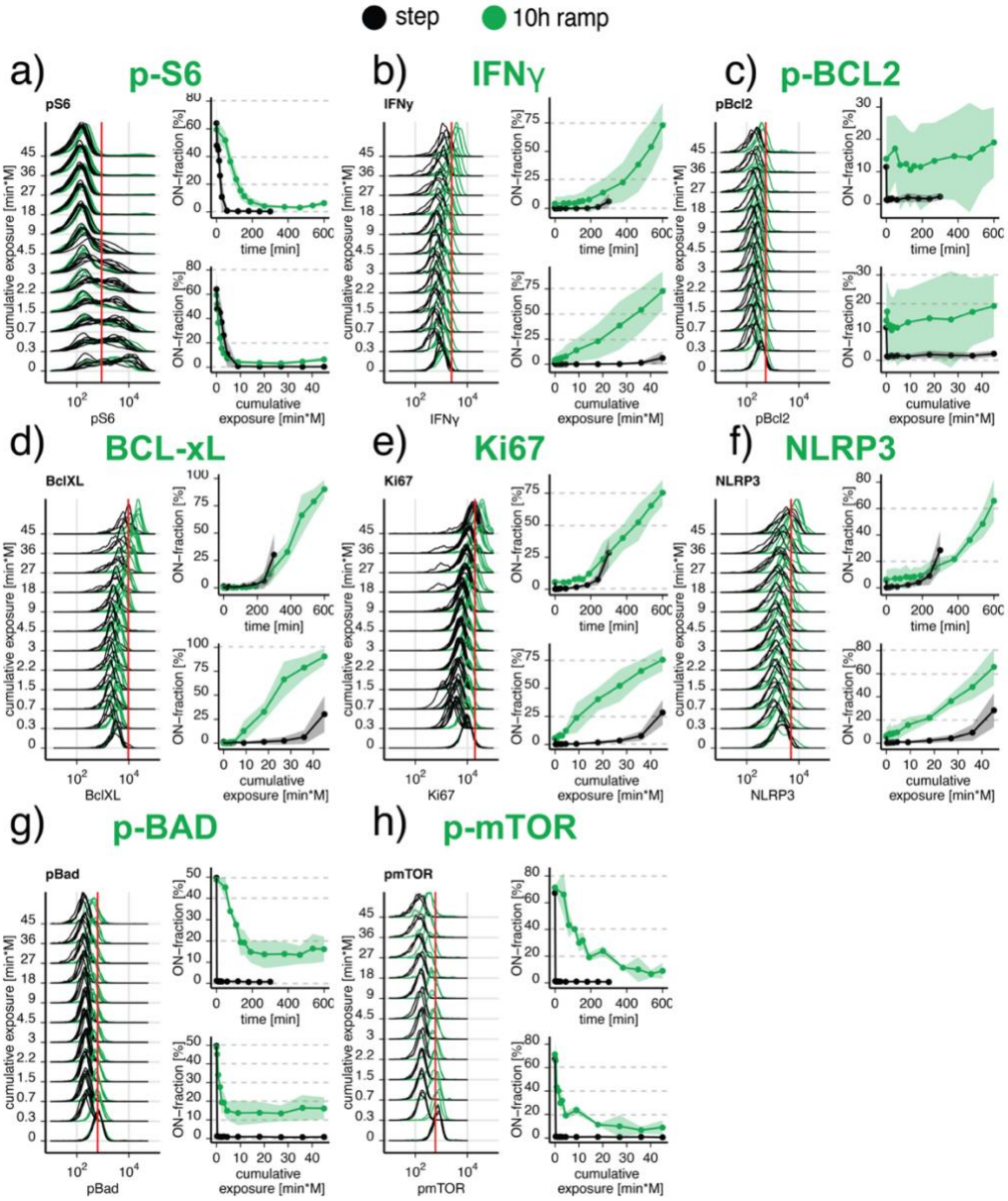

Figure 3.7: Markers for growth and proliferation.

a-h) Markers for growth/proliferation in Jurkat cells exposed to 300 mosmol/l NaCl by a step (black) or a 10h ramp (green). The left panel shows single-cell distributions over the cumulative exposure with individual lines representing independent experiments. The Red line indicates the threshold for determining the ON-fraction. Right panels represent the mean and standard deviation of 3-10 independent experiments over time (top panel) and cumulative exposure (lower panel).

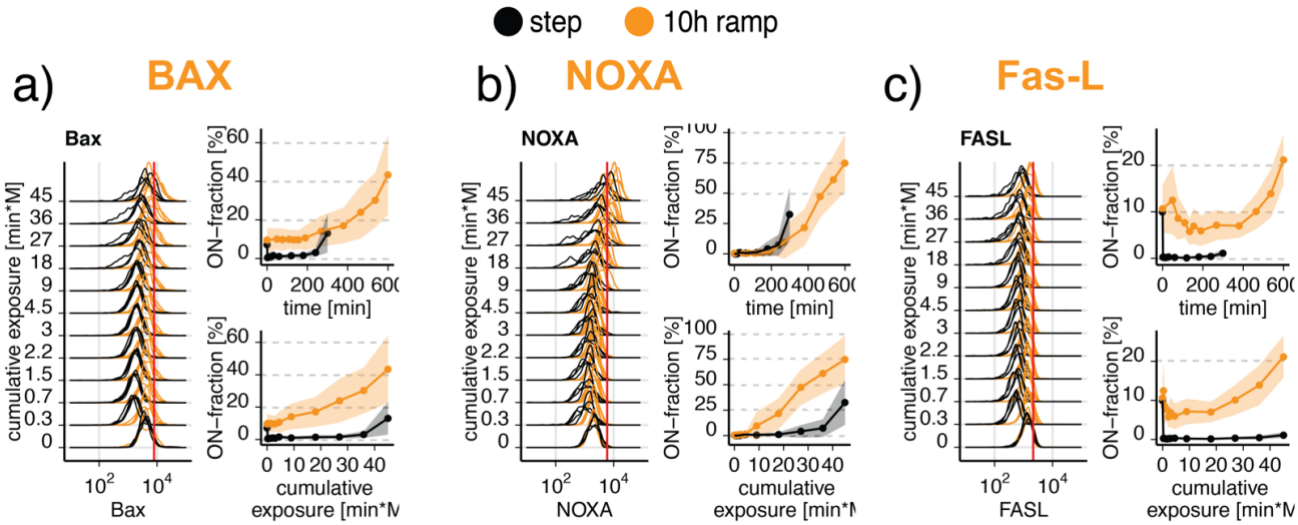

Figure 3.8: Markers for DNA damage.

In a-e) Markers for DNA damage in Jurkat cells exposed to 300 mosmol/l NaCl by a step (black) or a 10h ramp (yellow). The left panel shows single-cell distributions over the cumulative exposure with individual lines representing independent experiments. The Red line indicates the threshold for determining the ON-fraction. Right panels represent the mean and standard deviation of 3-10 independent experiments over time (top panel) and cumulative exposure (lower panel).

To understand which cellular mechanisms, contribute to improved viability during the slow ramp, we performed a temporal functional screen using a selected set of 27 well-established key markers of cell state and signaling that contribute to cell viability (Figure 3.5b). We grouped these into four cellular processes known to have an impact on cellular viability: stress signaling (blue), caspase signaling (magenta), DNA damage (orange) and growth/survival & inflammation (green) (Figure 3.5b). Each of these processes is known to be affected by increased NaCl concentrations (Burg, Ferraris, and Dmitrieva 2007). The process ‘stress signaling’ (blue) consists of markers belonging to stress/mitogen-activated protein kinases (SAPK/MAPK) pathways such as phosphorylated proteins p38 (Kleinewietfeld et al. 2013; Ko et al. 2002), JNK (Luo, Li, and Pflugfelder 2007), MK2 (Soni, Anand, and Padwad 2019), ASK1 (Takeda et al. 2008), MKK4 (Brancho et al. 2003), HSP27 (Niswander and Dokas 2006), CREB (Sulen et al. 2016), ATF2

(Humphreys et al. 2013), as well as total protein levels of HSP70 (Woo et al. 2002) and NFAT5/TonEBP (Jeon et al. 2006; Cheung and Ko 2013). MAPK pathways are known to convey stress signals to alter gene expression and cell phenotype (J. M. J. Kyriakis and Avruch 2012). Proteins in the 'caspase signaling' group are initiator caspases (Slee et al. 1999), such as activated caspase 8 (extrinsic pathway) (S. Y. Choi et al. 2013) and caspase 9 (intrinsic pathway) (S. Y. Choi et al. 2013), effector caspase 3 (McComb et al. 2019; Lazebnik et al. 1994), cleaved PARP(Kaufmann et al. 1993; Lazebnik et al. 1994) (cPARP) as a substrate of caspase 3 and γH2AX, as a marker for the excessive DNA damage caused by DNA degradation during apoptosis (Kuo and Yang 2008). The markers of 'growth/survival & inflammation' contain proteins that counteract apoptotic responses or indicate growth, proliferation, and inflammatory stimulation. The group contains phosphorylated forms of Bad (Grethe and Pörn-Ares 2006), Bcl2 (Pihán, Carreras-Sureda, and Hetz 2017), two anti-apoptotic proteins, mTOR (Peña-Oyarzun et al. 2017), a key node in the cell growth pathway, S6 (Magnuson, Ekim, and Fingar 2012), a marker for active translation, and phosphorylated ZAP70 (Fischer et al. 2010; Chan et al. 1992), a marker for activated inflammatory signaling. The group also contains total proteins Bcl-XL (Chao et al. 1995; Clem et al. 1998), an anti-apoptotic protein, Ki67 (Miller et al. 2018), a general marker of a cell proliferative activity, and NLRP3 (P. Ma et al. 2019; Abderrazak et al. 2015), a marker for the inflammasome, and intracellular IFNγ (Lawrence and Chow 2012), a marker for inflammatory cytokine production. In response to DNA damage (Dmitrieva, Cai, and Burg 2004) proteins such as Noxa (Flinterman et al. 2005; Fei, Bernhard, and El-Deiry 2002; Roos and Kaina 2006), Fas-L (Kasibhatla et al. 1998; Roos and Kaina 2006), and BAX (Fei, Bernhard, and El-Deiry 2002) are expressed and fall into the group DNA damage.

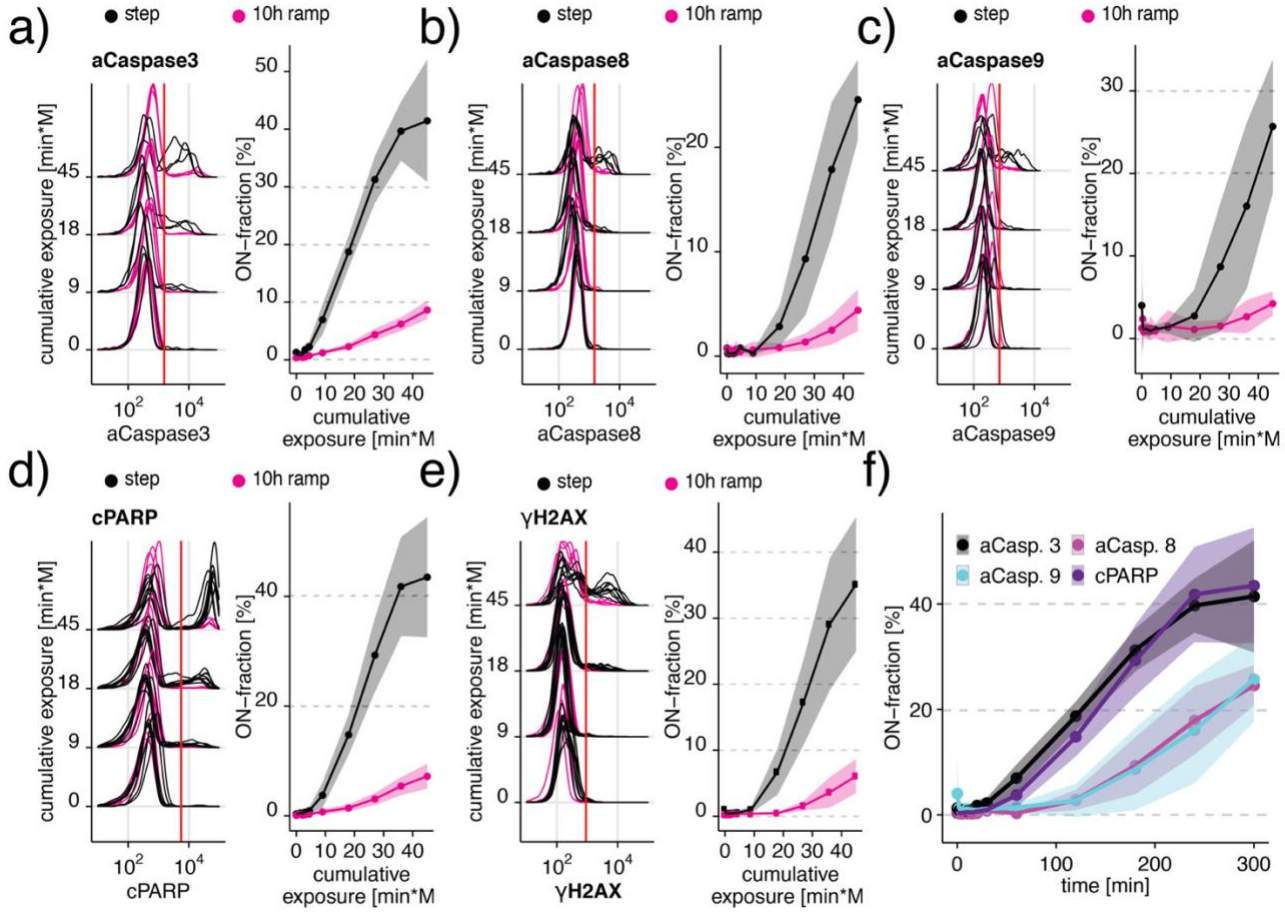

Figure 3.9: Differential caspase signaling regulates cell viability.

a-d) Differential regulation of (a) cleaved Caspase 3, (b) cleaved Caspase 8 and (c) cleaved Caspase 9, (d) cleaved PARP, (e) γH2AX in Jurkat cells exposed to 300 mosmol/l NaCl by a step (black) or a 10h ramp (magenta). The left panel shows selected single-cell distributions over the cumulative exposure with individual lines representing independent experiments. Redline indicates the threshold for determining the ON-fraction. Right panels represent ON-fraction mean and standard deviation of 3-10 independent experiments as a function of cumulative exposure of NaCl. f) ON-fraction kinetics of caspase signaling markers over time indicate early (Caspase 3 and cPARP) and late (Caspase 8 and 9) activation. Lines indicate mean and SD of 3-10 independent experiments.

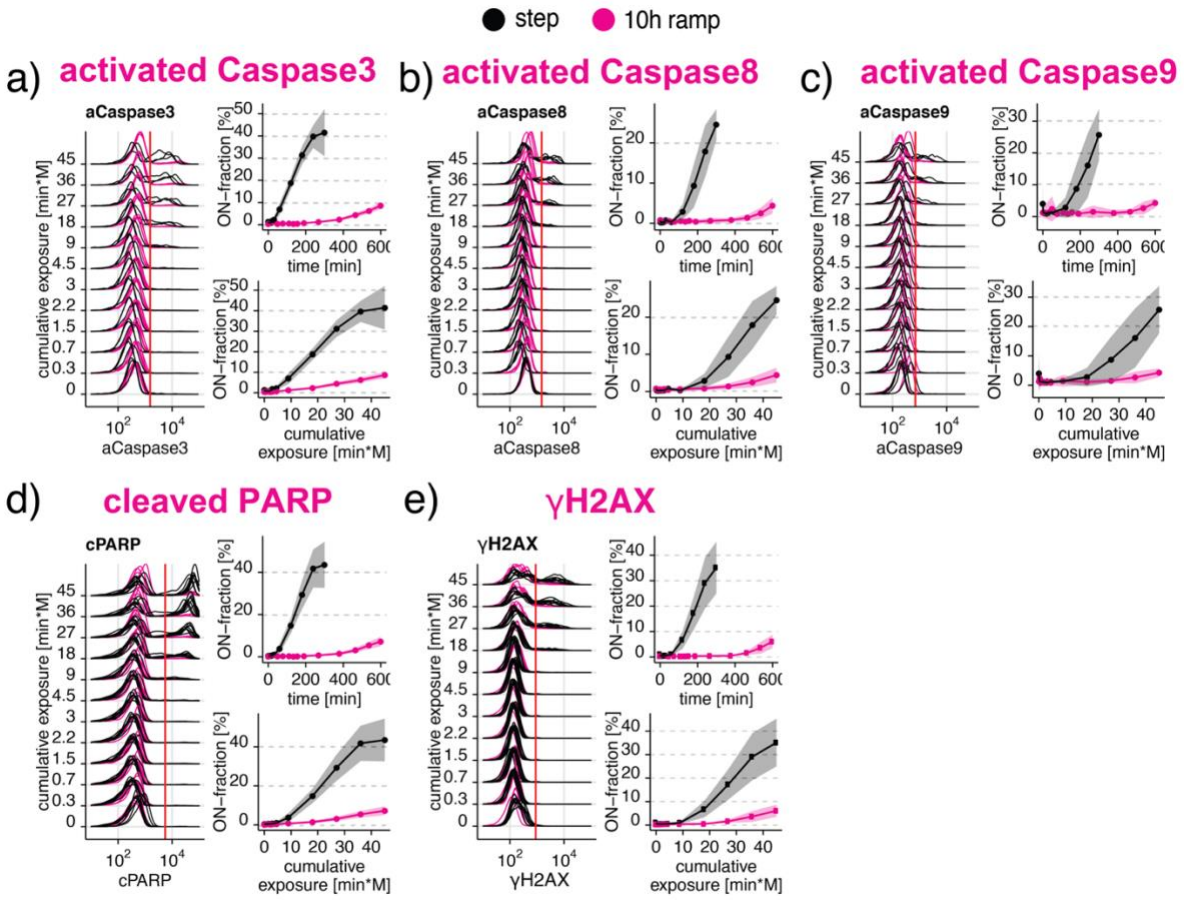

Figure 3.10: Differential caspase signaling regulates cell viability.

a-d) Differential regulation of (a) cleaved Caspase 3, (b) cleaved Caspase 8 and (c) cleaved Caspase 9, (d) cleaved PARP, (e) γH2AX in Jurkat cells exposed to 300 mosmol/l NaCl by a step (black) or a 10h ramp (magenta). The left panel shows selected single-cell distributions over the cumulative exposure with individual lines representing independent experiments. The Red line indicates the threshold for determining the ON-fraction. Right panels represent ON-fraction mean and standard deviation of 3-10 independent experiments as a function of time (top panel) or cumulative exposure of NaCl (lower panel).

We use Fluorescent Cell Barcoding for multiplex flow cytometry to identify differentially regulated markers over time in step or ramp conditions (Krutzik and Nolan 2006; Earl et al. 2018). This functional temporal screen allows us to uniquely encode each time point sample with a combination of two dye concentrations (Figure 3.5c). We pooled barcoded

samples and then split them again into different tubes to stain each split sample with antibodies. The advantages of barcoding and then sample splitting is reduced variability between samples, increased throughput, and reduced cost for different markers. Using this approach, we screened protein markers in Jurkat cells for their change over time in step versus 10h ramp experiments to an additional concentration of 300 mosmol/l NaCl. After data collection, we demultiplexed each sample with one or two protein markers to extract the individual time points (Figure 3.5c, d). To quantify each marker's response, we next computed the fraction of positive cells for this marker and called this population 'ON-fraction' (Figure 3.5e). We then plot the ON-fraction of each marker at the end of the time course experiment between the ramp and the step treatment to understand the correlation between the markers in each group (Figure 3.5f). This analysis revealed several distinct response patterns: (a) We observed strong activation in step but not ramp condition in cells with phosphorylated proteins of the caspase signaling group and p38 of the stress signaling group (Figure 3.2g, 3.6). (b) We observed minimal activation in step but strong activation in ramp conditions for some markers of stress response (pASK, NFAT5, and HSP70) (Figure 3.5g (blue), 3.6), growth (Ki67), anti-apoptotic (Bcl-XL), and inflammation (IFNγ, NLRP3) (Fig. 3.5h (green), 3.7), and markers of DNA damage (Figure 3.5h (orange), 3.8). (c) A screen for other markers of cell survival, growth, and DNA damage reveals no significant differential changes over time. Based on this temporal functional screen, we focused on protein markers of the caspase signaling group.

3.3.3 Caspases differentially regulate step and ramp conditions.

Activated caspases 3, 8, 9, cleaved PARP and γH2AX all showed strong activation (ON-fraction) during the 300 mosmol/l NaCl step treatment (Figure 3.9a-e (black), 3.10). Strikingly, caspase, and γH2AX activation, as well as PARP cleavage, are negligible during the 10h ramp treatment condition to the same final concentration (Figure 3.9a-e (magenta), 3.10). Phosphorylation of γH2AX is also entirely prevented when caspase activity is inhibited during step NaCl treatment by a pan-caspase inhibitor (Figure 3.13), which suggests prevention of apoptosis-associated destruction of DNA. Next, we investigated the contributions of caspases 3, 8, and 9 to the cell viability phenotype by

quantifying the time course of activation for each member of the caspase signaling group relative to cleavage of PARP (Figure 3.9f). We found that caspase 3 (grey) is activated slightly before its target cPARP (purple), as expected (Figure 3.9f). Surprisingly, we found activation of the initiator caspases 8 (magenta) and 9 (cyan) after caspase 3 and cPARP. These results suggest that caspase 3 contributes to the induction of apoptosis, but not cleaved caspase 8 and 9. To understand if these population-level effects are indeed observable in the same cell, we co-stained cells with antibodies for activated caspase 9 and cPARP (Figure 3.11a). We found that single cells that are negative for cPARP are never positive for activated caspase 9 at any point during the treatment (Figure 3.11a, b). Cells positive for activated caspase 9 already have a high level of cPARP, suggesting that caspase 9 cleavage is not causative for apoptosis induction in single cells. Similarly, single cells co-stained for cPARP and activated caspase 8 are never negative for cPARP and positive for activated caspase 8, at the same time throughout the time course (Fig. 3.11c). These results indicate no activation of caspase 8 before apoptosis induction (Figure 3.11d). In summary, these results suggest that activated caspase 3, but not activated caspase 8 and 9 contribute to PARP cleavage and subsequent induction of apoptosis (Figure 3.11d).

3.3.4 Caspase signaling is the main contributor to cell death in step conditions.

We next tested if these different caspases contributed to cell viability and addressed their mechanism in an attempt to link dynamics in caspase activation to apoptosis and cell phenotype (Figure 3.11e). In our ramp treatment condition to additional 300 mosmol/l NaCl in 10h, we find that cell viability increases to 40% in comparison to 15% in step treatment of the same final concentration and the total amount of NaCl relative to cells grown in control conditions (100% viability) (Figure 3.11e, magenta area). We asked if this increase in viability is entirely related to the lack of caspase activation and PARP cleavage, as observed in Figures 3.9 & 3.10. To test this idea, we treated cells with a step of 300 mosmol/l NaCl in the presence of potent and different pan-caspase inhibitors (panCas-i-a = Z-VAD-FMK (Slee, E. Cohen 1996); panCas-i-b = Q-VD-OPH (Caserta et al. 2003)) (Figure 3.11e). We observed an increase in cell viability to 40%, which is the same as for the ramp treatment. This result suggests that caspase activation and

caspase-mediated apoptosis are necessary to explain the reduction in viability during the step treatment relative to the ramp treatment. Therefore, we hypothesize that caspase-dependent apoptosis is the main contributor to the difference in viability between the step and the long ramp treatment conditions.

We predicted that early caspase 3 activation triggers PARP cleavage and apoptosis compared to late caspase 8 and 9 activation (Figures 3.10, 3.11a-d). To test this prediction, we exposed cells to inhibitors of caspase 8, caspase 9, or both of them. We found that inhibitors for caspase 8 and 9 do not substantially improve viability after step exposure to 300 mosmol/l NaCl (Figure 3.11e). As expected, we found that pan-caspase inhibition prevents the cleavage of caspase 3 during the step treatment (Figure 3.11f). We also tested if necroptosis may be activated during the step treatment by inhibiting the process with necrostatin. We did not see an improvement in viability, when adding necrostatin alone (Figure 3.12). When added in combination with Z-VAD-FMK, pan-caspase inhibitor, we did not observe an improvement in viability above Z-VAD-FMK addition alone (Figure 3.12). This suggests that Necroptosis does not mediate cell death during the step treatment. We also added Bid inhibitor BI-6C9 to test the dependence of cell death on Bid cleavage. We observe that viability is improved to the same level as in pan-caspase inhibition (Figure 3.12), suggesting that Bid cleavage is critical for cell death in the step treatment.

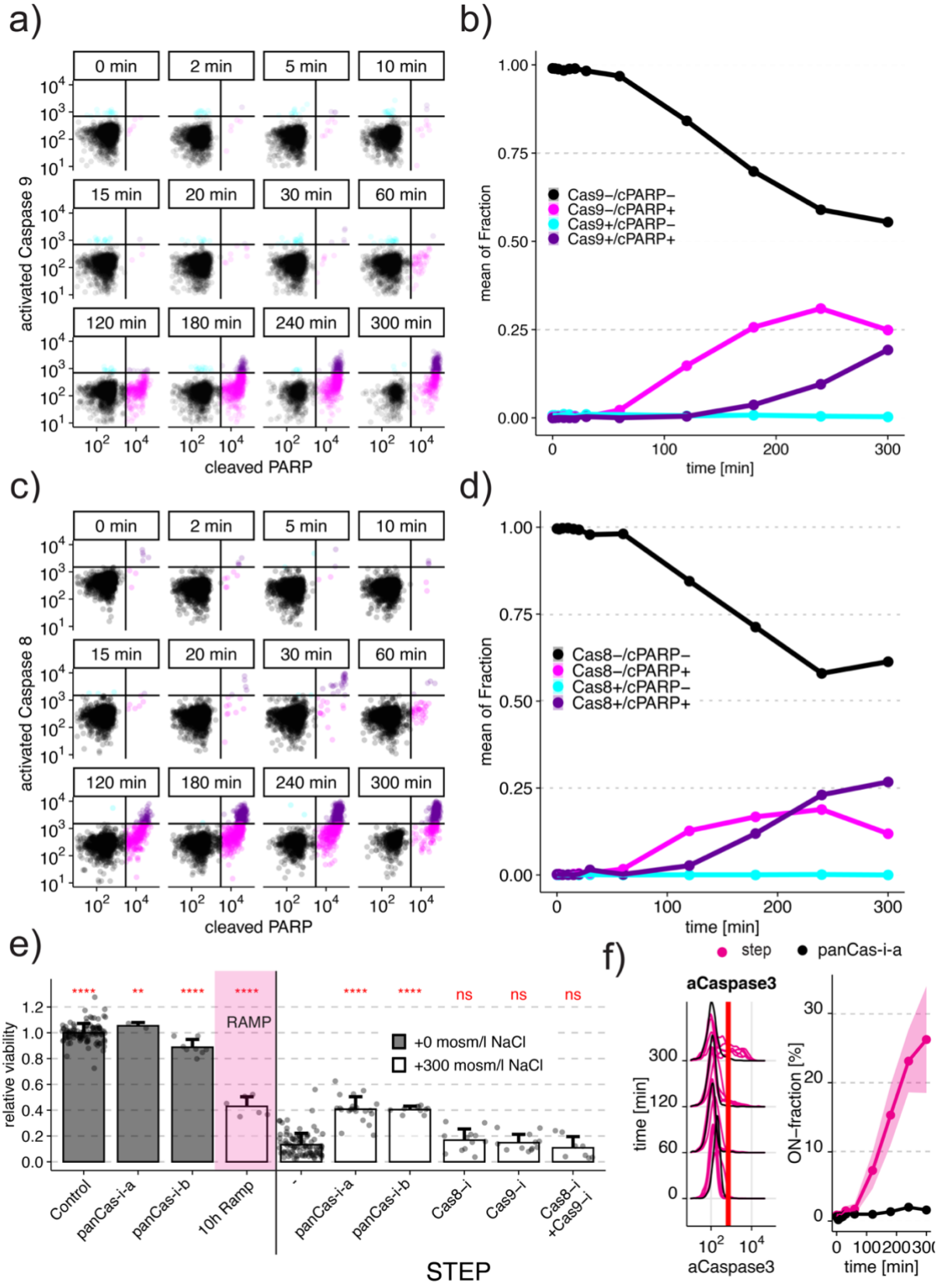
a)
0 min
2 min
5 min
10 min
15 min
20 min
30 min
60 min
120 min
180 min
240 min
300 min
activated Caspase 9
cleaved PARP
b)
mean of Fraction
Cas9−/cPARP−
Cas9−/cPARP+
Cas9+/cPARP−
Cas9+/cPARP+
time [min]
c)
activated Caspase 8
cleaved PARP
d)
mean of Fraction
Cas8−/cPARP−
Cas8−/cPARP+
Cas8+/cPARP−
Cas8+/cPARP+
time [min]
e)
relative viability
RAMP
+0 mosm/l NaCl
+300 mosm/l NaCl
Control
panCas-i-a
panCas-i-b
10h Ramp
Cas8–i
Cas9–i
Cas8–i +Cas9–i
STEP
f)
step
panCas-i-a
aCaspase3
time [min]
ON−fraction [%]
time [min]

Figure 3.11: Activated Caspase 8 or 9 are not initiating apoptosis in hyperosmotic stress.

*a, Single-cell scatter plots of Jurkat cells co-stained with antibodies for cPARP and activated Caspase 9 measured by flow cytometry after exposure to 300 mosmol/l NaCl for 5h. Black lines indicate thresholds to determine individual fractions of low aCaspase9 and low cPARP (black), low aCaspase9, and high cPARP (magenta), high aCaspase9 and high cPARP (purple) and high aCaspase9 and low cPARP (cyan). Circles represent single cells. b, Quantification of fraction of cells stained for Caspase 9 activation and PARP cleavage over the time course using the thresholds indicated in a c) Single-cell scatter plots of Jurkat cells co-stained with antibodies for cPARP and activated Caspase 8 measured by flow cytometry after exposure to 300 mosmol/l NaCl for 5h. Black lines indicate thresholds to determine individual fractions of low aCaspase8 and low cPARP (black), low aCaspase8, and high cPARP (magenta), high aCaspase8 and high cPARP (purple) and high aCaspase8 and low cPARP (cyan). d) Quantification of fraction of cells stained for Caspase 8 activation and PARP cleavage over the time course using the thresholds indicated in c. e) Relative viability of untreated cells (grey), cells exposed to a 10h ramp (magenta) or 5h step treatment both to 300 mosmol/l NaCl (white) exposed to different inhibitors. Inhibitors were added 30 min before NaCl at concentrations as follows: "panCas-i-a" (pan-caspase inhibitor Z-VAD-FMK, 100 μM), "panCas-i-b" (pan-caspase inhibitor Q-VD-OPH, 100 μM), "Cas8-i" (Caspase 8 inhibitor Z-IETD-FMK, 100 μM), "Cas9-i" (Caspase 9 inhibitor Z-LEHD-FMK, 100 μM). Bars indicate the mean and SD of at least 3 replicates. Two-sided unpaired student's t-test: **p<0.01, ***p<0.001, ****p<0.001, ns=not significant. f) Activated Caspase 3 (aCasapse 3) in Jurkat cells exposed to 300 mosmol/l NaCl step in presence (black) or absence (magenta) of pan-caspase inhibitor (Z-VAD-FMK, 20 μM). The left panel shows single-cell distributions over the cumulative exposure with individual lines representing independent experiments. The Red line indicates the threshold for determining the ON-fraction. Right panels represent the mean and standard deviation of 1-4 independent experiments as a function of cumulative exposure.*

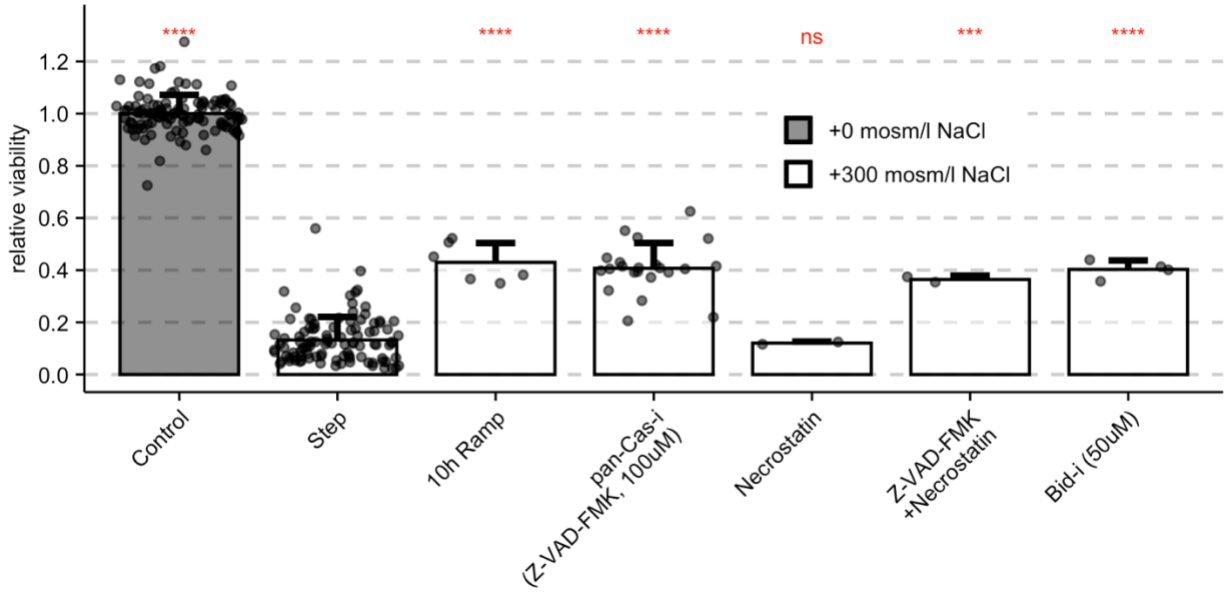

Figure 3.12: Inhibtion of other cell death pathways.

Jurkat cells were pretreated with inhibitors for Bid (50 μM), Z-VAD-FMK (100 μM), Necrostation (5 μM) or a combination of them for 30 minutes after which 300 mosmol/l NaCl were added to the cells by a step treatment. Viability was determined by measuring intracellular ATP by the CellTiterGlo assay.

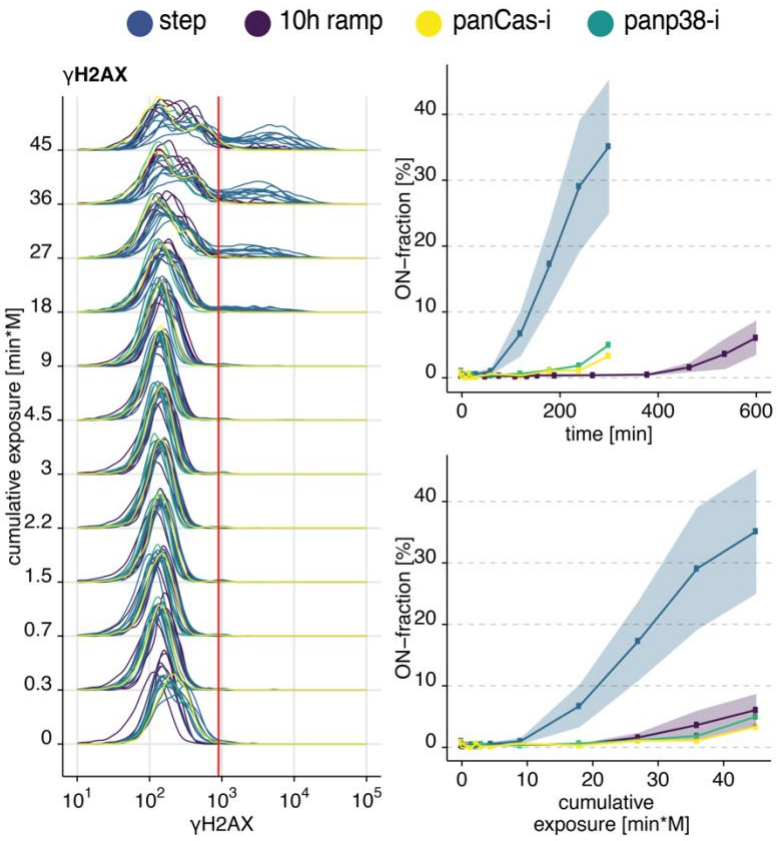

Figure 3.13: Caspases and p38 mediate γH2AX phosphorylation during hyperosmotic stress.

γH2AX phosphorylation in Jurkat cells exposed to 300 mosmol/l NaCl as a step without (blue), with inhibitor pan-Cas-I (Z-VAD-FMK, yellow), with inhibitor pan-p38-I (BIRB796, green), or as a ramp for 10h (purple) Left panel shows single-cell distributions over the cumulative exposure with individual lines representing independent experiments. The Red line indicates the threshold for determining the ON-fraction. Right panels represent the mean and standard deviation of 1-10 independent experiments over time (top panel) and cumulative exposure (lower panel). Z-VAD-FMK (panCas-i) was added 30 min before NaCl at 20 μM.

Through our functional temporal screen, we also observed that p38 is strongly activated in NaCl step treatment condition, as previously reported to occur in other mammalian cells (Figure 3.14a) (Han et al. 1994; Ip et al. 2015). However, during a 10h

ramp treatment, we find that p38 is only slightly activated, perhaps playing a role in the decreased cell viability phenotype following step stimulation relative to the ramp stimulation. To understand how phospho-p38 and cPARP are expressed in single cells over time, we costained cells with antibodies for both proteins. We observed a correlation of p38 phosphorylation and PARP cleavage and at later timepoints an anticorrelation of positive cPARP and negative phospho-p38 (Figure 3.15-3.16). This could suggest a role for p38 in mediating cell death. However, when we inhibited all p38 isoforms by using a pan-p38 inhibitor (BIRB 796) (Pargellis et al. 2002), we found that it had a statistically significant, but biologically small effect on cell viability following step treatment condition (Figure 3.14b). From these results, we conclude that the rate of hypertonic stress addition differentially regulates p38, but that p38 activity is not essential for the reduction in cell viability following step treatment.

Compared to p38, NFAT5, pASK, and HSP70 signals are reduced in step but not in ramp conditions shortly after osmotic stress (Figure 3.6c, d, e). Followed by this initial drop are similar temporal profiles for step and ramp conditions. These results demonstrate that the dynamics of NFAT5, pASK, and HSP70 are not differentially regulated. We also observed similar dynamics for markers of the growth (Ki67), anti-apoptosis (Bcl-xL), inflammation (IFNγ, NLRP3), and the DNA damage (BAX, NOXA, and Fas-L) signaling groups (Figure 3.6-8). Markers that did change over time but not strongly between step and ramp conditions are the proliferation markers p-S6 and p-mTOR and pro-apoptotic protein p-BAD (Figure 3.7a, g, h). We observed no change given the error in the measurements between step and ramp conditions for selected markers of stress signaling (p-MK2, p-JINK, p-MKK4, p-HSP27, p-ATF2, and p-CREB), and anti-apoptotic protein p-Bcl2 (Figures A3.6a, b, f, g, h, p).

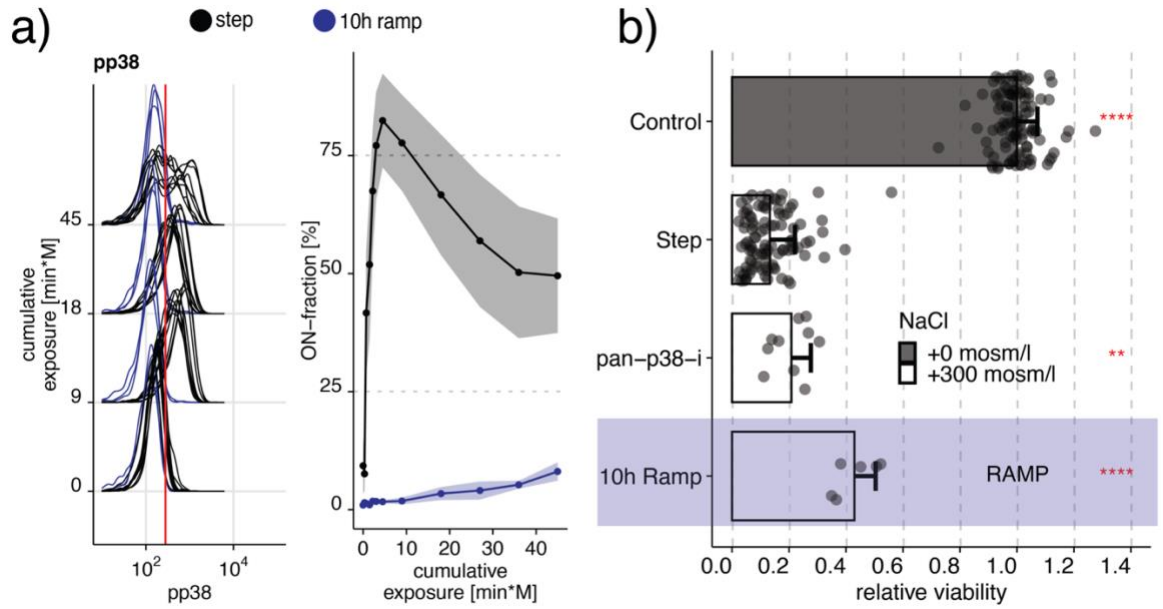

Figure 3.14: Contribution of p38 to apoptosis in hypertonic stress is minimal.

*a) Phosphorylation of p38 in Jurkat cells exposed to 300 mosmol/l NaCl by a step (black) or a 10h ramp (blue). The left panel shows selected single-cell distributions over the cumulative exposure with individual lines representing independent experiments. The Red line indicates the threshold for determining a cell that is p38 phosphorylation positive (ON-fraction). The right panel represents the ON-fraction mean and standard deviation of 3-10 independent experiments as a function of cumulative exposure. b) Viability of Jurkat cells relative to untreated cells (control) exposed to an additional 0 (grey) or 300 mosmol/l (white) NaCl for 5h (step) or 10h (ramp, purple), respectively. Pan p38 inhibitor (pan-p38-I, BIRB796) was added 30 min before NaCl at concentrations at 10 μM. Inhibitor was added 30 min before NaCl at concentrations for pan-p38-i (BIRB796, 10 μM). Circles represent single experiments. Bars indicate the mean and SD of at least 3 replicates. Two-sided unpaired student's t-test: **p<0.01, ****p<0.001.*

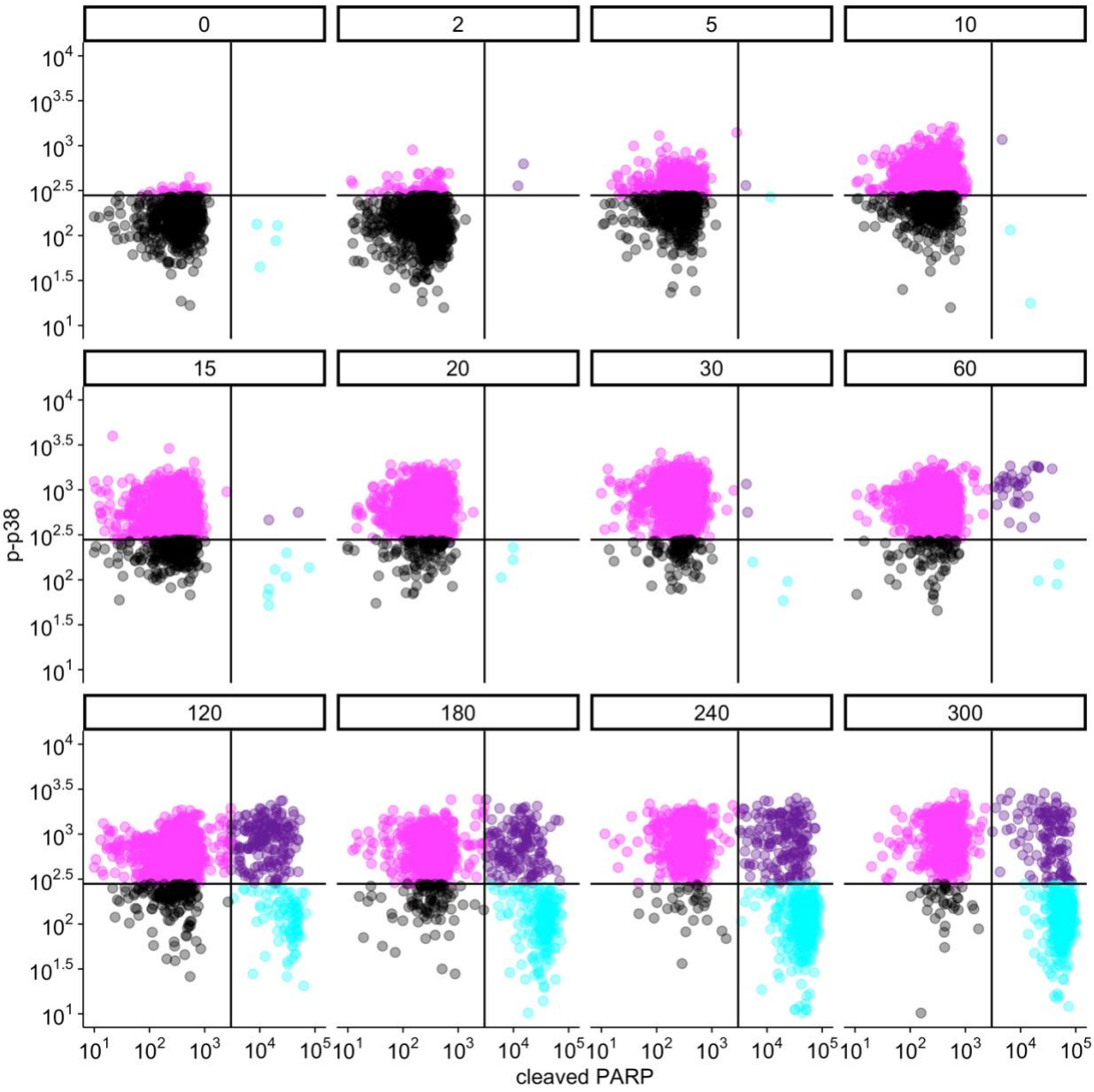

Figure 3.15: Phosphorylation of p38 is correlated with PARP cleavage.

Jurkat cells costained for p-p38 and cPARP antibodies after a step treatment to additional 300 mosmol/l NaCl measured by Flow cytometry. Black lines indicate thresholds to classify each population. Colors represent the different populations.

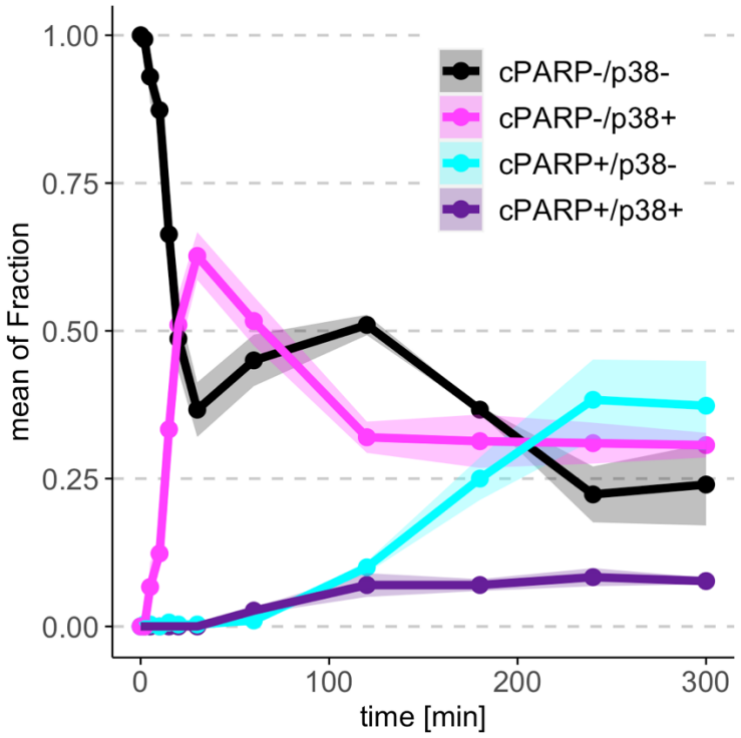

Figure 3.16: cPARP+/p-p38+ fraction precedes appearance of cPARP+/p-p38- fraction

Jurkat cells costained for p-p38 and cPARP antibodies after a step treatment to additional 300 mosmol/l NaCl measured by Flow cytometry. Fractions were quantified using the thresholds indicated in Figure 3.15. Lines represent meand and SD of 3 biological replicates.

3.3.5 Intracellular proline levels improve viability in ramp stress conditions

To better understand the protective mechanisms contributing to improved viability during the ramp condition, we analyzed the abundance and fold changes of metabolites that may function as cell internal osmolytes (Figure 3.17, 3.18). We found that the most abundant metabolites are the amino acid proline, glutamic acid, and arginine. In comparison, traditional osmolytes such as betaine, inositol, sorbitol, taurine, or urea are significantly less abundant in the cell (Figure 3.18). Interestingly, of these amino acids, only proline is differentially regulated in step and ramp conditions, rejecting the possibility that these amino acids are only byproducts of protein degradation (Figure 3.17a). This

result suggests that proline may act as an osmoprotective molecule in human cells in ramp treatment conditions. The increase in abundance of cell internal proline levels relative to other amino acids and organic molecules suggests that cells import proline from the growth media. Elevated protein degradation in the cell, would presumably result in an equal distribution of increased amino acid abundance. We then tested if intracellular proline levels are independent of the activation of the caspase pathway or if preventing caspase-mediated cell death results in higher levels of proline in the cells. In these experiments, we exposed cells to a step treatment of NaCl with or without pan-caspase inhibitor Z-VAD-FMK (Fig. 3.17b). As in all previous experiments, we exposed cells to the same cumulative exposure of NaCl for the same final NaCl concentration and compared the results. We found that regardless of pan-caspase inhibition, cells accumulated significantly less proline during the step treatment than cells exposed to the ramp treatment (Figure 3.17b). We conclude that caspase inhibition during hypertonic stress does not result in additional proline accumulation during the step treatment. This result indicates that caspase activation and proline accumulation are independent. To test if extracellular levels of proline can improve cell viability in the step treatment to 300 mosmol/l NaCl, we added free L-proline to the media of the cells before applying hypertonic stress (Figure 3.17c). We found a significant increase in viability due to added proline, in comparison to cells were no additional proline was added (Figure 3.17c). This result suggests that proline is transported into the cells and can protect mammalian cells from hypertonic stress. It is well established that hyperosmotic stress upregulates transporters for glutamine (Izumi et al. 2015). Therefore, we tested if additional external L-glutamine, a precursor of proline (H. Li et al. 2016), can also improve viability. When we added additional L-glutamine to the media before adding NaCl, we observed a significant improvement in cell viability, similar to adding proline. Because proline is a yet unidentified compound in the mammalian response to hyperosmotic stress, we tested the effect of typical mammalian osmolytes on cell viability (James Ming Phang et al. 2012b; James M. Phang, Liu, and Zabirnyk 2010). When we added compounds identified as physiological osmoprotectants to the media, such as taurine, sorbitol, or betaine, we observe that these compounds seem to provide less or the same protection as proline or glutamine, during hypertonic stress. These results demonstrate that proline and glutamine

are as effective as traditional osmolytes in protecting the cell from osmotic stress (Figure 3.19). In addition, we analyzed publicly available data on gene expression under step hypertonic stress in murine embryonic fibroblasts (Ferreiro et al. 2010; Farabaugh et al. 2020). These data suggest that gene expression changes to benefit the transport and biosynthesis of proline in the cell (Figure 3.20).

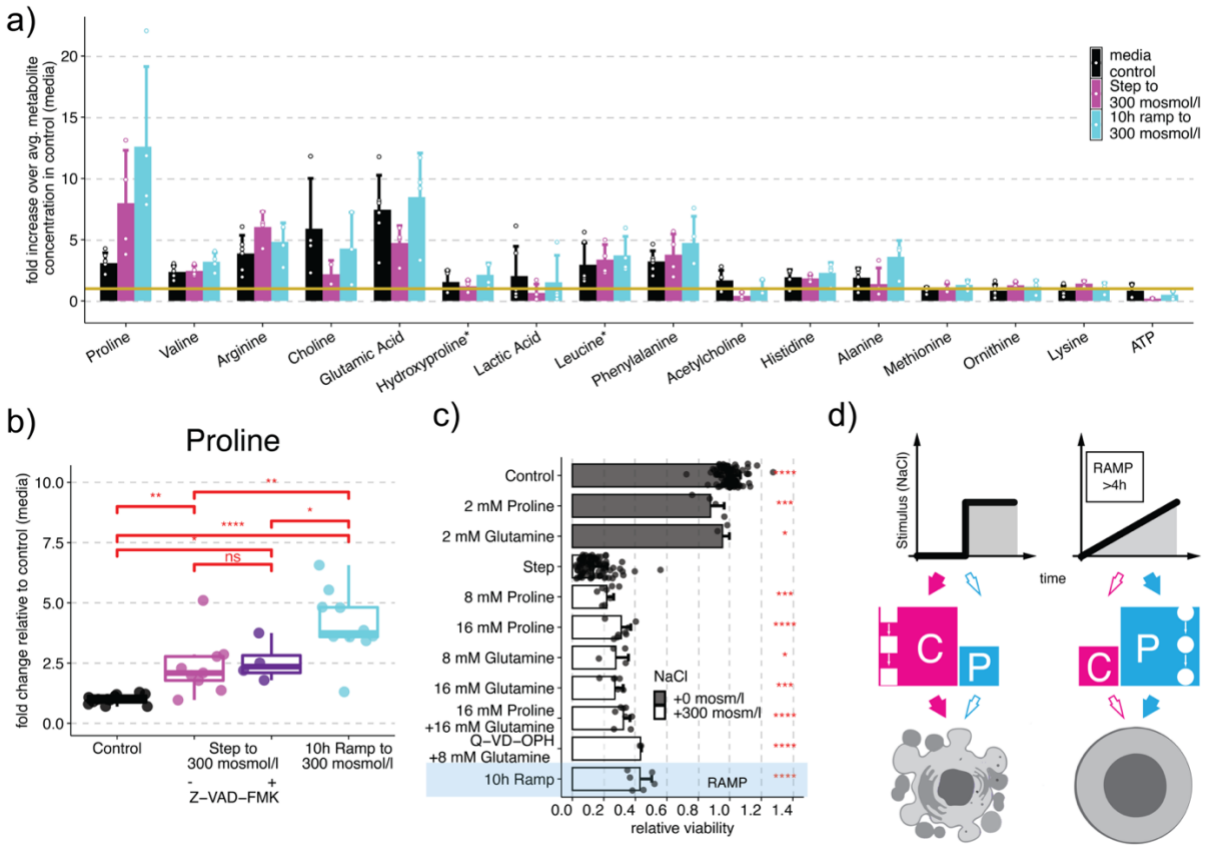

Figure 3.17: Intracellular proline protects human cells during ramp stress conditions.

a) Fifteen most abundant metabolites detected in Jurkat cells without stimulation (control media, black), after treatment with step (magenta) or 10h ramp (cyan) to 300 mosmol/l NaCl. Bars represent the mean and standard deviation of the fold change of each metabolite to the average metabolite concentration in the control condition (yellow line) with circles representing individual replicates. b) Change of proline levels in Jurkat cells relative to control (no additional NaCl) in 0 (black) or 300 mosmol/l NaCl for 5h without (step, magenta) or with pan-caspase inhibitor "a" (Z-VAD-FMK, 100 μM)(purple) or a 300 mosmol/l NaCl ramp for 10h (cyan). Boxplots represent data of 4-10 replicates with circles

*represent individual replicates as determined by Mass spectrometry. c) External amino acid treatment impacts viability relative to untreated cells (control, grey) in Jurkat cells exposed to an additional 0 or 300 mosmol/l NaCl for 5h (step) or 10h (10h ramp, blue shade), respectively. Amino acids were added 60 min before NaCl at indicated concentrations. Pan-caspase inhibitor (Q-VD-OPH) was added 30 min before NaCl at 100 μM. Bars indicate the mean and SD of at least 3 replicates. Two-sided unpaired student's t-test: *p<0.05, **p<0.01, ***p<0.001, ****p<0.0001, ns=not significant. d) Model summarizing how instant stress conditions cause activation of caspase signaling and cell death (left, magenta) whereas the gradual increase of the same stress to the same final concentration does not activate caspase signaling but instead increases intracellular proline as an osmolyte to protect cells against increasing stress (right, cyan).*

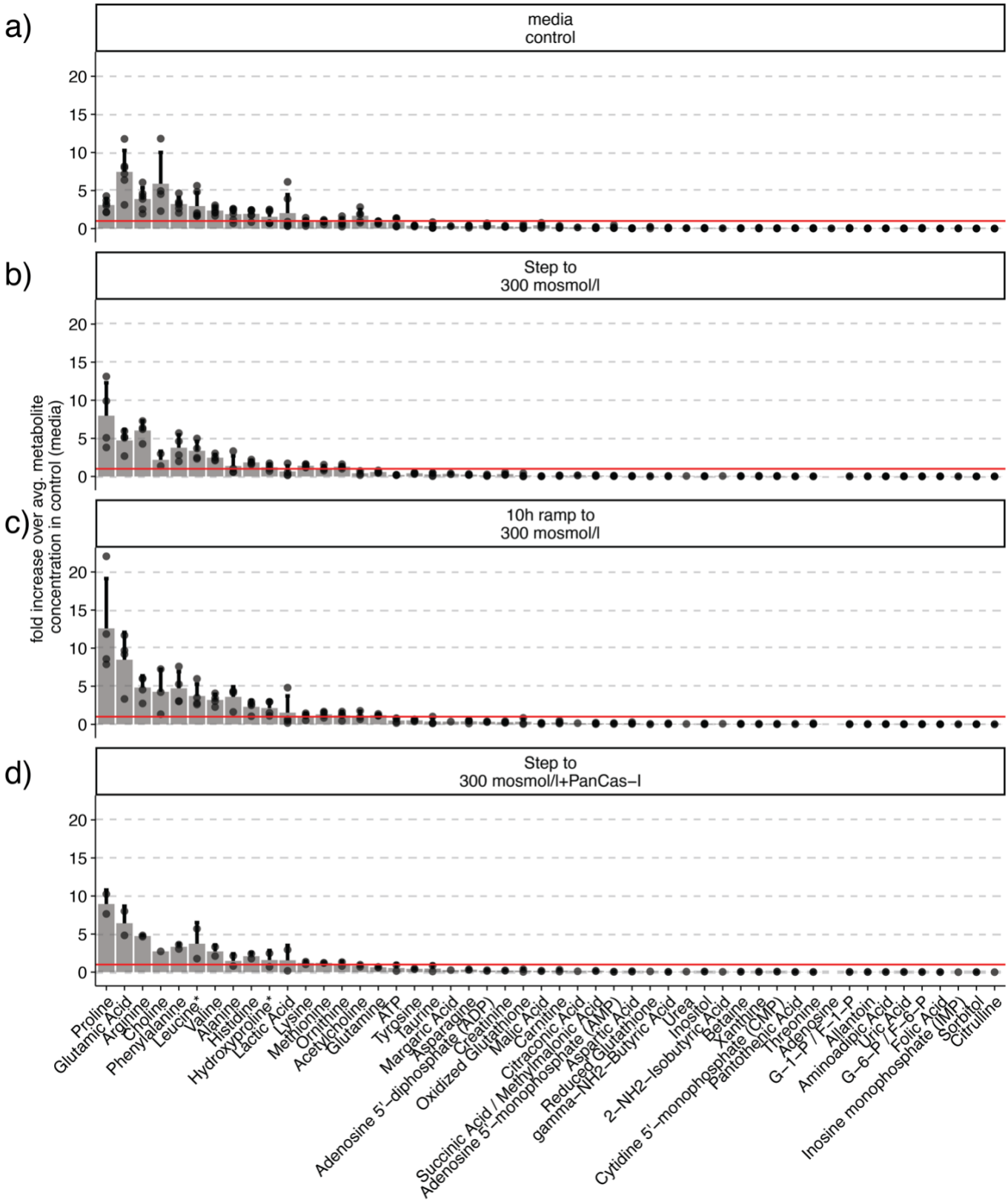
a)
media
control
b)
Step to
300 mosmol/l
c)
10h ramp to
300 mosmol/l
d)
Step to
300 mosmol/l+PanCas−I
fold increase over avg. metabolite
concentration in control (media)
0
5
10
15
20
Proline
Glutamic Acid
Arginine
Choline
Phenylalanine*
Leucine*
Valine
Alanine
Histidine*
Hydroxyproline*
Lactic Acid
Lysine
Methionine
Ornithine
Acetylcholine
Glutamine
ATP
Tyrosine
Taurine
Margaric Acid
Asparagine
Adenosine 5'−diphosphate (ADP)
Creatinine
Oxidized Glutathione
Malic Acid
Carnitine
Citraconic Acid
Succinic Acid / Methylmalonic Acid
Adenosine 5'−monophosphate (AMP)
Aspartic Acid
Reduced Glutathione
gamma−NH2−Butyric Acid
Urea
Inositol
2−NH2−Isobutyric Acid
Betaine
Xanthine
Cytidine 5'−monophosphate (CMP)
Pantothenic Acid
Threonine
Adenosine
G−1−P / F−1−P
Allantoin
Aminoadipic Acid
Uric Acid
G−6−P / F−6−P
Folic Acid
Inosine monophosphate (IMP)
Sorbitol
Citrulline

Figure 3.18: Metabolite distribution changes in hypertonic stress.

a-d) All metabolites detected in Jurkat cells (a) without stimulation, (b) after treatment with 300 mosmol/l NaCl as a step, (c) a 10h ramp, and (d) step preincubated with Pan-Caspase inhibitor (PanCas-I = 100 μM Z-VAD-FMK). Bars represent the mean and standard deviation of the fold change of each metabolite to the average metabolite concentration in the control condition. The Red line is a visual aid to identify metabolites that are above and below the average concentration in the control condition and indicates the relative average amino acid concentration.

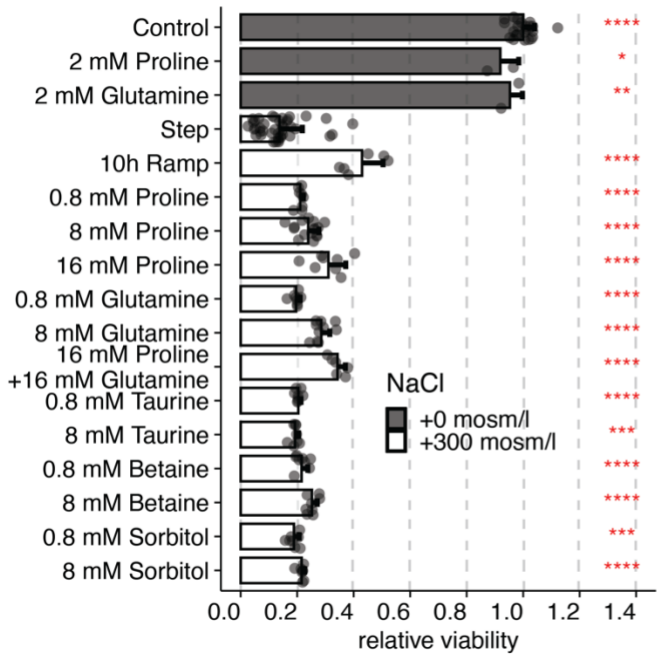

Figure 3.19: External proline and glutamine improve viability in step treated cells similarly to ramp treated cells without external proline or glutamine in comparison to established osmolytes.

*Viability relative to untreated cells (control) in Jurkat cells exposed to additional 0 or 300 mosmol/l NaCl for 5h (step) or 10h (10h ramp), respectively. Bars indicate mean and SD of at least 3 replicates. Osmolytes were added 60 min before NaCl at indicated concentrations. Error bar represent SD. t-test: *p<0.05, **p<0.01, ***p<0.001, ****p<0.0001, ns=not significant.*

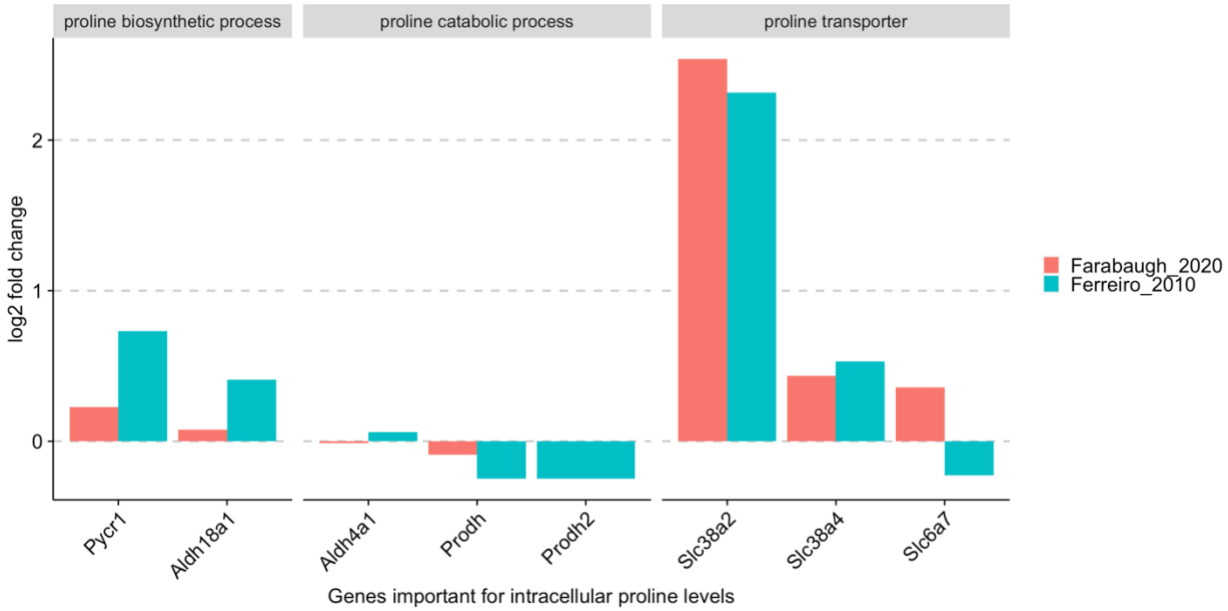

Figure 3.20: Gene expression changes in MEFs is indicative of proline accumulation.

Publicly available data on gene expression of Murine embryonic fibroblasts from RNA Microarray (Ferreiro et al. 2010) *and RNAseq* (Farabaugh et al. 2020) *was analyzed to show changes in genes affecting proline concentration in cells. Bars represent log2 fold change for each gene after 2h step treatment to 200 mosmol/l Nacl (Ferreiro_2010) or 3h step treatment to 200 mosmol/l sucrose (Farabaugh_2020).*

3.4 Discussion

Previous studies have established that acute changes in environmental stimulus concentrations can control cell fate. However, cells in physiological environments may not necessarily experience such acute concentration changes. It is conceivable that typical solute concentration changes are gradual over time with different kinetics (Neuhofer and Beck 2005; Ullrich et al. 1963; Gottschalk and Mylle 1959; Thiemicke et al. 2019). However, there is a limited understanding of how a gradual change of stimulus concentrations affect cellular responses. We investigated stress responses of human immune cells to ramp increases in the concentrations of different osmolytes to address the key question of how varying the kinetics of stimulation affect cellular responses. We

found that in comparison to instantly changing osmolyte concentrations, slow changes protect human immune cells from otherwise deadly insults (Figures 3.1b-d, 3.3). These results indicate that sensitivity to the rate of change of external osmolyte concentrations is a fundamental feature of human cells. These results are important because they demonstrate that immune cells that migrate into and through hypertonic tissues such as renal, intestinal, or epidermal tissue can survive hypertonic conditions better if these changes occur at a low rate over time. These results are consistent with pioneering studies indicating partial protection of renal medullary cells from slowly increasing external osmolytes (Cai, Ferraris, and Burg 2004; Cai et al. 2002a). The authors of these pioneering studies postulate an increase in cell internal organic osmolytes is responsible for protecting cells exposed to gradually increasing osmolyte gradients (Cai, Ferraris, and Burg 2004). Perhaps surprisingly, we found that well-established osmolytes such as betaine, inositol, sorbitol, taurine, or urea do not increase at the end of our experiments (Figure 3.5a). One reason for this observation is likely that kidney cells respond differently to hypertonic stress than immune cells. Another reason is that we quantify cell internal osmolytes at the end of the 10h ramp experiment, whereas the previous study analyzed the response of cells 24h after the ramp treatment. We hypothesize that increases in traditional cell internal osmolytes after 24h may function as a secondary and long-term protection against osmotic stress but are not significant for short term protection. Because the step and ramp conditions do not differentially regulate the concentrations of these osmolytes (Figure 3.5a), we studied the cellular pathways that are important in the regulation of cell viability during hyperosmotic stress. We discovered differential regulation between ramp and step conditions of caspases 3, 8, and 9 (Figure 3.10a-c). In step conditions a large fraction of cleaved caspases is observed, whereas in ramp conditions only a small fraction of cells show cleaved caspases (Figure 3.10a-c). This mechanism enables a population of cells to respond gradually to stresses that change over time without changing the individual cell's ability to undergo apoptosis. It is conceivable that in the kidney or the intestine, immune cells need to adjust not only to the absolute change but also to the rate of change in hypertonicity to avoid apoptosis. A property of an adapting system is to distinguish between a rapid and a slow increase of a stimulus. It has been studied in several important model systems, such as in yeast

osmotic stress response signaling (Muzzey et al. 2009; Granados et al. 2017; Johnson et al. 2020; Goulev et al. 2017), chemotaxis signaling in bacteria (Alon et al. 1999; J. W. Young, Locke, and Elowitz 2013), and mitogen(Albeck, Mills, and Brugge 2013; Sasagawa et al. 2005; Fujita et al. 2010), as well as developmental(Sorre et al. 2014) signaling. These studies demonstrate that differential regulation of cell signaling between step and ramp stimulation might be a universal feature of signal transduction pathways by determining the presence or absence of a response to changes in the environment over time.

To better understand the mechanism of this observation, we analyzed the timing of caspase activation in single cells. We discovered that activated caspase 3 and cleaved PARP increase before activated caspase 8 and 9 (Figure 3.9f). These findings support previous studies demonstrating that activated caspase 3 cleaves PARP (Lazebnik et al. 1994; Kaufmann et al. 1993). This observation is consistent with published studies of apoptosis induction through caspase 9 protein recruitment, but not its cleavage. Recruited caspase 9 then cleaves caspase 3, which subsequently cleaves PARP (Slee et al. 1999; McComb et al. 2019; S. Y. Choi et al. 2013). However, these cell population experiments cannot determine if indeed in a single cell, caspase 3 cleaves PARP and not caspase 8 or 9 (Figure 3.11a-d). To test if indeed caspase 3 cleaves PARP in single cells, we quantified co-stained cells for cleaved caspase 3 and cleaved PARP. Our single-cell analysis demonstrates that PARP gets cleaved before caspase 8 or 9, supporting our results and are consistent with previous cell population studies (Slee et al. 1999; McComb et al. 2019). From these single-cell time-course experiments, we predict that inhibition of caspase signaling in step conditions increases cell viability similar to ramp conditions in single cells (Figure 3.11e). Because PARP activates before caspases 8 and 9, we predict that these caspases do not contribute significantly to cell death. We indeed find that inhibiting caspase 8 or 9 or both together does not improve viability (Figure 3.11e).

To better understand which proteins contribute to differential caspase activation and cell survival, we analyzed changes in protein levels or phosphorylation states of upstream markers for proteins contributing to and indicating stress, growth, pro-apoptosis, anti-apoptosis, inflammation, and DNA damage. We separate these proteins into three groups. In the first group of protein markers of stress (NFAT5, pASK, and HSP70), growth

(Ki67), anti-apoptosis (Bcl-xL), inflammation (IFNg, NLRP3), and DNA damage (BAX, NOXA, and Fas-L) drop rapidly in step but not ramp conditions. These results could indicate that these markers can sense the difference in the type of stress gradient in a switch-like manner, although the dynamics of their distributions do not change overall. The second group of markers, such as proliferation markers p-S6 and p-mTOR and pro-apoptotic protein p-BAD, decrease over time but show no differences between step and ramp conditions relative to the cumulative osmolyte exposure. These results indicate that a strong reduction of these markers is independent of the stress kinetics. The third group of proteins, such as stress signaling (p-MK2, p-JINK, p-MKK4, p-HSP27, p-ATF2, and p-CREB), and the pro-apoptotic protein p-Bcl2 do not show a clear difference between step and ramp treatments given the experimental constraints.

We also investigated the well-established link between osmotic stress and p38 signaling. We observed that p38 phosphorylation and phosphorylation of its target H2AX are also differentially regulated in ramp and step conditions (Figures 3.10e, 3.14). However, inhibition of p38 does not contribute to cell viability improvement as much as caspase inhibition (Figure 3.14b). These results are consistent with previous studies in macrophages where inhibition of stress response pathways such as p38 or JNK does not contribute to caspase signaling (Ip et al. 2015). This large temporal functional screen establishes caspase signaling as the main contributor to differential regulation in step versus ramp stress condition compared to alternative signaling pathways of stress, proliferation, anti-apoptosis, pro-apoptosis, inflammation, and DNA damage.

Together these results indicate that human immune cells can survive shallow gradients to high osmolarity. This protective capability might be important because monocytes need to migrate inside the kidney from the low osmolarity cortex, to the very high osmolarity medulla to prevent bacterial infection (Berry et al. 2017). These results then beg the question of how do cells survive gradients of osmotic stresses that would otherwise be deadly?

We extended our initial analysis of cell internal organic osmolytes to a wide range of metabolites measured in step and ramp conditions. Although we can detect many well-established osmolytes, their concentration is significantly lower than many other

metabolites that we detected (Figures 3.5a, 3.18). Also, none of these osmolytes change significantly in step and ramp conditions (Figure 3.5a, 3.18). Instead, from this analysis, we discovered disproportional proline increases compared to the other amino acids. This disproportional increase for one amino acid excludes differential global protein degradation as a mechanism to increase proline levels (Figure 3.17a, b). Supplementing external proline or one of its precursors, glutamine, protected cells from acute hypertonic stress, similar to stress protection in ramp conditions (Figure 3.17c). Although not well established in mammalian cells, in plants, proline acts as an osmoprotective molecule, and its accumulation is a well-described mechanism applied by plants to endure droughts and other stresses (Szabados and Savouré 2010; Liang et al. 2013). Our results strongly suggest that the accumulation of intracellular proline plays a role in the protection of human immune cells from slowly increasing hypertonicity and the prevention of apoptosis (Figure 3.17c, 3.18).

In summary, we propose a model (Figure 3.17d) in which step increases in hypertonicity activate caspase signaling, PARP cleavage, and cause cell death. Whereas slowly increasing hypertonicity does not activate caspase signaling, but instead causes accumulation of intracellular proline. Proline is known to be upregulated during hypertonic stress in plants and bacteria and to have an osmoprotective function. Proline functions as an organic osmolyte, molecular chaperone, metal chelator, and ROS scavenger independent of caspase activation (Hare and Cress 1997; Szabados and Savouré 2010; Rudolph and Crowe 1985; Csonka 1989). These properties make proline an efficient stress response molecule. We argue that proline may have a yet underestimated critical role in protecting human cells from cell death in hypertonic conditions and could explain how immune cells can survive in microenvironments within the body that have extreme osmolarities that change over time such as the renal papilla or the intestine.

3.5 Methods

Human cell culture

THP1 (ATCC® TIB-202™) cells were cultured at 0.5–1 × 10^6 cells/ml in RPMI 1640 media (Corning, Catalog#: 15-040-CV) containing 10% Heat inactivated FBS (Gibco,

Catalog#: 16140-071), 100 U/ml Penicillin-Streptomycin (Gibco, Catalog#: 15140-122), 2 mM L-alanyl-L-glutamine dipeptide (GlutaMAX™, Gibco, Catalog#: 35050-061) and 0.05 mM 2-Mercaptoethanol (Sigma, Catalog#: M3148) at 37 °C in a 5% CO2 humidity controlled environment. Jurkat cells (Clone E6-1, ATCC® TIB-152™) and PBMCs (Stemcell technologies, Catalog # 70025.1) were cultured at 0.5–1.5 × 10^6 cells/ml in RPMI 1640 media (Corning, Catalog#: 15-040-CV) containing 10% Heat inactivated FBS (Gibco, Catalog#: 16140-071), 100 U/ml Penicillin-Streptomycin (Gibco, Catalog#: 15140-122) and 2 mM L-alanyl-L-glutamine dipeptide (GlutaMAX™, Gibco, Catalog#: 35050-061) at 37 °C in a 5% CO2 humidity controlled environment. Experiments with PMBCs were carried out 30 min after thawing.

Experimental procedure for step and ramp stimuli application

We used a programmable pump (New Era Syringe Pump Systems, NE-1200) to apply gradually increasing (ramp) profiles. In brief, the pumping rate and dispensed volume per interval were calculated as described (Thiemicke et al. 2019) and uploaded to the pump via a computer. A syringe pump driving a syringe (BD™, Catalog#: 309628) filled with 5 M NaCl (Corning, Catalog#: 46-032-CV) solution connected to a needle (Jensen Global, Catalog#: JG21-1.0x) with tubing (Scientific Commodities, Catalog#: BB31695-PE/4). The tubing was inserted into a foam stopper on an autoclaved glass flask (Pyrex, Catalog#: 4980-500) holding the suspension cells. Cells were shaken at 100 rpm during the entire experiment using a CO2 resistant shaker, ensuring proper mixing (Thermo Fisher Scientific, Catalog#: 88881101). For step stimulation, appropriate amount of 5 M NaCl (Corning® 500 mL 5M Sodium Chloride, #46-032-CV) solution was added by a syringe within 5 seconds to reach the desired final concentration. 5 ml of cells were removed with a syringe (BD™, Catalog#: 309628) through autoclaved silicone tubing (Thermo Scientific, Catalog#: 8600-0020) to collect time point samples.

Cell viability assay

We measured cell viability with CellTiterGlo (Promega, Cat.#: G7571). Cells were transferred to a white 96 well plate according to the manufacturer's instructions and equilibrated to room temperature for 10 minutes. We added CellTiterGlo reagent in a ratio

1:8 to cell suspension. Luminescence was measured using a plate reader (Promega, GloMax Discover plate reader, GM3000). Relative viability was calculated by dividing luminescence values for each replicate by mean luminescence of media control for each experiment.

Flow cytometry

We fixed cells with 1.6% formaldehyde (Fisher, Catalog#: F79-4) in a 15 ml falcon tube. We quenched fixation by adding 200 mM Glycine after 8 minutes. Cells were washed with PBS (Corning, Catalog#: 46-013-CM) and permeabilized with Methanol (Fisher, Catalog#: A454-4) for 15 minutes on ice. Cells were washed with PBS and stained with Pacific-Blue NHS ester (Pacific Blue™ Succinimidyl Ester, Thermo Fisher Scientific, #P10163) and Pacific-Orange NHS ester (Pacific Orange™ Succinimidyl Ester, Triethylammonium Salt, Thermo Fisher Scientific, #P30253) for 30 minutes. We blocked cells with 1% BSA (Rpi, Catalog#: A30075-100.0) in PBS. We washed and stained cells with a primary monoclonal antibody for 60 minutes at room temperature. We performed flow cytometry on BD LSRII (five lasers). We listed all antibodies used in this study in Table 3.1.

Antibody target	Site	Manufacturer	Catalog#	Lot
aCasp3		BD	561011	8130555
aCasp9	D315	Cell Signaling	31245S	1
cPARP	D214	BD	558710	5253919
FASL		BD	564261	8174746
IFNγ		BD	561024	7201908
Ki67		BD	561277	7349946
p-Bcl2	S70	BD	562532	8043559
p-CREB	S133	BD	558434	7130853

p-H2Ax	S139	BD	560446	7125854
p-mTOR		BD	563489	8116629
p-S6	S235 236	BD	560435	7160990
p-ZAP70	Y292	BD	558515	7282572
aCasp8	D391	Cell Signaling	12602S	4
BclXl		Cell Signaling	54H6	2
p-ATF2	T71	Cell Signaling	13850S	1
p-BAD	S112	Cell Signaling	11865S	2
p-HSP27	S82	Cell Signaling	11892S	3
p-JNK	T183/Y185	Cell Signaling	9257	29
p-MK2	T334	BD	562472	8156894
p-MKK4	S257	Cell Signaling	59056S	1
p-p38	T180/Y182	Cell Signaling	8632S	3
NLRP3		RD	IC7578N	Adoro118051
BAX		Santa Cruz	Sc-20067	J1316
HSP70		Santa Cruz	Sc-32239	K2818
NFAT5		Santa Cruz	Sc-398171	F0518
NOXA		Santa Cruz	Sc-515840	D0819

p-ASK	S83	Santa Cruz	Sc-166967	D1219

Table 3.1: Antibodies used in this study.

This table lists the antibodies used in this study, binding site of the antibody (if known), the manufacturer of the antibody, the product catalog number and the lot number of the product that was used.

Flow cytometry analysis

We analyzed flow cytometry data with custom R software. We gate the primary cell population on FSC-A vs. SSC-A by using the 'flowcore' package (Meur, Hahne, and Ellis 2007). We debarcoded the cell populations automatically and analyzed the resulting data using custom software in R applying the following packages: 'ggplot2', 'data.table', 'plyr', 'dplyr', 'flowViz', 'flowCore', 'flowStats', 'ggcyto', 'RcppEigen', 'fields', 'ggridges', 'viridis', 'scales' and 'xml2'. The distributions between independent experiments with similar shapes are aligned for their 0 minute time point so that their means are identical. We applied this offset to all the distributions in each experiment. We performed experiments so that the total exposure to NaCl is identical between step and ramp experiments. We

plotted the distributions, and ON-fraction as a function of the cumulative exposure. Plotting data as a function of the cumulative NaCl expose helps to distinguish between changes related to the total NaCl exposure compared to the temporal change in the NaCl concentration.

Inhibitor studies

We listed all inhibitors used in this study in Table 3.2. Inhibitors were dissolved in DMSO and added 30 min before the start of the experiment to the cell culture media at indicated concentrations.

Inhibitor	Manufacturer	Catalog#	target
Z-VAD-FMK	Selleckchem	S7023	pan-caspase
Z-IETD-FMK,	Calbiochem	218759-1mg	Caspase8
Z-LEHD-FMK	BD	550382	Casaspe9
BIRB 796	Sigma-Aldrich	506172-10MG	pan-p38
Q-VD-OPH	BD	563828	pan-caspase
SB 203580	Sigma-Aldrich	559395-10MG	p38α/β
Necrostatin-1	Calbiochem	CAS 4311-88-0	RIPK 1
BI-6C9	Santa Cruz	CAS 791835-21-7	BID

Table 3.2: Inhibitors used in this study.

This table lists the inhibitors used in this study, the manufacturer of the inhibitor, the product catalog number and the targeted protein of the inhibitor.

Targeted Metabolomics Methodology

5 ml of cell suspension were pelleted, the supernatant was removed and resuspended in 90% Methanol. Analysis of metabolites was performed at the Vanderbilt University Mass Spectrometry Research Center using an Acquity UPLC system (Waters, Milford, MA) interfaced with a TSQ Quantum triple-stage quadrupole mass spectrometer (Thermo Scientific, San Jose, CA), using heated electrospray ionization operating in multiple

reaction monitoring (MRM) mode. 500 μl of each cell lysate sample was blown to dryness with N_2 and reconstituted with 150 ul of an Acetonitrile/H_2O (2:1) solution containing stable isotope-labeled internal standards: tyrosine-d_2 and lactate-$^{13}C_3$ (Cambridge Isotope Lab, Tewksbury, MA). Centrifuged the cell lysate at 10,000 g for 20 minutes, and injected 90 μl supernatant into UPLC. We separated the supernatant chromatographically with a Zic-cHILIC column, 3 μm, 150 x 2.1 mm (Merck SeQuant, Darmstadt, Germany) at a flow rate of 300 μl/min. The mobile phases were A) 15 mM ammonium acetate with 0.2% acetic acid in water/acetonitrile (90:10, v/v), and B) 15 mM ammonium acetate with 0.2% acetic acid in acetonitrile/water/methanol (90:5:5, v/v). The gradient was as follows: 0 min, 85%B, 2 min, 85%B, 5 min, 30%B, 9 min, 30%B, 11 min, 85%B, 20 min, 85%B. We set the spray voltage to 5 kV and the capillary and vaporizer temperatures to 300℃ and 185℃, with sheath gas and auxiliary gas set to 60 and 45 psi, respectively. The skimmer offset was -10 V, and the collision energy varied for each transition. Metabolites were identified based on predetermined peaks and elution times. We calculated the response ratio for each detected metabolite relative to the internal standard.

4 FCBapp: An interactive application to automatically debarcode multiplexed flow cytometry datasets

Adapted from:
Thiemicke A and Neuert G. FCBapp: An interactive application to automatically debarcode multiplexed flow cytometry datasets. 2020, in preparation.

4.1 Abstract

Flow cytometry is a powerful method to analyze protein levels in single cells through fluorescently-labeled molecules, such as antibodies. The spectral properties of Flow cytometers allow the measurement of several molecular events simultaneously. In addition, a new powerful method has been developed that allows the parallel analysis of different samples of cells by barcoding them first with dye dilutions unspecifically binding to proteins. The data of these experiments can be complex and demand the investment of significant amounts of time using conventionally available commercial flow cytometry software that often use manual gating. To address these issues, we developed an automated software application that allows the user to load barcoded flow cytometry data into an application, which then automatically debarcodes the data, visualizes the resulting distributions and, enables a threshold-based determination of positive fractions. Thereby, the software makes the data analysis faster than manual gating and results in more objective and reproducible gating. The application can be accessed online through a web browser or can be installed locally as an R package. In conclusion, we present one of the first debarcoding software applications that will improve data analysis of debarcoded flow cytometry data significantly.

4.2 Introduction

Fluorescent cell barcoding (FCB) is a method that was developed to facilitate the use of flow cytometry, to scale it, to reduce variability between samples and to reduce the cost of experiments by using reagents more effectively (Krutzik et al. 2011; Krutzik and Nolan

2006). It was pioneered in the field of phospho-specific flow cytometry (Davies et al. 2016; Skånland 2018; Tsai et al. 2019) and later adapted in immunophenotyping (Giudice et al. 2017; Lekishvili and Campbell 2018; Stam et al. 2011) and intracellular cytokine detection. Recently, it has been used in drug screening (Earl et al. 2018; Krutzik et al. 2008; Spurgeon et al. 2014) and time course studies (Kalland et al. 2011). The strength of FCB is a reduction in variability from antibody staining. Additionally, the time of measuring one sample is significantly reduced, which allows to measure several markers or several samples in parallel.This high-throughput process results in large amounts of data. While flow cytometry is one of the first large scale single cell assays in biomedical research, analysis is still mostly done with software that requires subjective manual input (Aghaeepour et al. 2013; Saeys, Gassen, and Lambrecht 2016). Current manually controlled flow cytometry software requires a lot of time for user input, which subtracts from the time advantage gained by high throughput FCB and potentially introduces human bias (Saeys, Gassen, and Lambrecht 2016).

In the past, several research groups have developed software to computationally analyze flow cytometry data. These studies are foundational for the development of new software, including machine learning algorithms, to identify new populations (Qiu et al. 2011). Despite the more widespread use of FCB, there is so far no complete software that allows automatic computational debarcoding (Tsai et al. 2019).

A similar method to flow cytometry is mass cytometry. Due to the reduction in spectral overlap and fine detection peaks the method can be scaled to measure many more different markers simultaneously even without barcoding. If barcoding is added, the resulting datasets become excessively large and require a lot of processing. It is no surprise that in this younger technology some computational analysis pipelines for barcoding have been developed (Zunder et al. 2015; Hartmann, Simonds, and Bendall 2018). However, these software pipelines are not readily applicable to flow cytometry.

To address this shortcoming, we developed a debarcoding software that provides a graphic user interface on a webhosted server. The software automatically gates for the main population of cells, debarcodes cells stained with two fluorescent labels, plots the debarcoded single cell distributions and enables the determination of an optimal threshold

for the positive population for all timepoints simultaneously to quantify the fraction of activated proteins.

4.3 Implementation and Results

FCBapp is developed in R with Shiny (Winston Chang, Joe Cheng, JJ Allaire , Yihui Xie 2020). It has been deployed at the RStudio Shinyapps.io cloud server and can be easily accessed through the internet accessed using any operating system or browser (https://alexanderthiemicke.shinyapps.io/deploy9). In addition, the app can be used locally by installing it as an R package. To install the app locally, one can simply run the following command in R: devtools::install_github("alexthie/FCBapp5"). This will try to install all the necessary underlying dependent packages and the complete app and allow the same functionality as the web based interactive browser interface, when installed.

The FCBapp allows users to upload data into the FCBapp, adjust gating parameters and visualize the data within the app. The debarcoded data can be downloaded as a .csv file for further analysis. It uses packages such as the flowcore package (Meur, Hahne, and Ellis 2007). The user needs to provide a ‘key’, which is a simple ‘.txt’ file stating the conditions used in the experiment separated by a space. The flow cytometry data should be an ‘.fcs’ file. Figure 4.1 illustrates the workflow and the layout of the user input of the FCBapp.

The software has been tested using Flow Cytometry data from Jurkat cells that we generated ourselves. In a first step, we uploaded the ‘.fcs’ file to the app and set the parameter for the determination of the main cell population (Figure 4.2). In a next step the barcoded fractions are plotted by the intensity of the stained fluorescent dyes. By adjusting the ‘bw’ parameter, one can control the gating process and the demultiplexing of the barcoded samples (Figure 4.3). In the next step, the populations are automatically assigned to the conditions supplied by the key file and shown in a similarly plotted way (Figure 4.4.) .Finally the distributions of each population are plotted over the conditions in the experiment and the positive population (On-fraction) is plotted as a bar plot on the right (Figure 4.5).

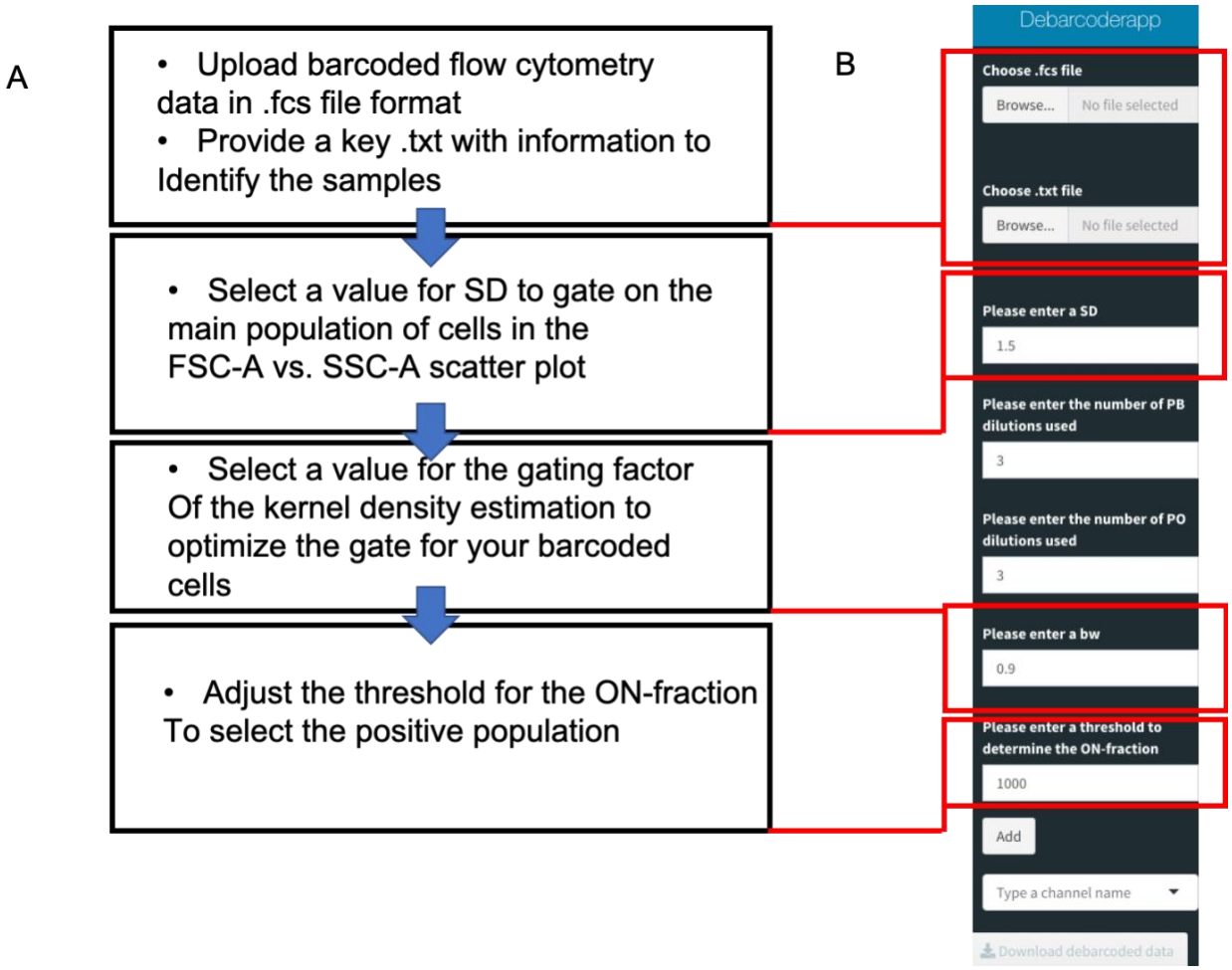

Figure 4.1: Workflow of the FCBapp

A) Upload of data and 'key' file, select parameters, visualize and download the processed data. B) User input interface of FCBapp. The app allows to set a threshold for the gate on the main population and for the determination of a positive fraction.

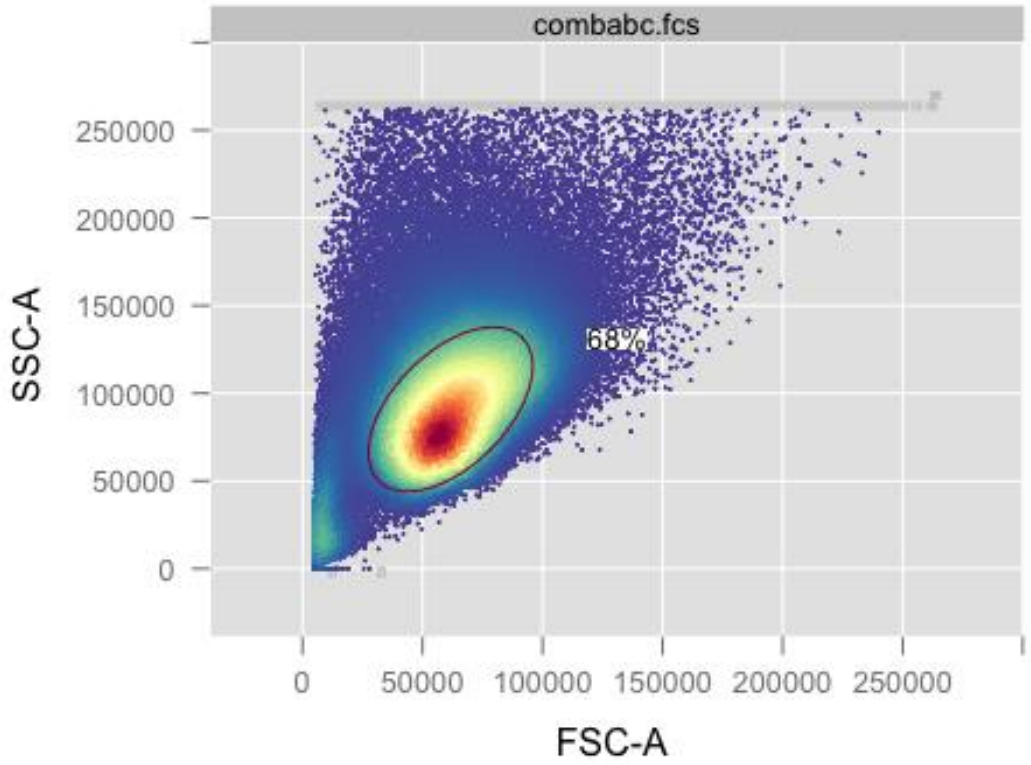

Figure 4.2: Gating using the FCBapp.

After uploading data to the app, the main population can be gated by changing the standard deviation of the bivariate normal distribution. The events collected by the flow cytometer and stored in the '.fcs' file are plotted for the forward vs. sideward scatter. The red circle indicates the gated cells and the number in the plot indicates the percentage gated relative to all events.

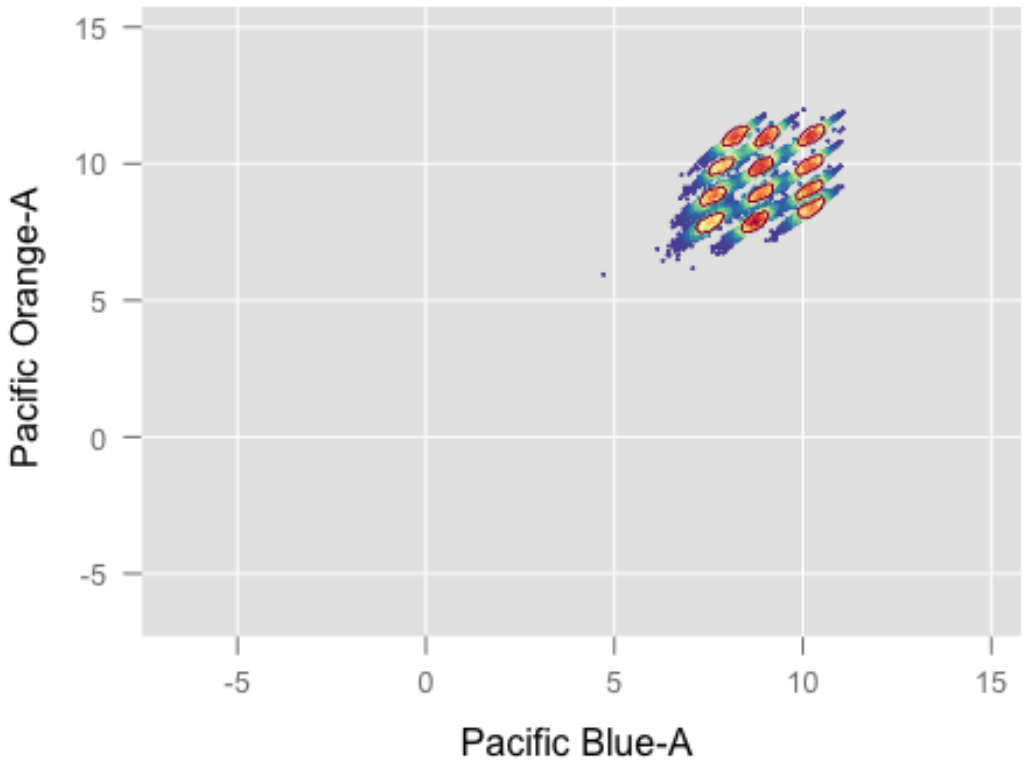

Figure 4.3: Debarcoding of fluorescently labeled cells using the FCBapp.

Jurkat cells are plotted for the intensity of the fluorescent dye labels that were used to achieve the barcoding. The red circles indicate the gates for the individual barcoded cell populations.

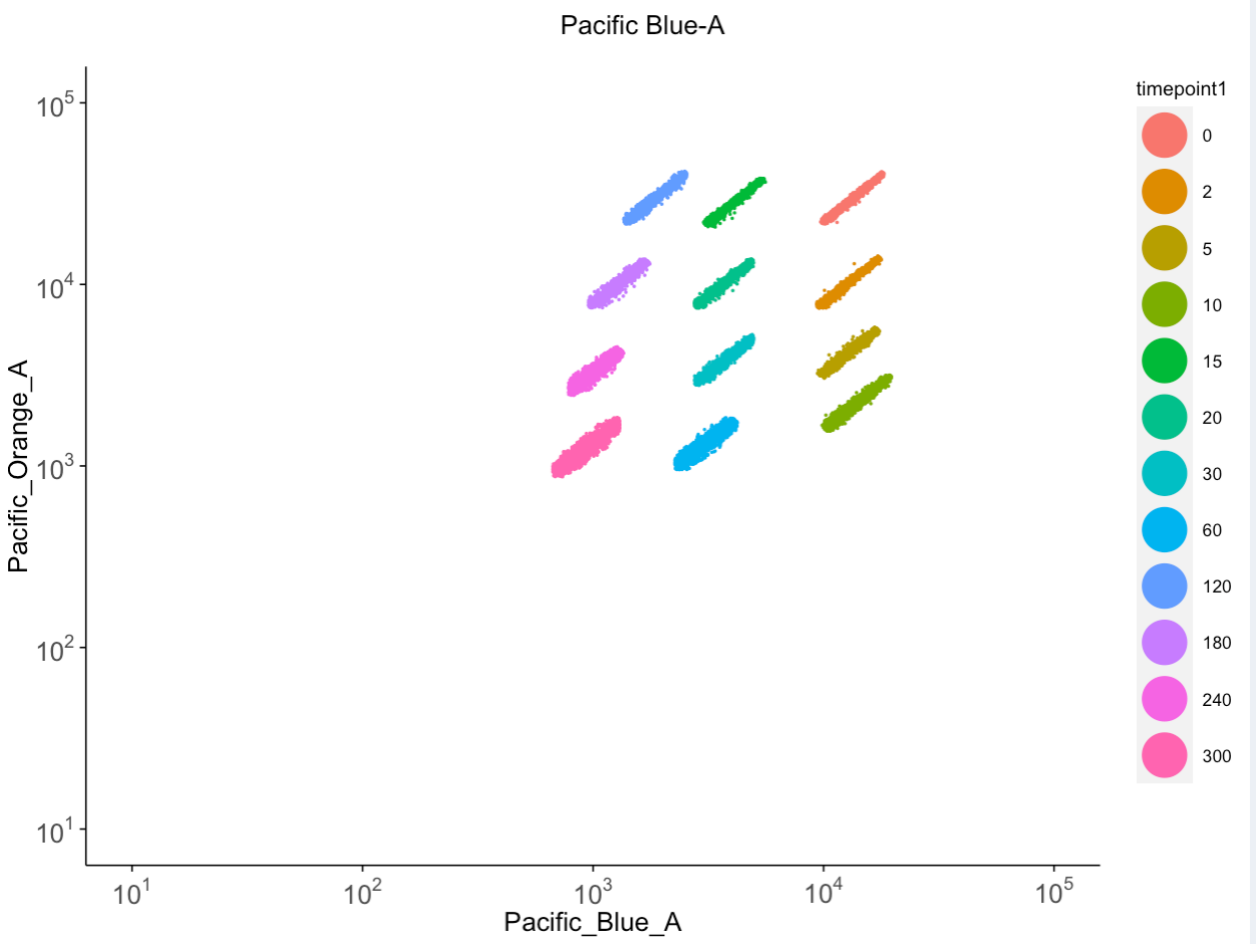

Figure 4.4: The debarcoded populations are assigned to the conditions used in the experiment.

Jurkat cells measured by Flow cytometry are plotted for the intensity of Pacific-Blue and Pacific-Orange. The colors indicate the timepoint samples each population corresponds to.

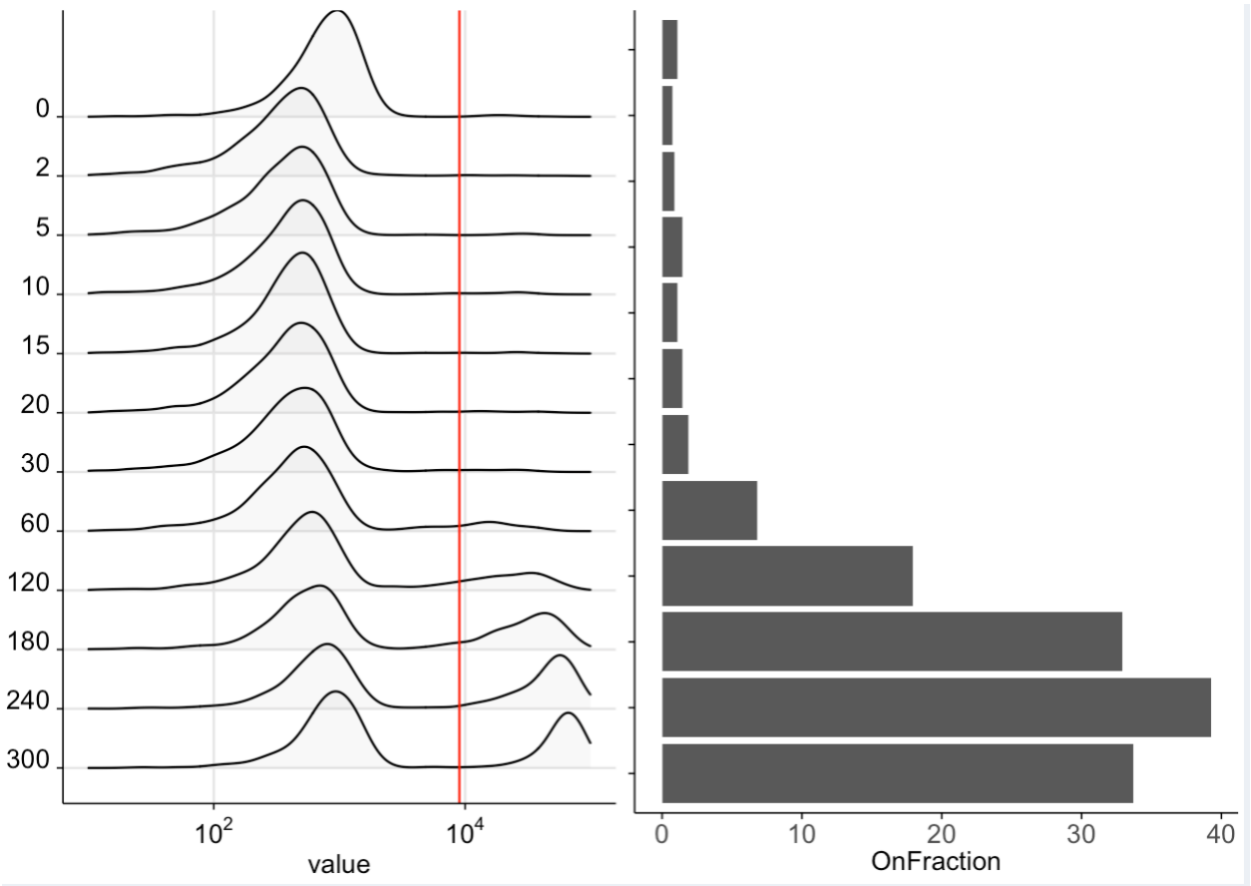

Figure 4.5: Visualizing the distributions of the debarcoded fractions.

The left panel shows the single cell distributions of the debarcoded flow cytometry data. Jurkat cells have been barcoded and stained with an antibody for cleaved PARP, exposed to add. 300 mosmol/l NaCl and fixed at timepoints indicated on the y-axis (min). The red line represents the threshold for the 'OnFraction' that can be controlled by the app. The right panel represents the 'OnFraction' as percentage of positively stained cells for each population.

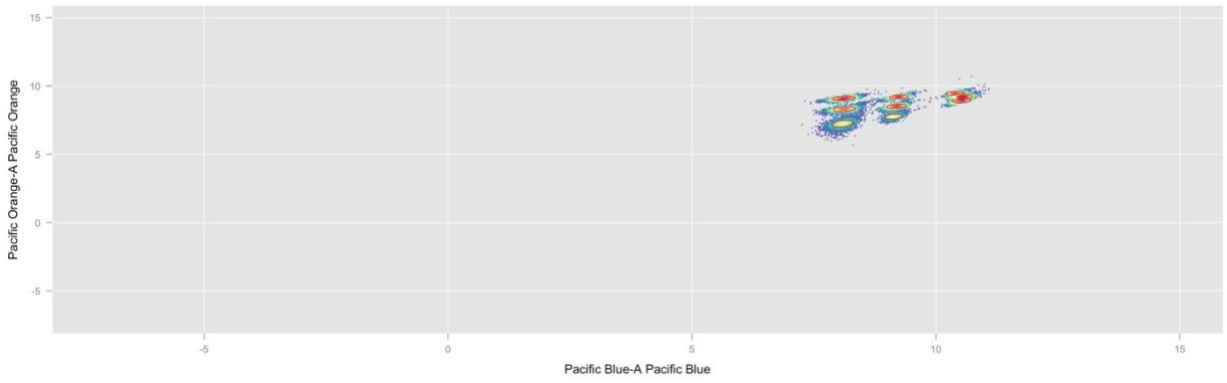

Figure 4.6: Sample data from the Flowrepository debarcoded by the FCBapp. *Screenshot of the FCBapp interface showing flow cytometry data of PBMCs deposited by the authors of Davies et al.* (Davies et al. 2016) *that has been automatically debarcoded using the FCBapp.*

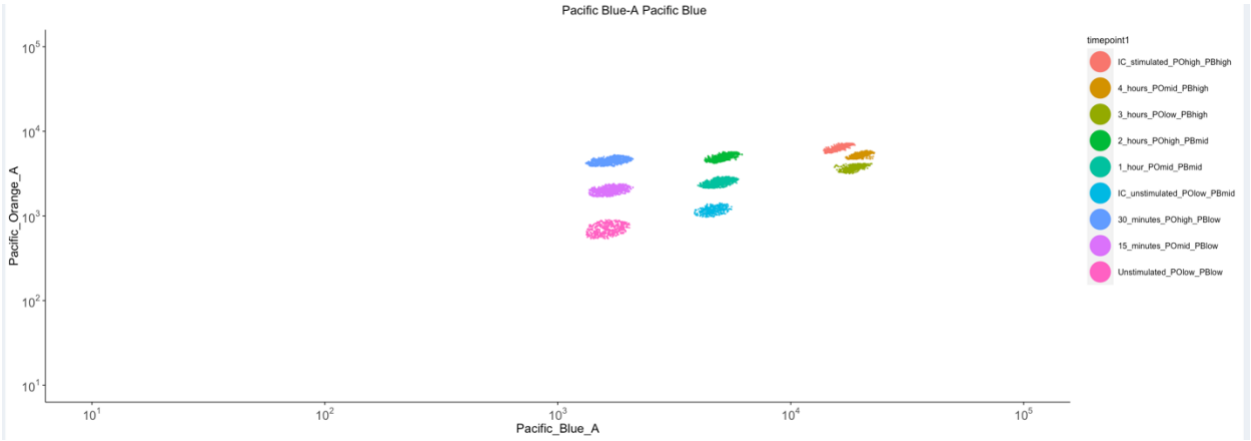

Figure 4.7: Assigning conditions to the Sample data from the Flowrepository. *Screenshot of the FCBapp interface showing the assignment of flow cytometry data of PBMCs deposited by the authors of Davies et al.* (Davies et al. 2016) *to the conditions used in the respective experiments as given in the uploaded key file.*

We aimed to test the software with publicly available data. To demonstrate the feasibility of the FCBapp, we tested the software on a publicly available dataset (Davies et al. 2016) that was deposited to the flowrepository (Spidlen et al. 2012). We downloaded the data, uploaded it to the FCBapp and generated a key file giving the conditions used in the experiment. Figure 4.6 shows the debarcoding result of the PBMC data from the publicly available dataset (Davies et al. 2016). The debarcoded populations are then assigned to the treatment conditions used in the experiment (Figure 4.7). The debarcoded data can then be visualized as distributions in the app and downloaded as a '.csv' file for further analysis. This approach shows that the FCBapp is able to debarcode new data from different cells (PBMCs vs. Jurkat cells) and a different number of barcoded populations (9 vs. 12).

4.4 Discussion

Big data flow cytometry data sets are more frequently generated due the development of methods such as FCB. Flow cytometry barcoding methods are more commonly used, but there is no software that automatically processes and deconvolutes the barcoded cell data. The software presented here was used in our own studies and provides a simple and accessible graphical interface. We expect the software to accelerate the analysis of Fluorescent cell barcoding in the application of various approaches of the method.

5 Conclusions and Future directions

5.1 Conclusions

In our approach we aimed to identify the response of human cells to additional NaCl concentrations and under which kinetic profiles cells are able to tolerate these. To do this, we developed a experimental setup that allows to grow cells under cell culture conditions and expose them to kinetic profiles of temporally-variable changes in osmolyte concentration. We identify a ramp duration above which human cells are able to survive high hypertonic NaCl concentrations. We elucidate the molecular response of many key markers of cell state and find that some markers are correlated with the cumulative exposure or the concentration, while others are differentially regulated between step and ramp exposure. We find that caspases 3, 8 and 9, as well as cPARP are only activated in step, but not in ramp exposure. We identify transient p38 activation in step but find that p38 does not get activated during a 10h ramp, despite reaching the same additional NaCl concentration. Lastly, we show for the first time that human cells accumulate proline during hypertonic stress and can be protected by proline. Exposure to a slow 10h ramp significantly increases the accumulation of proline.

5.2 Future directions

5.2.1 Morphological changes and Protein aggregation in hypertonic stress in step and ramp

Dehydration of proteins changes their conformation and can cause aggregation or phase separation (Boeynaems et al. 2018). Phase separation is a transient and reversible process, while protein aggregation may be more prolonged. Recent studies have found a link between cell shrinkage induced dehydration and a change in protein organization in the cell which results in a reversible phase separation of some proteins (Jalihal et al. 2019; Alexandrov et al. 2019).

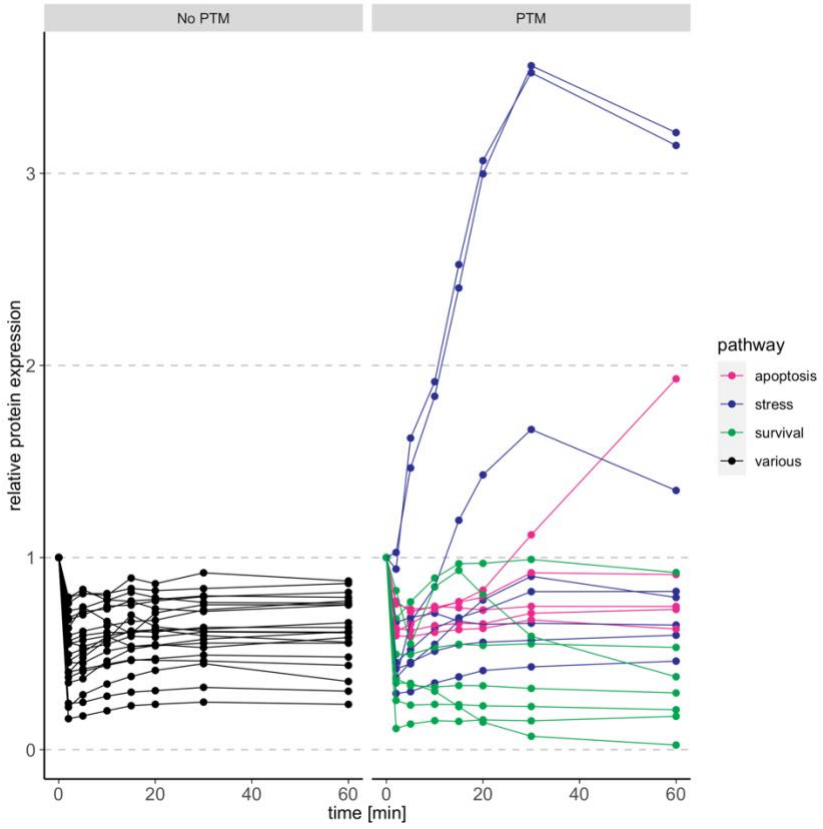

Figure 5.1: Response of proteins with and without posttranslational modifications

Flow cytometry data on protein markers expressed in a step exposure to 300 mosmol/l NaCl.

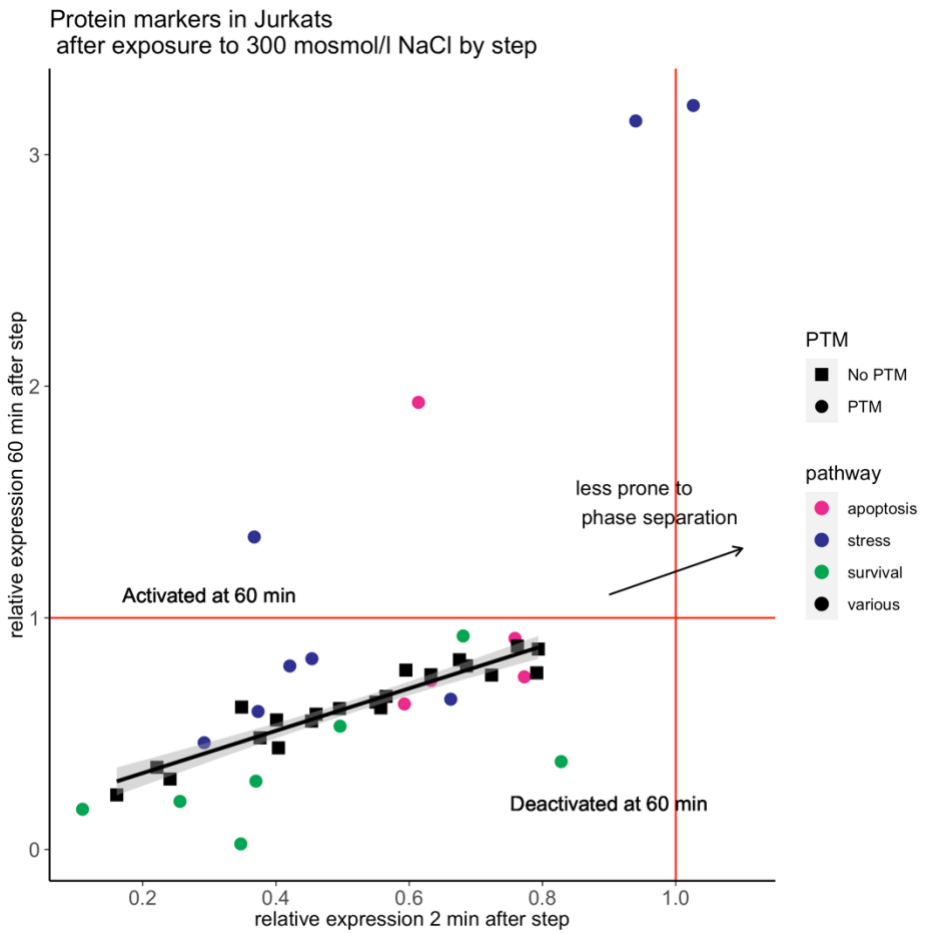

Figure 5.2: Expression of proteins markers relative to non-modified proteins

Flow cytometry data on protein markers expressed in a step exposure to 300 mosmol/l NaCl.

Proteins are affected by the dehydration stress of the hypertonic shock. As data in Figure 5.1 and 5.2 indicate the detected signal for the proteins generally decreases quickly after addition of the step NaCl. This decrease may be caused by a protein aggregation or phase separation that sterically prevents antibody binding. There is a difference in this decrease among the different proteins indicating a different response to dehydration. Further studies should test, if the supposed aggregation or phase separation is transient or prolonged.

5.2.2 Redefining the role and significance of proline in evolution, metabolism and disease

Proline is a proteinogenic amino acid present in the proteins of all forms of life. It's chemical properties as an imino acid have earned it a special role in structural biology as a helix breaker (Christgen and Becker 2019). Free L-Proline has particular properties that enable it to stabilize protein folds, chelate ions, scavenge ROS, stabilize the membrane and function as an organic osmolyte (Chattopadhyay et al. 2004; Yancey 2005; Krishnan, Dickman, and Becker 2008; Dandage et al. 2015; Ignatova and Gierasch 2006; Fisher 2006). All of these properties qualify proline as an ideal osmostress protectant.

It should therefore not be surprising that proline has been found to play a role in the osmotic stress response in many diverse species. Proline is important for the survival of bacteria in hyperosmotic stress (Brill et al. 2011) and has been found to play a role in the osmotic stress response in yeast (Takagi 2008). It also may be important in the virulence of bacteria (Christgen and Becker 2019; Wood 2011). Proline accumulates especially in plants as an adaptation to potential drought environments that plants evolved to survive in (Ashraf and Foolad 2007; Verbruggen and Hermans 2008). An interesting resulting question is, why did plants that accumulated proline, instead of a combination of or any other osmoprotective molecules did so much better throughout evolution? A possible reason is, that proline due its properties as a membrane and protein fold stabilizer, ROS and ion scavenger and, neutral osmolyte, is the best fit organic compound at the lowest metabolic cost to ensure the evolutionary advantage (Liang et al. 2013).

Proline as a molecule and its biosynthetic enzymes are evolutionarily conserved since the early stages of life (Fichman et al. 2015). In animals, proline has so far only been identified as a protective molecule during freezing stress (Rudolph and Crowe 1985). Animal cells did not have to adapt to survive extreme drought such as plants to confer an evolutionary advantage. The local changes in osmolarity are not as drastic and not as threatening as for an immobilized plant. Therefore, the level of proline needed to protect a cell from hypertonic stress is likely much lower.

As outlined in the introduction, chapter 1, the predominant opinion in human physiology has been that hypertonicity cannot persist in the human body. Studies investigating changes in osmolytes have therefore almost exclusively focused on kidney cells. Only recently, more studies are investigating the change of metabolite levels in other human tissues (Kitada et al. 2017; U. Y. Choi et al. 2020). For instance, it was recently found that proline becomes the most abundant amino acid in human cells infected with herpes virus (U. Y. Choi et al. 2020). The authors of this study argue that the virus is able to modify cellular metabolism to specifically accumulate proline. These changes then benefit the survival of their host and contribute to tumorigenesis.

In our own study (Chapter 3), we can demonstrate that proline accumulates in the cells and that proline protects cells during hypertonic stress. That amino acids are needed as osmolytes in hypertonic stress has been suggested for murine embryonic fibroblasts (Farabaugh et al. 2020; Krokowski et al. 2015; Ferreiro et al. 2010; Garcia-Perez and Burg 1991). These data show, the amino acid transporter is one of the most strongly and consistently upregulated genes in hypertonic stress (Farabaugh et al. 2020; Ferreiro et al. 2010). In addition, the data in these studies show an upregulation of collagenases and proline biosynthetic enzymes. In combination, the expression of these proteins may cause an intracellular accumulation of proline. Hypertonic stress has been shown to activate JNK which in turn contributes to the expression of collagenases (D. Q. Li et al. 2004).

Collagen is the main part of the extracellular matrix (ECM) and the most abundant protein (25% of all protein) in the body (James M. Phang et al. 2015). Proline and hydroxyproline in turn make up about 25% of the amino acid component of collagen. (W. Liu et al. 2015a), resulting in collagen-bound proline to make up about 6.25% of all amino acids in the body. This is in addition to free L-proline and proline bound in any other protein. This means there is a substantial amount of proline in the human body and It has been postulated that this proline storage is comparable in its relevance to the storage of glucose in glycogen and the storage of fatty acids in adipocytes (James M. Phang et al. 2015). This indicates that proline is an important molecule for the body and that together with the evidence cited above, proline as a molecule can serve as an osmostress-protectant in cells. It may be abundantly available in tissue through the degradation of

collagen and subsequently similarly effective as its function in bacteria and plant cells. Further studies need to test and confirm these relationships *in vitro* and *in vivo.*

An additional example is the skin. With age, sodium content and hypertonicity may increase in the skin (Kopp et al. 2013b). The skin consists of different layers with varying sodium contents that create sodium gradients (Nikpey et al. 2017). At the same time skin collagen, a store of proline, is known to decrease with age (Varani et al. 2006; Baumann 2007). Skin ageing is believed to be predominantly influenced by UV damage (Fligiel et al. 2003). The associated stresses contribute to the degradation of collagen. While this is a well-established anti-correlation, the same relationship is found in intrinsically aged (not damaged by UV light) skin (Jin et al. 2001). The effect of sodium deposition in the skin on collagen levels and skin aging is yet insufficiently understood but may reveal important insights on skin aging and the role of collagen in osmotic and stress protection in the skin.

Proline is metabolized by proline oxidase (POX/PRODH) to Pyrroline-5-Carboxylate (P5C). POX/PRODH is inhibited by lactate (Kowaloff et al. 1977) which contributes to a systemic correlation of proline and lactate. Lactate accumulates in conditions where anerobic glycolysis is favored to oxidative phosphorylation, such as in active muscle tissue or in cancer. Cancer cells or the cells in cancerous tissue are often thought of as being hypoxic which contributes to a shift from oxidative phosphorylation to glycolysis, also known as the Warburg effect (Warburg 1956; Heiden, Cantley, and Thompson 2009; Hamraz et al. 2020). POX/PRODH is coupled to the electron transport chain by supplying reducing agents, NADH and FADH2. Under conditions of low oxygen and high lactate, this reaction is suppressed and contributes to an accumulation of proline. The metabolism and activity of proline metabolic enzymes have been attributed to play a role in human stress response and contribute to tumor cell growth and survival (James M. Phang, Liu, and Zabirnyk 2010; James M. Phang, Pandhare, and Liu 2008; James M. Phang 2019, 1985; W. Liu et al. 2015b). An important function of these metabolic enzymes is that they regulate the redox balance in the cell (James M. Phang 1985). Several recent studies demonstrate that proline has several benefits to cancer cell growth (D'Aniello et al. 2020; Sahu et al. 2016). It can be imported and used as a nutrient (Y. Liu et al. 2020), play a role in metastasis formation (Elia et al. 2017) or in tumorigenesis in virus driven cancers (U. Y. Choi et al. 2020). A key regulator in establishing suppression of POX/PRODH

expression in cancer may be the oncogene MYC (W. Liu et al. 2012). The ECM or collagen, which serves as a proline reservoir, has also been found to be important to cancer survival (Gouirand and Vasseur 2018; Olivares et al. 2017).

Recent evidence, including the ones provided in this study suggest that proline as a molecule plays a critical role in cancer survival, growth and progression. Proline can get imported through amino acid channels that are overexpressed in hypertonic stress (Farabaugh et al. 2020) and cancer (Lieu et al. 2020).

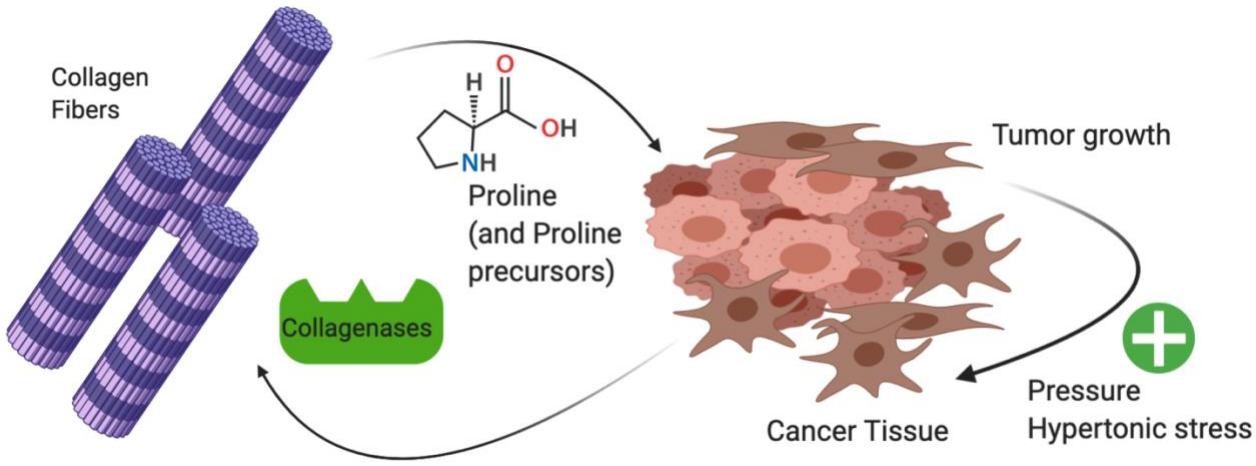

Figure 5.3: Proline supply affects tumor growth in the microenvironment

Collagen, proline, cancer axis outlines a potential future direction. In this model collagen serves as a reservoir for proline which is an osmoprotectant. A cancer growing in a hyperosmolar environment due to growth pressure and metabolism secretes collagenases, takes up proline (by overexpressed protein transporters) and uses proline as cytoprotectant and nutrient. Such a model suggests that proline metabolism is a key target for cancer therapy.

This makes proline and its metabolism (James M. Phang et al. 2015; James Ming Phang et al. 2012a; Ding et al. 2020) a new focused target in cancer therapy (Tanner, Fendt, and Becker 2018). Current approaches on targeting the metabolism seem to be promising in preventing tumor growth (Luengo, Gui, and Vander Heiden 2017). A recent data based model suggests that inhibiting proline synthesis and lipogenesis could be

sufficient to suppress tumor growth as well (M. Liu et al. 2020). Unfortunately, there are no good drugs available yet that inhibit these enzymes. However, they are actively being developed (Tanner, Fendt, and Becker 2018; Zeng et al. 2017; Milne et al. 2019)

References

Abderrazak, Amna, Tatiana Syrovets, Dominique Couchie, Khadija El Hadri, Bertrand Friguet, Thomas Simmet, and Mustapha Rouis. 2015. “NLRP3 Inflammasome: From a Danger Signal Sensor to a Regulatory Node of Oxidative Stress and Inflammatory Diseases.” *Redox Biology* 4 (April): 296–307. https://doi.org/10.1016/J.REDOX.2015.01.008.

Adewola, Adeola F., Dongyoung Lee, Tricia Harvat, Javeed Mohammed, David T. Eddington, Jose Oberholzer, and Yong Wang. 2010. “Microfluidic Perifusion and Imaging Device for Multi-Parametric Islet Function Assessment.” *Biomedical Microdevices* 12 (3): 409–17. https://doi.org/10.1007/s10544-010-9398-1.

Adler, Miri, and Uri Alon. 2018. “Fold-Change Detection in Biological Systems.” *Current Opinion in Systems Biology* 8 (April): 81–89. https://doi.org/10.1016/J.COISB.2017.12.005.

Aghaeepour, Nima, Greg Finak, Holger Hoos, Tim R. Mosmann, Ryan Brinkman, Raphael Gottardo, Richard H. Scheuermann, et al. 2013. “Critical Assessment of Automated Flow Cytometry Data Analysis Techniques.” *Nature Methods* 10 (3): 228–38. https://doi.org/10.1038/NMETH.2365.

Albeck, John G., Gordon B. Mills, and Joan S. Brugge. 2013. “Frequency-Modulated Pulses of ERK Activity Transmit Quantitative Proliferation Signals.” *Molecular Cell* 49 (2): 249–61. https://doi.org/10.1016/j.molcel.2012.11.002.

Alberts, Bruce, Alexander Johnson, Julian Lewis, David Morgan, and Martin Raff. 2015. *Molecular Biology of The Cell*. 6th ed. Garland Science.

Alexandrov, Alexander I., Erika V. Grosfeld, Alexander A. Dergalev, Vitaly V. Kushnirov, Roman N. Chuprov-Netochin, Pyotr A. Tyurin-Kuzmin, Igor I. Kireev, Michael D. Ter-Avanesyan, Sergey V. Leonov, and Michael O. Agaphonov. 2019. “Analysis of Novel Hyperosmotic Shock Response Suggests ‘Beads in Liquid’ Cytosol Structure.” *Biology Open* 8 (7). https://doi.org/10.1242/bio.044529.

Allen, Richard D., and Yutaka Naitoh. 2002. “Osmoregulation and Contractile Vacuoles of Protozoa.” *International Review of Cytology* 215 (January): 351–78. https://doi.org/10.1016/S0074-7696(02)15015-7.

Allison, Susan J. 2019. “Immune Topology of the Human Kidney.” *Nature Reviews Nephrology* 15 (12): 729–729. https://doi.org/10.1038/s41581-019-0223-7.

Alon, U, M G Surette, N Barkai, and S Leibler. 1999. “Robustness in Bacterial Chemotaxis.” *Nature* 397 (6715): 168–71. https://doi.org/10.1038/16483.

Andres-Hernando, Ana, Miguel A. Lanaspa, Nanxing Li, Christina Cicerchi, Carlos Roncal-Jimenez, Glenn H. Cantor, Victor Sorribas, Christopher J. Rivard, and Tomas Berl. 2010. “Effects of 2-Bromoethanamine on TonEBP Expression and Its Possible Role in Induction of Renal Papillary Necrosis in Mice.” *Toxicological Sciences* 118 (2): 510–20. https://doi.org/10.1093/toxsci/kfq261.

Aramburu, José, Katherine Drews-Elger, Anaïs Estrada-Gelonch, Jordi Minguillón, Beatriz Morancho, Verónica Santiago, and Cristina López-Rodríguez. 2006. “Regulation of the Hypertonic Stress Response and Other Cellular Functions by the Rel-like Transcription Factor NFAT5.” *Biochemical Pharmacology* 72 (11): 1597–1604. https://www.sciencedirect.com/science/article/pii/S0006295206004175#bib10.

Ashraf, M., and M.R. Foolad. 2007. “Roles of Glycine Betaine and Proline in Improving Plant Abiotic Stress Resistance.” *Environmental and Experimental Botany* 59 (2): 206–16. https://doi.org/10.1016/J.ENVEXPBOT.2005.12.006.

Atherton, J. C., M. A. Hai, and S. Thomas. 1968. “Effects of Water Diuresis and Osmotic (Mannitol) Diuresis on Urinary Solute Excretion by the Conscious Rat.” *The Journal of Physiology* 197 (2): 395–410. https://doi.org/10.1113/jphysiol.1968.sp008566.

Babazadeh, Roja, Caroline Beck Adiels, Maria Smedh, Elzbieta Petelenz-Kurdziel, Mattias Goksör, Stefan Hohmann, S Hohmann, et al. 2013. “Osmostress-Induced Cell Volume Loss Delays Yeast Hog1 Signaling by Limiting Diffusion Processes and by Hog1-Specific Effects.” Edited by Michael Polymenis. *PLoS ONE* 8 (11): e80901. https://doi.org/10.1371/journal.pone.0080901.

Baetica, Ania-Ariadna, Alexandra Westbrook, and Hana El-Samad. 2019. “Control Theoretical Concepts for Synthetic and Systems Biology.” *Current Opinion in Systems Biology* 14 (April): 50–57. https://doi.org/10.1016/J.COISB.2019.02.010.

Bansal, A., C. Li, F. Xin, A. Duemler, W. Li, C. Rashid, M. S. Bartolomei, and R. A. Simmons. 2019. “Transgenerational Effects of Maternal Bisphenol: A Exposure on

Offspring Metabolic Health." *Journal of Developmental Origins of Health and Disease* 10 (2): 164–75. https://doi.org/10.1017/S2040174418000764.

Barbaro, Natalia R., Jason D. Foss, Dmytro O. Kryshtal, Nikita Tsyba, Shivani Kumaresan, Liang Xiao, Raymond L. Mernaugh, et al. 2017. "Dendritic Cell Amiloride-Sensitive Channels Mediate Sodium-Induced Inflammation and Hypertension." *Cell Reports* 21 (4): 1009–20. https://doi.org/10.1016/j.celrep.2017.10.002.

Barrett, Tristan, Frank Riemer, Mary A. McLean, Josh Kaggie, Fraser Robb, James S. Tropp, Anne Warren, et al. 2018. "Quantification of Total and Intracellular Sodium Concentration in Primary Prostate Cancer and Adjacent Normal Prostate Tissue With Magnetic Resonance Imaging." *Investigative Radiology* 53 (8): 450–56. https://doi.org/10.1097/RLI.0000000000000470.

Baumann, L. 2007. "Skin Ageing and Its Treatment." *Journal of Pathology*. John Wiley & Sons, Ltd. https://doi.org/10.1002/path.2098.

Behar, Marcelo, Nan Hao, Henrik G. Dohlman, and Timothy C. Elston. 2008. "Dose-to-Duration Encoding and Signaling beyond Saturation in Intracellular Signaling Networks." Edited by Rama Ranganathan. *PLoS Computational Biology* 4 (10): e1000197. https://doi.org/10.1371/journal.pcbi.1000197.

Bennett, Matthew R., Wyming Lee Pang, Natalie A. Ostroff, Bridget L. Baumgartner, Sujata Nayak, Lev S. Tsimring, and Jeff Hasty. 2008. "Metabolic Gene Regulation in a Dynamically Changing Environment." *Nature* 454 (7208): 1119–22. https://doi.org/10.1038/nature07211.

Bernard, Claude. 1859. *Lecons Sur Les Proprietes Physiologiques et Les Alterations Pathologiques Des Liquides de l'Organisme.*

Berry, Miriam R., Rebeccah J. Mathews, John R. Ferdinand, Chenzhi Jing, Kevin W. Loudon, Elizabeth Wlodek, Thomas W. Dennison, Christoph Kuper, Wolfgang Neuhofer, and Menna R. Clatworthy. 2017. "Renal Sodium Gradient Orchestrates a Dynamic Antibacterial Defense Zone." *Cell* 170 (5): 860-874.e19. https://doi.org/10.1016/j.cell.2017.07.022.

Beusecum, Justin P Van, Natalia R Barbaro, Zoe McDowell, Luul A Aden, Liang Xiao, Arvind K Pandey, Hana A Itani, Lauren E Himmel, David G Harrison, and Annet

Kirabo. 2019. “High Salt Activates CD11c+ Antigen-Presenting Cells via SGK (Serum Glucocorticoid Kinase) 1 to Promote Renal Inflammation and Salt-Sensitive Hypertension.” *Hypertension (Dallas, Tex. : 1979)*, July, HYPERTENSIONAHA11912761. https://doi.org/10.1161/HYPERTENSIONAHA.119.12761.

Block, S. M., J. E. Segall, and H. C. Berg. 1983. “Adaptation Kinetics in Bacterial Chemotaxis.” *Journal of Bacteriology* 154 (1): 312–23. https://doi.org/10.1128/jb.154.1.312-323.1983.

Boeynaems, Steven, Simon Alberti, Nicolas L. Fawzi, Tanja Mittag, Magdalini Polymenidou, Frederic Rousseau, Joost Schymkowitz, et al. 2018. “Protein Phase Separation: A New Phase in Cell Biology.” *Trends in Cell Biology*. Elsevier Ltd. https://doi.org/10.1016/j.tcb.2018.02.004.

Brancho, Deborah, Nobuyuki Tanaka, Anja Jaeschke, Juan-Jose Ventura, Nyaya Kelkar, Yoshinori Tanaka, Masanao Kyuuma, Toshikazu Takeshita, Richard A Flavell, and Roger J Davis. 2003. “Mechanism of P38 MAP Kinase Activation in Vivo.” *Genes & Development* 17 (16): 1969–78. https://doi.org/10.1101/gad.1107303.

Brewster, J. L, T de Valoir, N. D Dwyer, E Winter, and M. C Gustin. 1993. “An Osmosensing Signal Transduction Pathway in Yeast.” *Science* 259 (5102): 1760–63. https://doi.org/10.1126/science.7681220.

Brewster, Jay L, and Michael C Gustin. 2014. “Hog1: 20 Years of Discovery and Impact.” *Science Signaling* 7 (343): re7. https://doi.org/10.1126/scisignal.2005458.

Brill, Jeanette, Tamara Hoffmann, Monika Bleisteiner, and Erhard Bremer. 2011. “Osmotically Controlled Synthesis of the Compatible Solute Proline Is Critical for Cellular Defense of Bacillus Subtilis against High Osmolarity.” *Journal of Bacteriology* 193 (19): 5335–46. https://doi.org/10.1128/JB.05490-11.

Brocker, C, D C Thompson, and V Vasiliou. 2012. “The Role of Hyperosmotic Stress in Inflammation and Disease.” *Biomol Concepts* 3 (4): 345–64. https://doi.org/10.1515/bmc-2012-0001.

Broe, Marc E. De, and Monique M. Elseviers. 2009. “Over-the-Counter Analgesic Use.” *Journal of the American Society of Nephrology*. American Society of Nephrology.

https://doi.org/10.1681/ASN.2008101097.

Bunge, Frank, Sander van den Driesche, and Michael J Vellekoop. 2017. “Microfluidic Platform for the Long-Term On-Chip Cultivation of Mammalian Cells for Lab-On-A-Chip Applications.” *Sensors (Basel, Switzerland)* 17 (7). https://doi.org/10.3390/s17071603.

Burg, Maurice B., Eugene D. Kwon, and Dietmar KÜltz. 1997. “REGULATION OF GENE EXPRESSION BY HYPERTONICITY.” *Annual Review of Physiology* 59 (1): 437–55. https://doi.org/10.1146/annurev.physiol.59.1.437.

Burg, Maurice B, Joan D Ferraris, and Natalia I Dmitrieva. 2007. “Cellular Response to Hyperosmotic Stresses.” *Physiological Reviews* 87 (4): 1441–74. https://doi.org/10.1152/physrev.00056.2006.

Bush, Peter G., Peter D. Hodkinson, Georgina L. Hamilton, and Andrew C. Hall. 2005. “Viability and Volume of in Situ Bovine Articular Chondrocytes - Changes Following a Single Impact and Effects of Medium Osmolarity.” *Osteoarthritis and Cartilage* 13 (1): 54–65. https://doi.org/10.1016/j.joca.2004.10.007.

Bustamante, Mauro, Frank Roger, Marie-Luce Bochaton-Piallat, Giulio Gabbiani, Pierre-Yves Martin, and Eric Féraille. 2003. “Regulatory Volume Increase Is Associated with P38 Kinase-Dependent Actin Cytoskeleton Remodeling in Rat Kidney MTAL.” *American Journal of Physiology-Renal Physiology* 285 (2): F336–47. https://doi.org/10.1152/ajprenal.00003.2003.

Caen, Ouriel, Heng Lu, Philippe Nizard, and Valerie Taly. 2017. “Microfluidics as a Strategic Player to Decipher Single-Cell Omics?” *Trends in Biotechnology*. https://doi.org/10.1016/j.tibtech.2017.05.004.

Cai, Qi, Joan D Ferraris, and Maurice B Burg. 2004. “Greater Tolerance of Renal Medullary Cells for a Slow Increase in Osmolality Is Associated with Enhanced Expression of HSP70 and Other Osmoprotective Genes.” *American Journal of Physiology. Renal Physiology* 286 (1): F58--67. https://doi.org/10.1152/ajprenal.00037.2003.

Cai, Qi, Luis Michea, Peter Andrews, Zheng Zhang, Gerson Rocha, Natalia Dmitrieva, and Maurice B. Burg. 2002a. “Rate of Increase of Osmolality Determines Osmotic Tolerance of Mouse Inner Medullary Epithelial Cells.” *American Journal of*

Physiology. Renal Physiology 283 (4): F792–98. https://doi.org/10.1152/ajprenal.00046.2002.

———. 2002b. “Rate of Increase of Osmolality Determines Osmotic Tolerance of Mouse Inner Medullary Epithelial Cells.” *American Journal of Physiology-Renal Physiology* 283 (4): F792–98. https://doi.org/10.1152/ajprenal.00046.2002.

Cannon, Walter Bradford. 1932. *The Wisdom of the Body*.

Cano, Eva, and Louis C. Mahadevan. 1995. “Parallel Signal Processing among Mammalian MAPKs.” *Trends in Biochemical Sciences* 20 (3): 117–22. https://doi.org/10.1016/S0968-0004(00)88978-1.

Cao, Yangxiaolu, Marc D Ryser, Stephen Payne, Bochong Li, Christopher V Rao, and Lingchong You. 2016. “Collective Space-Sensing Coordinates Pattern Scaling in Engineered Bacteria.” *Cell* 165 (3): 620–30. https://doi.org/10.1016/j.cell.2016.03.006.

Caserta, T. M., A. N. Smith, A. D. Gultice, M. A. Reedy, and T. L. Brown. 2003. “Q-VD-OPh, a Broad Spectrum Caspase Inhibitor with Potent Antiapoptotic Properties.” *APOPTOSIS* 8 (4): 345–52. https://doi.org/10.1023/A:1024116916932.

CHA, JUNG H., SEUNG KYOON WOO, KI H. HAN, YOUNG H. KIM, JOSEPH S. HANDLER, JIN KIM, and H. MOO KWON. 2001. “Hydration Status Affects Nuclear Distribution of Transcription Factor Tonicity Responsive Enhancer Binding Protein in Rat Kidney.” *Journal of the American Society of Nephrology* 12 (11).

Chan, Andrew C., Makio Iwashima, Christoph W. Turck, and Arthur Weiss. 1992. “ZAP-70: A 70 Kd Protein-Tyrosine Kinase That Associates with the TCR ζ Chain.” *Cell* 71 (4): 649–62. https://doi.org/10.1016/0092-8674(92)90598-7.

Chao, Debra T., Gerald P. Linette, Lawrence H. Boise, Lynn S. White, Craig B. Thompson, and Stanley J. Korsmeyer. 1995. “Bcl-XL and Bcl-2 Repress a Common Pathway of Cell Death.” *Journal of Experimental Medicine* 182 (3): 821–28. https://doi.org/10.1084/jem.182.3.821.

Chattopadhyay, Madhab K, Renée Kern, Michel-Yves Mistou, Abhaya M Dandekar, Sandra L Uratsu, and Gilbert Richarme. 2004. “The Chemical Chaperone Proline Relieves the Thermosensitivity of a DnaK Deletion Mutant at 42 Degrees C.” *Journal of Bacteriology* 186 (23): 8149–52. https://doi.org/10.1128/JB.186.23.8149-

8152.2004.

Cheung, Chris Yk, and Ben Cb Ko. 2013. “NFAT5 in Cellular Adaptation to Hypertonic Stress - Regulations and Functional Significance.” *Journal of Molecular Signaling* 8 (1): 5. https://doi.org/10.1186/1750-2187-8-5.

Chevrier, Stéphane, Jacob Harrison Levine, Vito Riccardo Tomaso Zanotelli, Karina Silina, Daniel Schulz, Marina Bacac, Carola Hermine Ries, et al. 2017. “An Immune Atlas of Clear Cell Renal Cell Carcinoma.” *Cell* 169 (4): 736-749.e18. http://linkinghub.elsevier.com/retrieve/pii/S0092867417304294.

Choi, Soo Youn, Whaseon Lee-Kwon, Hwan Hee Lee, Jun Ho Lee, Satoru Sanada, and Hyug Moo Kwon. 2013. “Multiple Cell Death Pathways Are Independently Activated by Lethal Hypertonicity in Renal Epithelial Cells.” *American Journal of Physiology-Cell Physiology* 305 (10): C1011–20. https://doi.org/10.1152/ajpcell.00384.2012.

Choi, Un Yung, Jae Jin Lee, Angela Park, Wei Zhu, Hye Ra Lee, Youn Jung Choi, Ji Seung Yoo, et al. 2020. “Oncogenic Human Herpesvirus Hijacks Proline Metabolism for Tumorigenesis.” *Proceedings of the National Academy of Sciences of the United States of America* 117 (14): 8083–93. https://doi.org/10.1073/pnas.1918607117.

Chou, Yung-Chen, Joen-Rong Sheu, Chi-Li Chung, Che-Jen Hsiao, Po-Jen Hsueh, and George Hsiao. 2011. “Hypertonicity-Enhanced TNF-α Release from Activated Human Monocytic THP-1 Cells Requires ERK Activation.” *Biochimica et Biophysica Acta (BBA) - General Subjects* 1810 (4): 475–84. https://doi.org/10.1016/j.bbagen.2011.01.004.

Christgen, Shelbi L., and Donald F. Becker. 2019. “Role of Proline in Pathogen and Host Interactions.” *Antioxidants & Redox Signaling* 30 (4): 683–709. https://doi.org/10.1089/ars.2017.7335.

Ciano-Oliveira, Caterina Di, Gábor Sirokmány, Katalin Szászi, William T. Arthur, András Masszi, Mark Peterson, Ori D. Rotstein, and András Kapus. 2003. “Hyperosmotic Stress Activates Rho: Differential Involvement in Rho Kinase-Dependent MLC Phosphorylation and NKCC Activation.” *American Journal of Physiology - Cell Physiology* 285 (3). http://ajpcell.physiology.org/content/285/3/C555.long.

Ciano, Caterina Di, Zilin Nie, Katalin Szászi, Alison Lewis, Takehito Uruno, Xi Zhan, Ori

D. Rotstein, Alan Mak, and András Kapus. 2002. “Osmotic Stress-Induced Remodeling of the Cortical Cytoskeleton.” *American Journal of Physiology - Cell Physiology* 283 (3 52-3). https://doi.org/10.1152/ajpcell.00018.2002.

Clem, Rollie J., Emily H.Y. Cheng, Christopher L. Karp, David G. Kirsch, Kazuyoshi Ueno, Atsushi Takahashi, Michael B. Kastan, et al. 1998. “Modulation of Cell Death by BCl-XL through Caspase Interaction.” *Proceedings of the National Academy of Sciences of the United States of America* 95 (2): 554–59. https://doi.org/10.1073/pnas.95.2.554.

Cohen-Saidon, Cellina, Ariel A Cohen, Alex Sigal, Yuvalal Liron, and Uri Alon. 2009. “Dynamics and Variability of ERK2 Response to EGF in Individual Living Cells.” *Molecular Cell* 36 (5): 885–93. https://doi.org/10.1016/j.molcel.2009.11.025.

Crane, Matthew M., Ivan B. N. Clark, Elco Bakker, Stewart Smith, Peter S. Swain, V Shahrezaei, PS Swain, et al. 2014. “A Microfluidic System for Studying Ageing and Dynamic Single-Cell Responses in Budding Yeast.” Edited by Alan M. Moses. *PLoS ONE* 9 (6): e100042. https://doi.org/10.1371/journal.pone.0100042.

Csonka, L N. 1989. “Physiological and Genetic Responses of Bacteria to Osmotic Stress.” *Microbiol. Mol. Biol. Rev.* 53 (1): 121–47. http://mmbr.asm.org/content/53/1/121.short.

Cuadrado, Ana, and Angel R Nebreda. 2010. “Mechanisms and Functions of P38 MAPK Signalling.” *The Biochemical Journal* 429 (3): 403–17. https://doi.org/10.1042/BJ20100323.

Cvetkovic, Ljiljana, Stojan Perisic, Jens Titze, Hans-Martin Jäck, and Wolfgang Schuh. 2019. “The Impact of Hyperosmolality on Activation and Differentiation of B Lymphoid Cells.” *Frontiers in Immunology* 10 (April): 828. https://doi.org/10.3389/fimmu.2019.00828.

D’Aniello, Cristina, Eduardo J. Patriarca, James M. Phang, and Gabriella Minchiotti. 2020. “Proline Metabolism in Tumor Growth and Metastatic Progression.” *Frontiers in Oncology*. Frontiers Media S.A. https://doi.org/10.3389/fonc.2020.00776.

Dahl, Stephen C., Joseph S. Handler, and H. Moo Kwon. 2001. “Hypertonicity-Induced Phosphorylation and Nuclear Localization of the Transcription Factor TonEBP.” *American Journal of Physiology-Cell Physiology* 280 (2): C248–53.

https://doi.org/10.1152/ajpcell.2001.280.2.C248.

Dandage, Rohan, Anannya Bandyopadhyay, Gopal Gunanathan Jayaraj, Kanika Saxena, Vijit Dalal, Aritri Das, and Kausik Chakraborty. 2015. “Classification of Chemical Chaperones Based on Their Effect on Protein Folding Landscapes.” *ACS Chemical Biology* 10 (3): 813–20. https://doi.org/10.1021/cb500798y.

Davies, Richard, Petra Vogelsang, Roland Jonsson, and Silke Appel. 2016. “An Optimized Multiplex Flow Cytometry Protocol for the Analysis of Intracellular Signaling in Peripheral Blood Mononuclear Cells.” *Journal of Immunological Methods* 436 (September): 58–63. https://doi.org/10.1016/j.jim.2016.06.007.

Deen, Surrin S., Frank Riemer, Mary A. McLean, Andrew B. Gill, Joshua D. Kaggie, James T. Grist, Robin Crawford, et al. 2019. “Sodium MRI with 3D-Cones as a Measure of Tumour Cellularity in High Grade Serous Ovarian Cancer.” *European Journal of Radiology Open* 6 (January): 156–62. https://doi.org/10.1016/j.ejro.2019.04.001.

Deng, Shaoping, Marko Vatamaniuk, Xiaolun Huang, Nicolai Doliba, Moh Moh Lian, Adam Frank, Ergun Velidedeoglu, et al. 2004. “Structural and Functional Abnormalities in the Islets Isolated from Type 2 Diabetic Subjects.” *Diabetes* 53 (3): 624–32. https://doi.org/10.2337/diabetes.53.3.624.

Ding, Zhaobing, Russell E. Ericksen, Nathalie Escande-Beillard, Qian Yi Lee, Abigail Loh, Simon Denil, Michael Steckel, et al. 2020. “Metabolic Pathway Analyses Identify Proline Biosynthesis Pathway as a Promoter of Liver Tumorigenesis.” *Journal of Hepatology* 72 (4): 725–35. https://doi.org/10.1016/j.jhep.2019.10.026.

Dmitrieva, Natalia I., and Maurice B. Burg. 2004. “Living with DNA Breaks Is an Everyday Reality for Cells Adapted to High NaCl.” *Cell Cycle* 3 (5): 561–63. https://doi.org/10.4161/cc.3.5.869.

———. 2008. “Analysis of DNA Breaks, DNA Damage Response, and Apoptosis Produced by High NaCl” 295 (6): F1678–88. https://doi.org/10.1152/ajprenal.90424.2008.

Dmitrieva, Natalia I, Qi Cai, and Maurice B Burg. 2004. “Cells Adapted to High NaCl Have Many DNA Breaks and Impaired DNA Repair Both in Cell Culture and in Vivo.” *Proceedings of the National Academy of Sciences of the United States of*

America 101 (8): 2317–22. https://doi.org/10.1073/PNAS.0308463100.

Dmitrieva, Natalia I, Arkady Celeste, André Nussenzweig, and Maurice B Burg. 2005. "Ku86 Preserves Chromatin Integrity in Cells Adapted to High NaCl." *Proceedings of the National Academy of Sciences of the United States of America* 102 (30): 10730–35. https://doi.org/10.1073/pnas.0504870102.

Douros, Jonathan D., Jingjing Niu, Sophia Sdao, Trillian Gregg, Kelsey Fisher-Wellman, Manish Bharadwaj, Anthony Molina, et al. 2019. "Sleeve Gastrectomy Rapidly Enhances Islet Function Independently of Body Weight." *JCI Insight* 4 (6). https://doi.org/10.1172/jci.insight.126688.

Dreskin, S. C., G. W. Thomas, S. N. Dale, and L. E. Heasley. 2001. "Isoforms of Jun Kinase Are Differentially Expressed and Activated in Human Monocyte/Macrophage (THP-1) Cells." *The Journal of Immunology* 166 (9): 5646–53. https://doi.org/10.4049/jimmunol.166.9.5646.

Earl, David C., P. Brent Ferrell, Nalin Leelatian, Jordan T. Froese, Benjamin J. Reisman, Jonathan M. Irish, and Brian O. Bachmann. 2018. "Discovery of Human Cell Selective Effector Molecules Using Single Cell Multiplexed Activity Metabolomics." *Nature Communications* 9 (1): 39. https://doi.org/10.1038/s41467-017-02470-8.

Elia, Ilaria, Dorien Broekaert, Stefan Christen, Ruben Boon, Enrico Radaelli, Martin F. Orth, Catherine Verfaillie, Thomas G.P. Grünewald, and Sarah Maria Fendt. 2017. "Proline Metabolism Supports Metastasis Formation and Could Be Inhibited to Selectively Target Metastasizing Cancer Cells." *Nature Communications* 8 (1): 1–11. https://doi.org/10.1038/ncomms15267.

Erickson, Geoffrey R, Leonidas G Alexopoulos, and Farshid Guilak. 2001. "Hyper-Osmotic Stress Induces Volume Change and Calcium Transients in Chondrocytes by Transmembrane, Phospholipid, and G-Protein Pathways." *Journal of Biomechanics* 34 (12): 1527–35. https://doi.org/10.1016/S0021-9290(01)00156-7.

Farabaugh, Kenneth T., Dawid Krokowski, Bo Jhih Guan, Zhaofeng Gao, Xing Huang Gao, Jing Wu, Raul Jobava, et al. 2020. "PACT-Mediated Pkr Activation Acts as a Hyperosmotic Stress Intensity Sensor Weakening Osmoadaptation and Enhancing Inflammation." *ELife* 9 (March). https://doi.org/10.7554/eLife.52241.

Farabaugh, Kenneth T., Mithu Majumder, Bo-Jhih Guan, Raul Jobava, Jing Wu, Dawid Krokowski, Xing-Huang Gao, et al. 2017. “Protein Kinase R Mediates the Inflammatory Response Induced by Hyperosmotic Stress.” *Molecular and Cellular Biology* 37 (4). https://doi.org/10.1128/mcb.00521-16.

Fechner, Gustav Theodor. 1860. *Elemente Der Psychophysik*. Volume 2.

Fei, Peiwen, Eric J. Bernhard, and Wafik S. El-Deiry. 2002. “Tissue-Specific Induction of P53 Targets in Vivo.” *Cancer Research* 62 (24).

Ferraris, J D, C K Williams, K Y Jung, J J Bedford, M B Burg, and A García-Pérez. 1996. “ORE, a Eukaryotic Minimal Essential Osmotic Response Element. The Aldose Reductase Gene in Hyperosmotic Stress.” *The Journal of Biological Chemistry* 271 (31): 18318–21. https://doi.org/10.1074/jbc.271.31.18318.

Ferraris, Joan D., and Maurice B. Burg. 2006. “Tonicity-Dependent Regulation of Osmoprotective Genes in Mammalian Cells.” In *Mechanisms and Significance of Cell Volume Regulation*, 152:125–41. Basel: KARGER. https://doi.org/10.1159/000096320.

Ferreiro, Isabel, Manel Joaquin, Abul Islam, Gonzalo Gomez-Lopez, Montserrat Barragan, Luís Lombardía, Orlando Domínguez, et al. 2010. “Whole Genome Analysis of P38 SAPK-Mediated Gene Expression upon Stress.” *BMC Genomics* 11 (1): 144. https://doi.org/10.1186/1471-2164-11-144.

Ferrell, James E. 2009. “Signaling Motifs and Weber’s Law.” *Molecular Cell* 36 (5): 724–27. https://doi.org/10.1016/j.molcel.2009.11.032.

———. 2016. “Perfect and Near-Perfect Adaptation in Cell Signaling.” *Cell Systems*. Cell Press. https://doi.org/10.1016/j.cels.2016.02.006.

Fichman, Yosef, Svetlana Y. Gerdes, Hajnalka Kovács, László Szabados, Aviah Zilberstein, and Laszlo N. Csonka. 2015. “Evolution of Proline Biosynthesis: Enzymology, Bioinformatics, Genetics, and Transcriptional Regulation.” *Biological Reviews* 90 (4): 1065–99. https://doi.org/10.1111/brv.12146.

Finan, John D., and Farshid Guilak. 2009. “The Effects of Osmotic Stress on the Structure and Function of the Cell Nucleus.” *Journal of Cellular Biochemistry* 109 (3): n/a-n/a. https://doi.org/10.1002/jcb.22437.

Firsov, Dmitri, and Olivier Bonny. 2018. “Circadian Rhythms and the Kidney.” *Nature*

Reviews Nephrology 14 (10). http://www.nature.com/articles/s41581-018-0048-9.

Fischer, Alain, Capucine Picard, Karine Chemin, Stéphanie Dogniaux, Françoise Le Deist, and Claire Hivroz. 2010. “ZAP70: A Master Regulator of Adaptive Immunity.” *Seminars in Immunopathology*. Springer Verlag. https://doi.org/10.1007/s00281-010-0196-x.

Fisher, Mark T. 2006. “Proline to the Rescue.” *Proceedings of the National Academy of Sciences of the United States of America*. National Academy of Sciences. https://doi.org/10.1073/pnas.0606106103.

Fligiel, Suzanne E.G., James Varani, Subhash C. Datta, Sewon Kang, Gary J. Fisher, and John J. Voorhees. 2003. “Collagen Degradation in Aged/Photodamaged Skin in Vivo and after Exposure to Matrix Metalloproteinase-1 in Vitro.” *Journal of Investigative Dermatology* 120 (5): 842–48. https://doi.org/10.1046/j.1523-1747.2003.12148.x.

Flinterman, Marcella, Lars Guelen, Samira Ezzati-Nik, Richard Killick, Gerry Melino, Kazuya Tominaga, Joe S. Mymryk, Joop Gäken, and Mahvash Tavassoli. 2005. “E1A Activates Transcription of P73 and Noxa to Induce Apoptosis.” *Journal of Biological Chemistry* 280 (7): 5945–59. https://doi.org/10.1074/jbc.M406661200.

Foss, Jason D, Annet Kirabo, and David G Harrison. 2016. “Do High Salt Microenvironments Drive Hypertensive Inflammation?” *American Journal of Physiology - Regulatory, Integrative and Comparative Physiology*.

Frick, Christopher L, Clare Yarka, Harry Nunns, and Lea Goentoro. 2017. “Sensing Relative Signal in the Tgf-β/Smad Pathway.” *Proceedings of the National Academy of Sciences of the United States of America* 114 (14). https://doi.org/10.1073/pnas.1611428114.

Fujita, Kazuhiro A, Yu Toyoshima, Shinsuke Uda, Yu-ichi Ozaki, Hiroyuki Kubota, and Shinya Kuroda. 2010. “Decoupling of Receptor and Downstream Signals in the Akt Pathway by Its Low-Pass Filter Characteristics.” *Science Signaling* 3 (132): ra56. https://doi.org/10.1126/scisignal.2000810.

Fuller, N., and R. P. Rand. 1999. “Water in Actin Polymerization.” *Biophysical Journal* 76 (6): 3261–66. https://doi.org/10.1016/S0006-3495(99)77478-3.

Galcheva-Gargova, Z, B Dérijard, I. H Wu, R. J Davis, B Derijard, I. H Wu, and R. J

Davis. 1994. “An Osmosensing Signal Transduction Pathway in Mammalian Cells.” *Science* 265 (5173): 806–8. https://doi.org/10.1126/science.8047888.

Galluzzi, Lorenzo, Ilio Vitale, Stuart A. Aaronson, John M. Abrams, Dieter Adam, Patrizia Agostinis, Emad S. Alnemri, et al. 2018. “Molecular Mechanisms of Cell Death: Recommendations of the Nomenclature Committee on Cell Death 2018.” *Cell Death and Differentiation*. Nature Publishing Group. https://doi.org/10.1038/s41418-017-0012-4.

Garcia-Perez, A, and M B Burg. 1991. “Renal Medullary Organic Osmolytes.” *Physiological Reviews* 71 (4): 1081–1115. https://doi.org/10.1152/physrev.1991.71.4.1081.

Genovese, Mark C. 2009. “Inhibition of P38: Has the Fat Lady Sung?” *Arthritis and Rheumatism* 60 (2): 317–20. https://doi.org/10.1002/art.24264.

Gianazza, Elisabetta, and Pier Giorgio Righetti. 1980. “Size and Charge Distribution of Macromolecules in Living Systems.” *Journal of Chromatography A* 193 (1): 1–8. https://doi.org/10.1016/S0021-9673(00)81438-7.

Giudice, Valentina, Xingmin Feng, Sachiko Kajigaya, Neal S. Young, and Angélique Biancotto. 2017. “Optimization and Standardization of Fluorescent Cell Barcoding for Multiplexed Flow Cytometric Phenotyping.” *Cytometry Part A* 91 (7): 694–703. https://doi.org/10.1002/cyto.a.23162.

Goentoro, Lea, and Marc W Kirschner. 2009. “Evidence That Fold-Change, and Not Absolute Level, of Beta-Catenin Dictates Wnt Signaling.” *Molecular Cell* 36 (5): 872–84. https://doi.org/10.1016/j.molcel.2009.11.017.

Goentoro, Lea, Oren Shoval, Marc W Kirschner, and Uri Alon. 2009. “The Incoherent Feedforward Loop Can Provide Fold-Change Detection in Gene Regulation.” *Molecular Cell* 36 (5): 894–99. https://doi.org/10.1016/j.molcel.2009.11.018.

Gonçalves, Guilherme Lopes, Juliana Martins Costa-Pessoa, Karina Thieme, Bruna Bezerra Lins, and Maria Oliveira-Souza. 2018. “Intracellular Albumin Overload Elicits Endoplasmic Reticulum Stress and PKC-Delta/P38 MAPK Pathway Activation to Induce Podocyte Apoptosis.” *Scientific Reports* 8 (1): 18012. https://doi.org/10.1038/s41598-018-36933-9.

Gottschalk, Carl W, and Margaret Mylle. 1959. “Micropuncture Study of the Mammalian

Urinary Concentrating Mechanism: Evidence for the Countercurrent Hypothesis." *Am J Physiol* 196 (4): 927–36. http://ajplegacy.physiology.org/content/196/4/927.

Gouirand, Victoire, and Sophie Vasseur. 2018. "Fountain of Youth of Pancreatic Cancer Cells: The Extracellular Matrix." *Cell Death Discovery*. Springer Nature. https://doi.org/10.1038/s41420-017-0004-7.

Goulev, Youlian, Sandrine Morlot, Audrey Matifas, Bo Huang, Mikael Molin, Michel B Toledano, Gilles Charvin, et al. 2017. "Nonlinear Feedback Drives Homeostatic Plasticity in H $_2$ O $_2$ Stress Response." *ELife* 6 (April): 84–97. https://doi.org/10.7554/eLife.23971.

Granados, Alejandro A, Matthew M Crane, Luis F Montano-Gutierrez, Reiko J Tanaka, Margaritis Voliotis, and Peter S Swain. 2017. "Distributing Tasks via Multiple Input Pathways Increases Cellular Survival in Stress." *ELife* 6 (May). https://doi.org/10.7554/eLife.21415.

Grespan, Eleonora, Toni Giorgino, Silva Arslanian, Andrea Natali, Ele Ferrannini, and Andrea Mari. 2018. "Defective Amplifying Pathway of β-Cell Secretory Response to Glucose in Type 2 Diabetes: Integrated Modeling of in Vitro and in Vivo Evidence." *Diabetes* 67 (3): 496–506. https://doi.org/10.2337/db17-1039.

Grethe, Simone, and M. Isabella Pörn-Ares. 2006. "P38 MAPK Regulates Phosphorylation of Bad via PP2A-Dependent Suppression of the MEK1/2-ERK1/2 Survival Pathway in TNF-α Induced Endothelial Apoptosis." *Cellular Signalling* 18 (4): 531–40. https://doi.org/10.1016/J.CELLSIG.2005.05.023.

Gudipaty, Swapna A., Christopher M. Conner, Jody Rosenblatt, and Denise J. Montell. 2018. "Unconventional Ways to Live and Die: Cell Death and Survival in Development, Homeostasis, and Disease." *Annual Review of Cell and Developmental Biology* 34 (1): 311–32. https://doi.org/10.1146/annurev-cellbio-100616-060748.

Guyton, Arthur, and John Hall. 2000. *Textbook of Medical Physiology*. 10th ed. Saunders Company.

Guzik, Tomasz J., Nyssa E. Hoch, Kathryn A. Brown, Louise A. McCann, Ayaz Rahman, Sergey Dikalov, Jorg Goronzy, Cornelia Weyand, and David G. Harrison. 2007. "Role of the T Cell in the Genesis of Angiotensin II–Induced Hypertension

and Vascular Dysfunction." *Journal of Experimental Medicine* 204 (10). http://jem.rupress.org/content/204/10/2449.long.

Haase, Stefanie, Nicola Wilck, Markus Kleinewietfeld, Dominik N. Müller, and Ralf A. Linker. 2018. "Sodium Chloride Triggers Th17 Mediated Autoimmunity." *Journal of Neuroimmunology*, June. https://doi.org/10.1016/J.JNEUROIM.2018.06.016.

Hai, M. A., and S. Thomas. 1969. "The Time-Course of Changes in Renal Tissue Composition during Lysine Vasopressin Infusion in the Rat." *Pflugers Archiv European Journal of Physiology* 310 (4): 297–319. https://doi.org/10.1007/BF00587241.

Hallbäck, D.-A., M. Jodal, M. Mannischeff, and O. Lundgren. 1991. "Tissue Osmolality in Intestinal Villi of Four Mammals in Vivo and in Vitro." *Acta Physiologica Scandinavica* 143 (3): 271–77. https://doi.org/10.1111/j.1748-1716.1991.tb09232.x.

Hammaker, D, and G S Firestein. 2010. ""Go Upstream, Young Man": Lessons Learned from the P38 Saga." *Annals of the Rheumatic Diseases* 69 Suppl 1 (Suppl 1): i77-82. https://doi.org/10.1136/ard.2009.119479.

Hamraz, Minoo, Raymond Abolhassani, Mireille Andriamihaja, Céline Ransy, Véronique Lenoir, Laurent Schwartz, and Frédéric Bouillaud. 2020. "Hypertonic External Medium Represses Cellular Respiration and Promotes Warburg/Crabtree Effect." *The FASEB Journal* 34 (1). https://doi.org/10.1096/fj.201900706RR.

Han, J, J. Lee, L Bibbs, and R. Ulevitch. 1994. "A MAP Kinase Targeted by Endotoxin and Hyperosmolarity in Mammalian Cells." *Science* 265 (5173): 808–11. https://doi.org/10.1126/science.7914033.

Hara, Masayuki, Yoichi Minami, Munehiro Ohashi, Yoshiki Tsuchiya, Tetsuro Kusaba, Keiichi Tamagaki, Nobuya Koike, Yasuhiro Umemura, Hitoshi Inokawa, and Kazuhiro Yagita. 2017. "Robust Circadian Clock Oscillation and Osmotic Rhythms in Inner Medulla Reflecting Cortico-Medullary Osmotic Gradient Rhythm in Rodent Kidney." *Scientific Reports* 7 (1): 7306. https://doi.org/10.1038/s41598-017-07767-8.

Hare, P.D., and W.A. Cress. 1997. "Metabolic Implications of Stress-Induced Proline Accumulation in Plants." *Plant Growth Regulation* 21 (2): 79–102. https://doi.org/10.1023/A:1005703923347.

Hartmann, Felix J., Erin F. Simonds, and Sean C. Bendall. 2018. “A Universal Live Cell Barcoding-Platform for Multiplexed Human Single Cell Analysis” 8 (1): 10770. https://doi.org/10.1038/s41598-018-28791-2.

Heemskerk, Idse, Kari Burt, Matthew Miller, Sapna Chhabra, M Cecilia Guerra, Lizhong Liu, and Aryeh Warmflash. 2019. “Rapid Changes in Morphogen Concentration Control Self-Organized Patterning in Human Embryonic Stem Cells.” *ELife* 8 (March). https://elifesciences.org/articles/40526.

Heer, Martina, Friedhelm Baisch, Joachim Kropp, Rupert Gerzer, and Christian Drummer. 2000. “High Dietary Sodium Chloride Consumption May Not Induce Body Fluid Retention in Humans.” *American Journal of Physiology - Renal Physiology* 278 (4 47-4). https://doi.org/10.1152/ajprenal.2000.278.4.f585.

Heer, Martina, Christian Drummer, Friedhelm Baisch, and Rupert Gerzer. 1993. “Long-Term Elevations of Dietary Sodium Produce Parallel Increases in the Renal Excretion of Urodilatin and Sodium.” *Pflügers Archiv European Journal of Physiology* 425 (5–6): 390–94. https://doi.org/10.1007/BF00374863.

Hegemann, Björn, Michael Unger, Sung Sik Lee, Ingrid Stoffel-Studer, Jasmin van den Heuvel, Serge Pelet, Heinz Koeppl, and Matthias Peter. 2015. “A Cellular System for Spatial Signal Decoding in Chemical Gradients.” *Developmental Cell* 35 (4): 458–70. https://doi.org/10.1016/J.DEVCEL.2015.10.013.

Heiden, Matthew G.Vander, Lewis C. Cantley, and Craig B. Thompson. 2009. “Understanding the Warburg Effect: The Metabolic Requirements of Cell Proliferation.” *Science*. American Association for the Advancement of Science. https://doi.org/10.1126/science.1160809.

Heldin, Carl Henrik, Kristofer Rubin, Kristian Pietras, and Arne Östman. 2004. “High Interstitial Fluid Pressure - An Obstacle in Cancer Therapy.” *Nature Reviews Cancer*. Nature Publishing Group. https://doi.org/10.1038/nrc1456.

Helge Wiig, Friedrich C Luft, and Jens Titze. 2017. “The Interstitium Conducts Extrarenal Storage of Sodium and Represents a Third Compartment for Extracellular Volume and Blood Pressure Homeostasis.” *ARPN Journal of Engineering and Applied Sciences* 12 (10): 3218–21. https://doi.org/10.1111/ijlh.12426.

Hersen, Pascal, Megan N McClean, L Mahadevan, and Sharad Ramanathan. 2008. "Signal Processing by the HOG MAP Kinase Pathway." *Proceedings of the National Academy of Sciences of the United States of America* 105 (20): 7165–70. https://doi.org/10.1073/pnas.0710770105.

Ho, Steffan N. 2003. "The Role of NFAT5/TonEBP in Establishing an Optimal Intracellular Environment." *Archives of Biochemistry and Biophysics* 413 (2): 151–57. https://doi.org/10.1016/S0003-9861(03)00130-9.

Hoffmann, E. K. 2001. "The Pump and Leak Steady-State Concept with a Variety of Regulated Leak Pathways." *Journal of Membrane Biology*. Springer. https://doi.org/10.1007/s00232-001-0102-5.

Hoffmann, Else K., Ian H. Lambert, and Stine F. Pedersen. 2009. "Physiology of Cell Volume Regulation in Vertebrates." *Physiological Reviews* 89 (1): 193–277. https://doi.org/10.1152/physrev.00037.2007.

Hoffmann, Else K., and Stine F. Pedersen. 2006. "Sensors and Signal Transduction Pathways in Vertebrate Cell Volume Regulation." In *Mechanisms and Significance of Cell Volume Regulation*, 152:54–104. Basel: KARGER. https://doi.org/10.1159/000096318.

Humphreys, John M, Alexander T Piala, Radha Akella, Haixia He, and Elizabeth J Goldsmith. 2013. "Precisely Ordered Phosphorylation Reactions in the P38 Mitogen-Activated Protein (MAP) Kinase Cascade." *The Journal of Biological Chemistry* 288 (32): 23322–30. https://doi.org/10.1074/jbc.M113.462101.

Ignatova, Zoya, and Lila M. Gierasch. 2006. "Inhibition of Protein Aggregation in Vitro and in Vivo by a Natural Osmoprotectant." *Proceedings of the National Academy of Sciences of the United States of America* 103 (36): 13357–61. https://doi.org/10.1073/pnas.0603772103.

Inglese, M., G. Madelin, N. Oesingmann, J. S. Babb, W. Wu, B. Stoeckel, J. Herbert, and G. Johnson. 2010. "Brain Tissue Sodium Concentration in Multiple Sclerosis: A Sodium Imaging Study at 3 Tesla." *Brain* 133 (3): 847–57. https://doi.org/10.1093/brain/awp334.

Ip, W. K.Eddie Eddie, Ruslan Medzhitov, M. A. Roti, F. Liu, and S. N. Ho. 2015. "Macrophages Monitor Tissue Osmolarity and Induce Inflammatory Response

through NLRP3 and NLRC4 Inflammasome Activation." *Nature Communications* 6 (May): 6931. https://doi.org/10.1038/ncomms7931.

Ivanova, L. N., V. K. Archibassova, and I. S. Sterental. 1978. "Sodium-Deposing Function of the Skin in the Albino Rat." *Fiziologicheskii Zhurnal SSSR Imeni I.M. Sechenova* 64 (3): 358–63.

Izumi, Yuichiro, Wenjing Yang, Jun Zhu, Maurice B. Burg, and Joan D. Ferraris. 2015. "RNA-Seq Analysis of High NaCl-Induced Gene Expression." *Physiological Genomics* 47 (10): 500–513. https://doi.org/10.1152/physiolgenomics.00057.2015.

Jaeckle Santos, Lane J., Changhong Li, Paschalis Thomas Doulias, Harry Ischiropoulos, G. Scott Worthen, and Rebecca A. Simmons. 2014. "Neutralizing Th2 Inflammation in Neonatal Islets Prevents β-Cell Failure in Adult IUGR Rats." *Diabetes* 63 (5): 1672–84. https://doi.org/10.2337/db13-1226.

Jalihal, Ameya, Sethuramasundaram Pitchiaya, Lanbo Xiao, Pushpinder Bawa, Xia Jiang, Karan Bedi, Marcin Cieslik, Mats Ljungman, Arul Chinnaiyan, and Nils Walter. 2019. "Multivalent Proteins Rapidly and Reversibly Phase-Separate upon Osmotic Cell Volume Change." *BioRxiv*, May, 748293. https://doi.org/10.1101/748293.

Jantsch, Jonathan, Valentin Schatz, Diana Friedrich, Agnes Schröder, Christoph Kopp, Isabel Siegert, Andreas Maronna, et al. 2015. "Cutaneous Na+ Storage Strengthens the Antimicrobial Barrier Function of the Skin and Boosts Macrophage-Driven Host Defense." *Cell Metabolism* 21 (3): 493–501. https://doi.org/10.1016/j.cmet.2015.02.003.

Jeon, U. S., J.-A. Kim, M. R. Sheen, and H. M. Kwon. 2006. "How Tonicity Regulates Genes: Story of TonEBP Transcriptional Activator." *Acta Physiologica* 187 (1–2): 241–47. https://doi.org/10.1111/j.1748-1716.2006.01551.x.

Ji, Hong, Amrita V. Pai, Crystal A. West, Xie Wu, Robert C. Speth, and Kathryn Sandberg. 2017. "Loss of Resistance to Angiotensin II-Induced Hypertension in the Jackson Laboratory Recombination-Activating Gene Null Mouse on the C57BL/6J Background." *Hypertension* 69 (6): 1121–27. https://doi.org/10.1161/HYPERTENSIONAHA.117.09063.

Jiang, Li-Bo, Lu Cao, Xiao-Fan Yin, Miersalijiang Yasen, Mumingjiang Yishake, Jian

Dong, and Xi-Lei Li. 2015. “Activation of Autophagy via Ca $^{2+}$ -Dependent AMPK/MTOR Pathway in Rat Notochordal Cells Is a Cellular Adaptation under Hyperosmotic Stress.” *Cell Cycle* 14 (6): 867–79. https://doi.org/10.1080/15384101.2015.1004946.

Jin, Ho Chung, Young Seo Jin, Ryung Choi Hai, Kyung Lee Mi, Shik Youn Choon, Gi Eun Rhie, Hyun Cho Kwang, Han Kim Kyu, Chan Park Kyung, and Chul Eun Hee. 2001. “Modulation of Skin Collagen Metabolism in Aged and Photoaged Human Skin in Vivo.” *Journal of Investigative Dermatology* 117 (5): 1218–24. https://doi.org/10.1046/j.0022-202X.2001.01544.x.

Johnson, Amanda N., Guoliang Li, Hossein Jashnsaz, Alexander Thiemicke, Benjamin K. Kesler, Dustin C. Rogers, and Gregor Neuert. 2020. “A Rate Threshold Mechanism Regulates MAPK Stress Signaling and Survival.” *BioRxiv*.

Johnston, Jermaine G., and David M. Pollock. 2018. “Circadian Regulation of Renal Function.” *Free Radical Biology and Medicine*, January. https://doi.org/10.1016/j.freeradbiomed.2018.01.018.

Jones, Douglas S, Anne P Jenney, Brian A Joughin, Peter K Sorger, and Douglas A Lauffenburger. 2018. “Inflammatory but Not Mitogenic Contexts Prime Synovial Fibroblasts for Compensatory Signaling Responses to P38 Inhibition.” *Science Signaling* 11 (520): eaal1601. https://doi.org/10.1126/scisignal.aal1601.

Jörg, Stefanie, Jan Kissel, Arndt Manzel, Markus Kleinewietfeld, Aiden Haghikia, Ralf Gold, Dominik N Müller, and Ralf A Linker. 2016. “High Salt Drives Th17 Responses in Experimental Autoimmune Encephalomyelitis without Impacting Myeloid Dendritic Cells.” *Experimental Neurology* 279 (March): 212–22. https://doi.org/10.1016/j.expneurol.2016.03.010.

Kalinin, Yevgeniy V., Lili Jiang, Yuhai Tu, and Mingming Wu. 2009. “Logarithmic Sensing in Escherichia Coli Bacterial Chemotaxis.” *Biophysical Journal* 96 (6): 2439–48. https://doi.org/10.1016/j.bpj.2008.10.027.

Kalland, Maria Elisabeth, Nikolaus Günter Oberprieler, Torkel Vang, Kjetil Taskén, and Knut Martin Torgersen. 2011. “T Cell-Signaling Network Analysis Reveals Distinct Differences between CD28 and CD2 Costimulation Responses in Various Subsets and in the MAPK Pathway between Resting and Activated Regulatory T Cells.” *The*

Journal of Immunology 187 (10): 5233–45. https://doi.org/10.4049/jimmunol.1101804.

Kandel, Eric. 2013. *Principles of Neural Science*.

Kasibhatla, Shailaja, Thomas Brunner, Laurent Genestier, Fernando Echeverri, Artin Mahboubi, and Douglas R. Green. 1998. “DNA Damaging Agents Induce Expression of Fas Ligand and Subsequent Apoptosis in T Lymphocytes via the Activation of NF-KB and AP-1.” *Molecular Cell* 1 (4): 543–51. https://doi.org/10.1016/S1097-2765(00)80054-4.

Kaufmann, Scott H., Serge Desnoyers, Yvonne Ottaviano, Nancy E. Davidson, and Guy G. Poirier. 1993. “Specific Proteolytic Cleavage of Poly(ADP-Ribose) Polymerase: An Early Marker of Chemotherapy-Induced Apoptosis.” *Cancer Research* 53 (17): 3976–85.

Kesavardhana, Sannula, R.K. Subbarao Malireddi, and Thirumala-Devi Kanneganti. 2020. “Caspases in Cell Death, Inflammation, and Gasdermin-Induced Pyroptosis.” *Annual Review of Immunology* 38 (1): annurev-immunol-073119-095439. https://doi.org/10.1146/annurev-immunol-073119-095439.

Kharroubi, Akram T. 2015. “Diabetes Mellitus: The Epidemic of the Century.” *World Journal of Diabetes* 6 (6): 850. https://doi.org/10.4239/wjd.v6.i6.850.

Kirabo, Annet, Natalia Barbaro, Jason David Foss, Kim Ramil Montaniel, Wei Chen, and David Glenn Harrison. 2016. “High Salt Activates Human Monocytes and Promotes Their Conversion into Dendritic Cells via Formation of Immunogenic Isoketal-Adducts.” *The FASEB Journal* 30 (1 Supplement): 1216.4-1216.4.

Kirabo, Annet, Vanessa Fontana, Ana P C de Faria, Roxana Loperena, Cristi L Galindo, Jing Wu, Alfiya T Bikineyeva, et al. 2014. “DC Isoketal-Modified Proteins Activate T Cells and Promote Hypertension.” *The Journal of Clinical Investigation* 124 (10): 4642–56. https://doi.org/10.1172/JCI74084.

Kitada, Kento, Steffen Daub, Yahua Zhang, Janet D. Klein, Daisuke Nakano, Tetyana Pedchenko, Louise Lantier, et al. 2017. “High Salt Intake Reprioritizes Osmolyte and Energy Metabolism for Body Fluid Conservation.” *Journal of Clinical Investigation* 123 (7): 2803–15. https://doi.org/10.1172/JCI88532.

Kitano, Hiroaki. 2001. *Foundations of Systems Biology*. 1st ed.

———. 2002a. “Systems Biology: A Brief Overview.” *Science*. American Association for the Advancement of Science. https://doi.org/10.1126/science.1069492.

———. 2002b. “Computational Systems Biology.” *Nature*. Nature Publishing Group. https://doi.org/10.1038/nature01254.

Kleinewietfeld, Markus, Arndt Manzel, Jens Titze, Heda Kvakan, Nir Yosef, Ralf A. Linker, Dominik N. Muller, and David A. Hafler. 2013. “Sodium Chloride Drives Autoimmune Disease by the Induction of Pathogenic TH17 Cells.” *Nature* 496 (7446): 518–22. https://doi.org/10.1038/nature11868.

Ko, Ben C B, Amy K M Lam, Andras Kapus, Lingzhi Fan, Sookja K Stephen S M Chung, and Sookja K Stephen S M Chung. 2002. “Fyn and P38 Signaling Are Both Required for Maximal Hypertonic Activation of the Osmotic Response Element-Binding Protein/Tonicity-Responsive Enhancer-Binding Protein (OREBP/TonEBP).” *The Journal of Biological Chemistry* 277 (48): 46085–92. https://doi.org/10.1074/jbc.M208138200.

Koepsell, H., W. A.P. P. Nicholson, W. Kriz, H. J. H�hling, and H. J. Höhling. 1974. “Measurements of Exponential Gradients of Sodium and Chlorine in the Rat Kidney Medulla Using the Electron Microprobe” 350 (2): 167–84. https://doi.org/10.1007/BF00586235.

Konopka, Michael C., Kem A. Sochacki, Benjamin P. Bratton, Irina A. Shkel, M. Thomas Record, and James C. Weisshaar. 2009. “Cytoplasmic Protein Mobility in Osmotically Stressed Escherichia Coli.” *Journal of Bacteriology* 91 (1): 231–37. https://doi.org/10.1128/JB.00536-08.

Kopp, Christoph, Christian Beyer, Peter Linz, Anke Dahlmann, Matthias Hammon, Jonathan Jantsch, Patrick Neubert, et al. 2016. “Na+ Deposition in the Fibrotic Skin of Systemic Sclerosis Patients Detected by 23Na-Magnetic Resonance Imaging.” *Rheumatology (Oxford, England)*, December, kew371. https://doi.org/10.1093/rheumatology/kew371.

Kopp, Christoph, Peter Linz, Anke Dahlmann, Matthias Hammon, Jonathan Jantsch, Dominik N. Müller, Roland E. Schmieder, et al. 2013a. “23Na Magnetic Resonance Imaging-Determined Tissue Sodium in Healthy Subjects and Hypertensive Patients.” *Hypertension* 61 (3): 635–40.

https://doi.org/10.1161/HYPERTENSIONAHA.111.00566.

———. 2013b. “23Na Magnetic Resonance Imaging-Determined Tissue Sodium in Healthy Subjects and Hypertensive Patients.” *Hypertension* 61 (3): 635–40. https://doi.org/10.1161/HYPERTENSIONAHA.111.00566.

Kopp, Christoph, Peter Linz, Matthias Hammon, Christof Schöfl, Martin Grauer, Kai Uwe Eckardt, Alexander Cavallaro, Michael Uder, Friedrich C. Luft, and Jens Titze. 2012. “Seeing the Sodium in a Patient with Hypernatremia.” *Kidney International*. Elsevier. https://doi.org/10.1038/ki.2012.314.

Kopp, Christoph, Peter Linz, Lydia Wachsmuth, Anke Dahlmann, Thomas Horbach, Christof Schöfl, Wolfgang Renz, et al. 2012. “23Na Magnetic Resonance Imaging of Tissue Sodium.” *Hypertension* 59 (1): 167–72. https://doi.org/10.1161/HYPERTENSIONAHA.111.183517.

Kowaloff, E. M., J. M. Phang, A. S. Granger, and S. J. Downing. 1977. “Regulation of Proline Oxidase Activity by Lactate.” *Proceedings of the National Academy of Sciences of the United States of America* 74 (12): 5368–71. https://doi.org/10.1073/pnas.74.12.5368.

Krishnan, Navasona, Martin B. Dickman, and Donald F. Becker. 2008. “Proline Modulates the Intracellular Redox Environment and Protects Mammalian Cells against Oxidative Stress.” *Free Radical Biology and Medicine* 44 (4): 671–81. https://doi.org/10.1016/J.FREERADBIOMED.2007.10.054.

Krokowski, Dawid, Raul Jobava, Bo Jhih Guan, Kenneth Farabaugh, Jing Wu, Mithu Majumder, Massimiliano G. Bianchi, Martin D. Snider, Ovidio Bussolati, and Maria Hatzoglou. 2015. “Coordinated Regulation of the Neutral Amino Acid Transporter SNAT2 and the Protein Phosphatase Subunit GADD34 Promotes Adaptation to Increased Extracellular Osmolarity.” *Journal of Biological Chemistry* 290 (29): 17822–37. https://doi.org/10.1074/jbc.M114.636217.

Krutzik, Peter O., Matthew R. Clutter, Angelica Trejo, Garry P. Nolan, Peter O. Krutzik, Matthew R. Clutter, Angelica Trejo, and Garry P. Nolan. 2011. “Fluorescent Cell Barcoding for Multiplex Flow Cytometry.” *Current Protocols in Cytometry* 55 (SUPPL.55): 1–15. https://doi.org/10.1002/0471142956.cy0631s55.

Krutzik, Peter O., Janelle M. Crane, Matthew R. Clutter, and Garry P. Nolan. 2008.

"High-Content Single-Cell Drug Screening with Phosphospecific Flow Cytometry." *Nature Chemical Biology* 4 (2): 132–42. https://doi.org/10.1038/nchembio.2007.59.

Krutzik, Peter O, and Garry P Nolan. 2006. "Fluorescent Cell Barcoding in Flow Cytometry Allows High-Throughput Drug Screening and Signaling Profiling." *Nature Methods* 3 (5): 361–68. https://doi.org/10.1038/nmeth872.

Kültz, D, D Chakravarty, Natalia I. Dmitrieva, Yusen Liu, Maurice B. Burg, Daniil A. Kitchaev, Keji Zhao, and Maurice B. Burg. 2001. "Hyperosmolality in the Form of Elevated NaCl but Not Urea Causes DNA Damage in Murine Kidney Cells." *Proceedings of the National Academy of Sciences of the United States of America* 98 (4): 1999–2004. https://doi.org/10.1073/pnas.98.4.1999.

Kültz, Dietmar, and Devulapalli Chakravarty. 2001. "Maintenance of Genomic Integrity in Mammalian Kidney Cells Exposed to Hyperosmotic Stress." *Comparative Biochemistry and Physiology Part A: Molecular & Integrative Physiology* 130 (3): 421–28. https://doi.org/10.1016/S1095-6433(01)00440-8.

Kumar, Raj, Jenna F DuMond, Shagufta H Khan, E Brad Thompson, Yi He, Maurice B Burg, and Joan D Ferraris. 2020. "NFAT5, Which Protects against Hypertonicity, Is Activated by That Stress via Structuring of Its Intrinsically Disordered Domain." *Proceedings of the National Academy of Sciences of the United States of America*, August. https://doi.org/10.1073/pnas.1911680117.

Kuo, Linda J, and Li-Xi Yang. 2008. "Gamma-H2AX - a Novel Biomarker for DNA Double-Strand Breaks." *In Vivo (Athens, Greece)* 22 (3): 305–9. https://doi.org/0258-851X/2008.

Kwon, Min Seong, Sun Woo Lim, and H. Moo Kwon. 2009. "Hypertonic Stress in the Kidney: A Necessary Evil." *Physiology* 24 (3). http://physiologyonline.physiology.org/content/24/3/186.

Kwon, Min Seong, Ki Young Na, Gilbert Moeckel, Sang Do Lee, and H. Moo Kwon. 2009. "Urea Promotes TonEBP Expression and Cellular Adaptation in Extreme Hypertonicity." *Pflügers Archiv - European Journal of Physiology* 459 (1): 183–89. https://doi.org/10.1007/s00424-009-0696-5.

Kyriakis, John M., Papia Banerjee, Eleni Nikolakaki, Tianang Dai, Elizabeth A. Rubie, Mir F. Ahmad, Joseph Avruch, and James R. Woodgett. 1994. "The Stress-

Activated Protein Kinase Subfamily of c-Jun Kinases." *Nature* 369 (6476): 156–60. https://doi.org/10.1038/369156a0.

Kyriakis, John M JM., and Joseph Avruch. 2012. "Mammalian MAPK Signal Transduction Pathways Activated by Stress and Inflammation: A 10-Year Update." *Physiological Reviews* 92 (2): 689–737. https://doi.org/10.1152/physrev.00028.2011.

Lamkanfi, M., W. Declercq, M. Kalai, X. Saelens, and P. Vandenabeele. 2002. "Alice in Caspase Land. A Phylogenetic Analysis of Caspases from Worm to Man." *Cell Death and Differentiation* 9 (4): 358–61. https://doi.org/10.1038/sj.cdd.4400989.

Lamkanfi, M., N. Festjens, W. Declercq, T. Vanden Berghe, and P. Vandenabeele. 2007. "Caspases in Cell Survival, Proliferation and Differentiation." *Cell Death and Differentiation*. Nature Publishing Group. https://doi.org/10.1038/sj.cdd.4402047.

Lang, Florian, and Else K. Hoffmann. 2013. "CrossTalk Proposal: Cell Volume Changes Are an Essential Step in the Cell Death Machinery." *The Journal of Physiology* 591 (24): 6119–21. https://doi.org/10.1113/jphysiol.2013.258632.

Lang, Florian, Anne C. Uhlemann, Albrecht Lepple-Wienhues, Ildiko Szabo, Detlef Siemen, Bernd Nilius, and Erich Gulbins. 1999. "Cell Volume Regulatory Mechanisms in Apoptotic Cell Death." *Herz* 24 (3): 232–35. https://doi.org/10.1007/BF03044966.

Larsen, Erik Hviid, and Else Kay Hoffmann. 2016. "Volume Regulation in Epithelia." In *Ion Channels and Transporters of Epithelia in Health and Disease*, 131–85. Springer New York. https://doi.org/10.1007/978-1-4939-3366-2_4.

Lawrence, C P, and S C Chow. 2012. "Suppression of Human T Cell Proliferation by the Caspase Inhibitors, z-VAD-FMK and z-IETD-FMK Is Independent of Their Caspase Inhibition Properties." *Toxicology and Applied Pharmacology* 265 (1): 103–12. https://doi.org/10.1016/j.taap.2012.09.002.

Lazebnik, Y. A., S. H. Kaufmann, S. Desnoyers, G. G. Poirier, and W. C. Earnshaw. 1994. "Cleavage of Poly(ADP-Ribose) Polymerase by a Proteinase with Properties like ICE." *Nature* 371 (6495): 346–47. https://doi.org/10.1038/371346a0.

Leaf, Alexander. 1959. "MAINTENANCE OF CONCENTRATION GRADIENTS AND REGULATION OF CELL VOLUME." *Annals of the New York Academy of Sciences*

72 (12): 396–404. https://doi.org/10.1111/j.1749-6632.1959.tb44168.x.

Lee, Pearl, Navdeep S. Chandel, and M. Celeste Simon. 2020. “Cellular Adaptation to Hypoxia through Hypoxia Inducible Factors and Beyond.” *Nature Reviews Molecular Cell Biology*. Nature Research. https://doi.org/10.1038/s41580-020-0227-y.

Lekishvili, Tamara, and Jonathan J. Campbell. 2018. “Rapid Comparative Immunophenotyping of Human Mesenchymal Stromal Cells by a Modified Fluorescent Cell Barcoding Flow Cytometric Assay.” *Cytometry Part A* 93 (9): 905–15. https://doi.org/10.1002/cyto.a.23248.

Lemp, Michael A., Christophe Baudouin, Jules Baum, Murat Dogru, Gary N. Foulks, Shigeru Kinoshita, Peter Laibson, et al. 2007. “The Definition and Classification of Dry Eye Disease: Report of the Definition and Classification Subcommittee of the International Dry Eye WorkShop (2007).” In *Ocular Surface*, 5:75–92. ETHIS COMMUNICATIONS, INC. https://doi.org/10.1016/s1542-0124(12)70081-2.

Lemp, Michael A., Anthony J. Bron, Christophe Baudouin, Jos M. Bentez Del Castillo, David Geffen, Joe Tauber, Gary N. Foulks, Jay S. Pepose, and Benjamin D. Sullivan. 2011. “Tear Osmolarity in the Diagnosis and Management of Dry Eye Disease.” *American Journal of Ophthalmology* 151 (5): 792-798.e1. https://doi.org/10.1016/j.ajo.2010.10.032.

Leslie, Theresa K., Andrew D. James, Fulvio Zaccagna, James T. Grist, Surrin Deen, Aneurin Kennerley, Frank Riemer, et al. 2019. “Sodium Homeostasis in the Tumour Microenvironment.” *Biochimica et Biophysica Acta (BBA) - Reviews on Cancer*, July. https://doi.org/10.1016/J.BBCAN.2019.07.001.

Levin-Salomon, Vered, Inbal Maayan, Liat Avrahami-Moyal, Irit Marbach, Oded Livnah, and David Engelberg. 2009. “When Expressed in Yeast, Mammalian Mitogen-Activated Protein Kinases Lose Proper Regulation and Become Spontaneously Phosphorylated.” *The Biochemical Journal* 417 (1): 331–40. https://doi.org/10.1042/BJ20081335.

Li, Changhong, Carol Buettger, Jae Kwagh, Andrea Matter, Yevgeny Daikhin, Ilana B. Nissim, Heather W. Collins, Marc Yudkoff, Charles A. Stanley, and Franz M. Matschinsky. 2004. “A Signaling Role of Glutamine in Insulin Secretion.” *Journal of*

Biological Chemistry 279 (14): 13393–401. https://doi.org/10.1074/jbc.M311502200.

Li, De Quan, Zhuo Chen, Xiu Jun Song, Lihui Luo, and Stephen C. Pflugfelder. 2004. "Stimulation of Matrix Metalloproteinases by Hyperosmolarity via a JNK Pathway in Human Corneal Epithelial Cells." *Investigative Ophthalmology and Visual Science* 45 (12): 4302–11. https://doi.org/10.1167/iovs.04-0299.

Li, Huatao, Weidan Jiang, Yang Liu, Jun Jiang, Yongan Zhang, Pei Wu, Juan Zhao, Xudong Duan, Xiaoqiu Zhou, and Lin Feng. 2016. "The Metabolites of Glutamine Prevent Hydroxyl Radical-Induced Apoptosis through Inhibiting Mitochondria and Calcium Ion Involved Pathways in Fish Erythrocytes." *Free Radical Biology and Medicine* 92 (March): 126–40. https://doi.org/10.1016/J.FREERADBIOMED.2016.01.007.

Li, Pulin, and Michael B. Elowitz. 2019. "Communication Codes in Developmental Signaling Pathways" 146 (12): dev170977. https://doi.org/10.1242/dev.170977.

Li, Pulin, Joseph S Markson, Sheng Wang, Siheng Chen, Vipul Vachharajani, and Michael B Elowitz. 2018. "Morphogen Gradient Reconstitution Reveals Hedgehog Pathway Design Principles." *Science (New York, N.Y.)* 360 (6388): 543–48. https://doi.org/10.1126/science.aao0645.

Li, Yiwei, Angelo S. Mao, Bo Ri Seo, Xing Zhao, Satish Kumar Gupta, Maorong Chen, Yu Long Han, Ting Yu Shih, David J. Mooney, and Ming Guo. 2020. "Compression-Induced Dedifferentiation of Adipocytes Promotes Tumor Progression." *Science Advances* 6 (4): eaax5611. https://doi.org/10.1126/sciadv.aax5611.

Liang, Xinwen, Lu Zhang, Sathish Kumar Natarajan, and Donald F. Becker. 2013. "Proline Mechanisms of Stress Survival." *Antioxidants & Redox Signaling* 19 (9): 998–1011. https://doi.org/10.1089/ars.2012.5074.

Lieu, Elizabeth L., Tu Nguyen, Shawn Rhyne, and Jiyeon Kim. 2020. "Amino Acids in Cancer." *Experimental and Molecular Medicine*. Springer Nature. https://doi.org/10.1038/s12276-020-0375-3.

Lim, Wendell, Bruce Meyer, and Tony Pawson. 2014. *Cell Signaling: Principles and Mechanisms*. *CRC Press*.

Liu, Miao, Yuanyuan Wang, Chuanzhen Yang, Yuxia Ruan, Changsen Bai, Qiaoyun

Chu, Yanfen Cui, Ceshi Chen, Guoguang Ying, and Binghui Li. 2020. “Inhibiting Both Proline Biosynthesis and Lipogenesis Synergistically Suppresses Tumor Growth.” *Journal of Experimental Medicine* 217 (3). https://doi.org/10.1084/jem.20191226.

Liu, Wei, Chad N. Hancock, Joseph W. Fischer, Meredith Harman, and James M. Phang. 2015a. “Proline Biosynthesis Augments Tumor Cell Growth and Aerobic Glycolysis: Involvement of Pyridine Nucleotides.” *Scientific Reports* 5 (November). https://doi.org/10.1038/srep17206.

———. 2015b. “Proline Biosynthesis Augments Tumor Cell Growth and Aerobic Glycolysis: Involvement of Pyridine Nucleotides.” *Scientific Reports* 5 (November). https://doi.org/10.1038/srep17206.

Liu, Wei, Anne Le, Chad Hancock, Andrew N. Lane, Chi V. Dang, Teresa W.M. Fan, and James M. Phang. 2012. “Reprogramming of Proline and Glutamine Metabolism Contributes to the Proliferative and Metabolic Responses Regulated by Oncogenic Transcription Factor C-MYC.” *Proceedings of the National Academy of Sciences of the United States of America* 109 (23): 8983–88. https://doi.org/10.1073/pnas.1203244109.

Liu, Yating, Chao Mao, Min Wang, Na Liu, Lianlian Ouyang, Shouping Shuang Liu, Haosheng Tang, et al. 2020. “Cancer Progression Is Mediated by Proline Catabolism in Non-Small Cell Lung Cancer.” *Oncogene* 39 (11): 2358–76. https://doi.org/10.1038/s41388-019-1151-5.

Loperena, Roxana, Wei Chen, Annet Kirabo, and David Glenn Harrison. 2016. “Hypertensive Mechanical Stretch: A Model for Monocyte-Derived Dendritic Cell Differentiation.” *The FASEB Journal* 30 (1 Supplement): 723.4-723.4.

López-Rodríguez, Cristina, José Aramburu, Lei Jin, Andrew S. Rakeman, Mayako Michino, and Anjana Rao. 2001. “Bridging the NFAT and NF-KB Families: NFAT5 Dimerization Regulates Cytokine Gene Transcription in Response to Osmotic Stress.” *Immunity* 15 (1): 47–58. https://doi.org/10.1016/S1074-7613(01)00165-0.

Low, Sylvia Y., and Peter M. Taylor. 1998. “Integrin and Cytoskeletal Involvement in Signalling Cell Volume Changes to Glutamine Transport in Rat Skeletal Muscle.” *Journal of Physiology* 512 (2): 481–85. https://doi.org/10.1111/j.1469-

7793.1998.481be.x.

Lu, Ming, and Changhong Li. 2018. “Nutrient Sensing in Pancreatic Islets: Lessons from Congenital Hyperinsulinism and Monogenic Diabetes.” *Annals of the New York Academy of Sciences*. Blackwell Publishing Inc. https://doi.org/10.1111/nyas.13448.

Luby-Phelps, Kate. 2013. “The Physical Chemistry of Cytoplasm and Its Influence on Cell Function: An Update.” *Molecular Biology of the Cell*. The American Society for Cell Biology . https://doi.org/10.1091/mbc.E12-08-0617.

Luby-Phelps, Katherine. 1999. “Cytoarchitecture and Physical Properties of Cytoplasm: Volume, Viscosity, Diffusion, Intracellular Surface Area.” *International Review of Cytology* 192 (January): 189–221. https://doi.org/10.1016/s0074-7696(08)60527-6.

Ludwig, Carl. 1861. *Lehrbuch Der Physiologie Des Menschen*. 2nd ed. Leipzig.

Luengo, Alba, Dan Y. Gui, and Matthew G. Vander Heiden. 2017. “Targeting Metabolism for Cancer Therapy.” *Cell Chemical Biology*. Elsevier Ltd. https://doi.org/10.1016/j.chembiol.2017.08.028.

Lundbaek, Knud. 1962. “Intravenous Glucose Tolerance as a Tool in Definition and Diagnosis of Diabetes Mellitus.” *British Medical Journal* 1 (5291): 1507–13. https://doi.org/10.1136/bmj.1.5291.1507.

Lunn, J. Adrian, and Enrique Rozengurt. 2004. “Hyperosmotic Stress Induces Rapid Focal Adhesion Kinase Phosphorylation at Tyrosines 397 and 577: Role of Src Family Kinases and Rho Family GTPases.” *Journal of Biological Chemistry* 279 (43): 45266–78. https://doi.org/10.1074/jbc.M314132200.

Luo, Lihui, De-Quan Li, and Stephen C Pflugfelder. 2007. “Hyperosmolarity-Induced Apoptosis in Human Corneal Epithelial Cells Is Mediated by Cytochrome c and MAPK Pathways.” *Cornea* 26 (4): 452–60. https://insights.ovid.com/pubmed?pmid=17457195.

Ma, Pingping, Shenfang Zha, Xinkun Shen, Yulan Zhao, Li Li, Li Yang, Mingxing Lei, and Wanqian Liu. 2019. “NFAT5 Mediates Hypertonic Stress-Induced Atherosclerosis via Activating NLRP3 Inflammasome in Endothelium.” *Cell Communication and Signaling* 17 (1): 102. https://doi.org/10.1186/s12964-019-0406-7.

Ma, Wenzhe, Ala Trusina, Hana El-Samad, Wendell A. Lim, and Chao Tang. 2009. “Defining Network Topologies That Can Achieve Biochemical Adaptation.” *Cell* 138 (4): 760–73. https://doi.org/10.1016/j.cell.2009.06.013.

MacMillen, Richard E., and Anthony K. Lee. 1967. “Australian Desert Mice: Independence of Exogenous Water.” *Science* 158 (3799): 383–85. https://doi.org/10.1126/science.158.3799.383.

Madhur, Meena S., Annet Kirabo, Tomasz J. Guzik, and David G. Harrison. 2020. “From Rags to Riches: Moving beyond Rag1 in Studies of Hypertension.” *Hypertension*. Lippincott Williams and Wilkins. https://doi.org/10.1161/HYPERTENSIONAHA.119.14612.

Maeno, E, Y Ishizaki, T Kanaseki, A Hazama, and Y Okada. 2000. “Normotonic Cell Shrinkage Because of Disordered Volume Regulation Is an Early Prerequisite to Apoptosis.” *Proceedings of the National Academy of Sciences of the United States of America* 97 (17): 9487–92. https://doi.org/10.1073/pnas.140216197.

Magnuson, Brian, Bilgen Ekim, and Diane C Fingar. 2012. “Regulation and Function of Ribosomal Protein S6 Kinase (S6K) within MTOR Signalling Networks.” *The Biochemical Journal* 441 (1): 1–21. https://doi.org/10.1042/BJ20110892.

Mathers, William. 2004. “Evaporation from the Ocular Surface.” *Experimental Eye Research* 78 (3): 389–94. https://doi.org/10.1016/S0014-4835(03)00199-4.

McComb, Scott, Pik Ki Chan, Anna Guinot, Holmfridur Hartmannsdottir, Silvia Jenni, Maria Pamela Dobay, Jean Pierre Bourquin, and Beat C. Bornhauser. 2019. “Efficient Apoptosis Requires Feedback Amplification of Upstream Apoptotic Signals by Effector Caspase-3 or -7.” *Science Advances* 5 (7): eaau9433. https://doi.org/10.1126/sciadv.aau9433.

McIlwain, David R, Thorsten Berger, and Tak W Mak. 2013. “Caspase Functions in Cell Death and Disease.” *Cold Spring Harbor Perspectives in Biology* 5 (4): a008656. https://doi.org/10.1101/cshperspect.a008656.

Mettetal, Jerome T, Dale Muzzey, Carlos Gómez-Uribe, and Alexander van Oudenaarden. 2008. “The Frequency Dependence of Osmo-Adaptation in Saccharomyces Cerevisiae.” *Science (New York, N.Y.)* 319 (5862): 482–84. https://doi.org/10.1126/science.1151582.

Meur, N. Le, F. Hahne, and B. Ellis. 2007. “FlowCore: Data Structures Package for Flow Cytometry Data.” *Bioconductor Project*, 1–34.

Miermont, Agnès, François Waharte, Shiqiong Hu, Megan Nicole McClean, Samuel Bottani, Sébastien Léon, and Pascal Hersen. 2013. “Severe Osmotic Compression Triggers a Slowdown of Intracellular Signaling, Which Can Be Explained by Molecular Crowding.” *Proceedings of the National Academy of Sciences of the United States of America* 110 (14): 5725–30. https://doi.org/10.1073/pnas.1215367110.

Miller, Iain, Mingwei Min, Chen Yang, Chengzhe Tian, Sara Gookin, Dylan Carter, and Sabrina L. Spencer. 2018. “Ki67 Is a Graded Rather than a Binary Marker of Proliferation versus Quiescence.” *Cell Reports* 24 (5): 1105-1112.e5. https://doi.org/10.1016/J.CELREP.2018.06.110.

Milligan, L. P., and B. W. McBride. 1985. “Energy Costs of Ion Pumping by Animal Tissues.” *The Journal of Nutrition*. Oxford Academic. https://doi.org/10.1093/jn/115.10.1374.

Milne, Kirsty, Jianhui Sun, Esther A. Zaal, Jenna Mowat, Patrick H.N. Celie, Alexander Fish, Celia R. Berkers, et al. 2019. “A Fragment-like Approach to PYCR1 Inhibition.” *Bioorganic and Medicinal Chemistry Letters* 29 (18): 2626–31. https://doi.org/10.1016/j.bmcl.2019.07.047.

Mitchell, Amir, Ping Wei, and Wendell A Lim. 2015. “Oscillatory Stress Stimulation Uncovers an Achilles’ Heel of the Yeast MAPK Signaling Network.” *Science (New York, N.Y.)* 350 (6266): 1379–83. https://doi.org/10.1126/science.aab0892.

Mocholi, Enric, Samuel D Dowling, Yair Botbol, Ross C Gruber, Alex K Ray, Sebastiaan Vastert, Bridget Shafit-Zagardo, Paul J Coffer, and Fernando Macian. 2018. “Autophagy Is a Tolerance-Avoidance Mechanism That Modulates TCR-Mediated Signaling and Cell Metabolism to Prevent Induction of T Cell Anergy.” *Cell Reports* 24 (5): 1136–50. https://doi.org/10.1016/j.celrep.2018.06.065.

Moeckel, Gilbert W. 2013. “*Hypertonic Stress and Cell Death* . Focus on ‘Multiple Cell Death Pathways Are Independently Activated by Lethal Hypertonicity in Renal Epithelial Cells.’” *American Journal of Physiology-Cell Physiology* 305 (10): C1009–10. https://doi.org/10.1152/ajpcell.00263.2013.

Moeckel, Gilbert W., Li Zhang, Agnes B. Fogo, Chuan Ming Hao, Ambra Pozzi, and Matthew D. Breyer. 2003. “COX2 Activity Promotes Organic Osmolyte Accumulation and Adaptation of Renal Medullary Interstitial Cells to Hypertonic Stress.” *Journal of Biological Chemistry* 278 (21): 19352–57. https://doi.org/10.1074/jbc.M302209200.

Mokashi, Chaitanya S., David L. Schipper, Mohammad A. Qasaimeh, and Robin E.C. Lee. 2019. “A System for Analog Control of Cell Culture Dynamics to Reveal Capabilities of Signaling Networks.” *IScience* 19 (September): 586–96. https://doi.org/10.1016/J.ISCI.2019.08.010.

Monteleone, Ivan, Irene Marafini, Vincenzo Dinallo, Davide Di Fusco, Edoardo Troncone, Francesca Zorzi, Federica Laudisi, and Giovanni Monteleone. 2016. “Sodium Chloride-Enriched Diet Enhances Inflammatory Cytokine Production and Exacerbates Experimental Colitis in Mice.” *Journal of Crohn’s & Colitis*, July, jjw139. https://doi.org/10.1093/ecco-jcc/jjw139.

Mountian, I., and W. Van Driessche. 1997. “Isovolumetric Regulation of C6 Rat Glioma Cells in Hyperosmotic Media.” *The American Journal of Physiology* 272 (1 Pt 1): C318-23. https://doi.org/10.1152/ajpcell.1997.272.1.C318.

Mourão, Márcio A., Joe B. Hakim, and Santiago Schnell. 2014. “Connecting the Dots: The Effects of Macromolecular Crowding on Cell Physiology.” *Biophysical Journal*. Biophysical Society. https://doi.org/10.1016/j.bpj.2014.10.051.

Müller, Dominik N., Nicola Wilck, Stefanie Haase, Markus Kleinewietfeld, and Ralf A. Linker. 2019. “Sodium in the Microenvironment Regulates Immune Responses and Tissue Homeostasis.” *Nature Reviews Immunology*. Nature Publishing Group. https://doi.org/10.1038/s41577-018-0113-4.

Müller, Silke, Thomas Quast, Agnes Schröder, Stephanie Hucke, Luisa Klotz, Jonathan Jantsch, Rupert Gerzer, Ruth Hemmersbach, and Waldemar Kolanus. 2013. “Salt-Dependent Chemotaxis of Macrophages.” *PloS One* 8 (9): e73439. https://doi.org/10.1371/journal.pone.0073439.

Muzzey, Dale, Carlos a Gómez-Uribe, Jerome T Mettetal, and Alexander van Oudenaarden. 2009. “A Systems-Level Analysis of Perfect Adaptation in Yeast Osmoregulation.” *Cell* 138 (1): 160–71. https://doi.org/10.1016/j.cell.2009.04.047.

Netzer, Nikolaus, Hannes Gatterer, Martin Faulhaber, Martin Burtscher, Stephan Pramsohler, and Dominik Pesta. 2015. “Hypoxia, Oxidative Stress and Fat.” *Biomolecules* 5 (2): 1143–50. https://doi.org/10.3390/biom5021143.

Neubert, Patrick, Arne Homann, David Wendelborn, Anna-Lorena Bär, Luka Krampert, Maximilian Trum, Agnes Schröder, et al. 2020. “NCX1 Represents an Ionic Na+ Sensing Mechanism in Macrophages.” Edited by Paula M. Oliver. *PLOS Biology* 18 (6): e3000722. https://doi.org/10.1371/journal.pbio.3000722.

Neubert, Patrick, Andrea Weichselbaum, Carmen Reitinger, Valentin Schatz, Agnes Schröder, John R. Ferdinand, Michaela Simon, et al. 2019. “HIF1A and NFAT5 Coordinate Na+-Boosted Antibacterial Defense via Enhanced Autophagy and Autolysosomal Targeting.” *Autophagy* 15 (11): 1899–1916. https://doi.org/10.1080/15548627.2019.1596483.

Neuert, Gregor, Brian Munsky, Rui Zhen Tan, Leonid Teytelman, Mustafa Khammash, and Alexander van Oudenaarden. 2013. “Systematic Identification of Signal-Activated Stochastic Gene Regulation.” *Science (New York, N.Y.)* 339 (6119): 584–87. https://doi.org/10.1126/science.1231456.

Neuhofer, Wolfgang, and Franz-X. Beck. 2005. “Cell Survival in the Hostile Environment of the Renal Medulla.” *Annual Review of Physiology* 67 (1): 531–55. https://doi.org/10.1146/annurev.physiol.67.031103.154456.

Nguyen, Minhtri K., and Ira Kurtz. 2006. “Quantitative Interrelationship between Gibbs-Donnan Equilibrium, Osmolality of Body Fluid Compartments, and Plasma Water Sodium Concentration.” *Journal of Applied Physiology* 100 (4): 1293–1300. https://doi.org/10.1152/japplphysiol.01274.2005.

Nielsen, M. B., S. T. Christensen, and E. K. Hoffmann. 2008. “Effects of Osmotic Stress on the Activity of MAPKs and PDGFR-β- Mediated Signal Transduction in NIH-3T3 Fibroblasts.” *American Journal of Physiology - Cell Physiology* 294 (4): 1046–55. https://doi.org/10.1152/ajpcell.00134.2007.

Nikpey, Elham, Tine V. Karlsen, Natalia Rakova, Jens M. Titze, Olav Tenstad, and Helge Wiig. 2017. “High-Salt Diet Causes Osmotic Gradients and Hyperosmolality in Skin Without Affecting Interstitial Fluid and Lymph” 69 (4): 660–68. https://doi.org/10.1161/HYPERTENSIONAHA.116.08539.

Niswander, Julie M., and Linda A. Dokas. 2006. “Phosphorylation of HSP27 and Synthesis of 14-3-3ε Are Parallel Responses to Hyperosmotic Stress in the Hippocampus.” *Brain Research* 1116 (1): 19–30. https://doi.org/10.1016/J.BRAINRES.2006.07.119.

———. 2007. “Hyperosmotic Stress-Induced Caspase-3 Activation Is Mediated by P38 MAPK in the Hippocampus.” *Brain Research* 1186 (December): 1–11. https://doi.org/10.1016/J.BRAINRES.2007.10.008.

Noguchi, Rei, Hiroyuki Kubota, Katsuyuki Yugi, Yu Toyoshima, Yasunori Komori, Tomoyoshi Soga, and Shinya Kuroda. 2013. “The Selective Control of Glycolysis, Gluconeogenesis and Glycogenesis by Temporal Insulin Patterns.” *Molecular Systems Biology* 9 (1): 664. https://doi.org/10.1038/msb.2013.19.

Norlander, Allison E, Mohamed A Saleh, Arvind K Pandey, Hana A Itani, Jing Wu, Liang Xiao, Jooeun Kang, et al. 2017. “A Salt-Sensing Kinase in T Lymphocytes, SGK1, Drives Hypertension and Hypertensive End-Organ Damage.” *JCI Insight* 2 (13). https://doi.org/10.1172/jci.insight.92801.

Norstedt, Gunnar, and Richard Palmiter. 1984. “Secretory Rhythm of Growth Hormone Regulates Sexual Differentiation of Mouse Liver.” *Cell* 36 (4): 805–12. https://doi.org/10.1016/0092-8674(84)90030-8.

Nunes, Paula, Isabelle Roth, Paolo Meda, Eric Féraille, Dennis Brown, and Udo Hasler. 2015. “Ionic Imbalance, in Addition to Molecular Crowding, Abates Cytoskeletal Dynamics and Vesicle Motility during Hypertonic Stress.” *Proceedings of the National Academy of Sciences of the United States of America* 112 (24): E3104–13. https://doi.org/10.1073/pnas.1421290112.

O’Callaghan, Carol, Liam J Fanning, and Orla P Barry. 2014. “P38δ MAPK: Emerging Roles of a Neglected Isoform.” *International Journal of Cell Biology* 2014: 272689. https://doi.org/10.1155/2014/272689.

Okada, Yasunobu, Emi Maeno, Takahiro Shimizu, Katsuya Dezaki, Jun Wang, and Shigeru Morishima. 2001. “Receptor-Mediated Control of Regulatory Volume Decrease (RVD) and Apoptotic Volume Decrease (AVD).” *Journal of Physiology*. John Wiley & Sons, Ltd. https://doi.org/10.1111/j.1469-7793.2001.0003g.x.

Okuda, T, and A Grollman. 1967. “Passive Transfer of Autoimmune Induced

Hypertension in the Rat by Lymph Node Cells." *Texas Reports on Biology and Medicine* 25 (2): 257–64. http://www.ncbi.nlm.nih.gov/pubmed/6040652.

Okumus, Burak, Dirk Landgraf, Ghee Chuan Lai, Somenath Bakhsi, Juan Carlos Arias-Castro, Sadik Yildiz, Dann Huh, et al. 2016. "Mechanical Slowing-down of Cytoplasmic Diffusion Allows in Vivo Counting of Proteins in Individual Cells." *Nature Communications* 7 (1): 1–11. https://doi.org/10.1038/ncomms11641.

Olivares, Orianne, Jared R. Mayers, Victoire Gouirand, Margaret E. Torrence, Tristan Gicquel, Laurence Borge, Sophie Lac, et al. 2017. "Collagen-Derived Proline Promotes Pancreatic Ductal Adenocarcinoma Cell Survival under Nutrient Limited Conditions." *Nature Communications* 8 (1): 1–14. https://doi.org/10.1038/ncomms16031.

Orlov, Sergei N., Aleksandra Shiyan, Francis Boudreault, Olga Ponomarchuk, and Ryszard Grygorczyk. 2018. "Search for Upstream Cell Volume Sensors: The Role of Plasma Membrane and Cytoplasmic Hydrogel." *Current Topics in Membranes* 81 (January): 53–82. https://doi.org/10.1016/BS.CTM.2018.07.001.

Overduin, Joost, Tracy S Tylee, R Scott Frayo, and David E Cummings. 2014. "Hyperosmolarity in the Small Intestine Contributes to Postprandial Ghrelin Suppression." *American Journal of Physiology. Gastrointestinal and Liver Physiology* 306 (12): G1108-16. https://doi.org/10.1152/ajpgi.00072.2014.

Pargellis, Christopher, Liang Tong, Laurie Churchill, Pier F. Cirillo, Thomas Gilmore, Anne G. Graham, Peter M. Grob, et al. 2002. "Inhibition of P38 MAP Kinase by Utilizing a Novel Allosteric Binding Site." *Nature Structural Biology* 9 (4): 268–72. https://doi.org/10.1038/nsb770.

Peña-Oyarzun, Daniel, Rodrigo Troncoso, Catalina Kretschmar, Cecilia Hernando, Mauricio Budini, Eugenia Morselli, Sergio Lavandero, and Alfredo Criollo. 2017. "Hyperosmotic Stress Stimulates Autophagy via Polycystin-2." *Oncotarget* 8 (34): 55984–97. https://doi.org/10.18632/oncotarget.18995.

Phang, James M. 1985. "The Regulatory Functions of Proline and Pyrroline-5-Carboxylic Acid." In *Current Topics in Cellular Regulation*, 25:91–132. Academic Press. https://doi.org/10.1016/B978-0-12-152825-6.50008-4.

———. 2019. "Proline Metabolism in Cell Regulation and Cancer Biology: Recent

Advances and Hypotheses.” *Antioxidants and Redox Signaling*. Mary Ann Liebert Inc. https://doi.org/10.1089/ars.2017.7350.

Phang, James M., Wei Liu, Chad N. Hancock, and Joseph W. Fischer. 2015. “Proline Metabolism and Cancer.” *Current Opinion in Clinical Nutrition and Metabolic Care* 18 (1): 71–77. https://doi.org/10.1097/MCO.0000000000000121.

Phang, James M., Wei Liu, and Olga Zabirnyk. 2010. “Proline Metabolism and Microenvironmental Stress.” *Annual Review of Nutrition* 30 (1): 441–63. https://doi.org/10.1146/annurev.nutr.012809.104638.

Phang, James M., Jui Pandhare, and Yongmin Liu. 2008. “The Metabolism of Proline as Microenvironmental Stress Substrate.” In *Journal of Nutrition*, 138:2008S-2015S. American Society for Nutrition. https://doi.org/10.1093/jn/138.10.2008s.

Phang, James Ming, Wei Liu, Chad Hancock, and Kyle J. Christian. 2012a. *The Proline Regulatory Axis and Cancer*. *Frontiers in Oncology*. Frontiers. https://doi.org/10.3389/fonc.2012.00060.

———. 2012b. “The Proline Regulatory Axis and Cancer.” *Frontiers in Oncology* 2 (June): 60. https://doi.org/10.3389/fonc.2012.00060.

Pihán, Philippe, Amado Carreras-Sureda, and Claudio Hetz. 2017. “BCL-2 Family: Integrating Stress Responses at the ER to Control Cell Demise.” *Cell Death and Differentiation* 24 (9): 1478–87. https://doi.org/10.1038/cdd.2017.82.

Purvis, Jeremy E, and Galit Lahav. 2012. “Decoding the Insulin Signal.” *Molecular Cell* 46 (6): 715–16. https://doi.org/10.1016/j.molcel.2012.06.005.

Qiu, Peng, Erin F. Simonds, Sean C. Bendall, Kenneth D. Gibbs, Robert V. Bruggner, Michael D. Linderman, Karen Sachs, Garry P. Nolan, and Sylvia K. Plevritis. 2011. “Extracting a Cellular Hierarchy from High-Dimensional Cytometry Data with SPADE.” *Nature Biotechnology* 29 (10): 886–93. https://doi.org/10.1038/nbt.1991.

Rafael Gómez-Sjöberg, †, † Anne A. Leyrat, ‡ Dana M. Pirone, ‡ and Christopher S. Chen, and † Stephen R. Quake*. 2007. “Versatile, Fully Automated, Microfluidic Cell Culture System.”

Rahi, Sahand Jamal, Johannes Larsch, Kresti Pecani, Alexander Y Katsov, Nahal Mansouri, Krasimira Tsaneva-Atanasova, Eduardo D Sontag, and Frederick R Cross. 2017. “Oscillatory Stimuli Differentiate Adapting Circuit Topologies.” *Nature*

Methods, no. July. https://doi.org/10.1038/nmeth.4408.

Rakova, Natalia, Kento Kitada, Kathrin Lerchl, Anke Dahlmann, Anna Birukov, Steffen Daub, Christoph Kopp, et al. 2017. “Increased Salt Consumption Induces Body Water Conservation and Decreases Fluid Intake.” *Journal of Clinical Investigation* 166 (4): 669–77. https://doi.org/10.1172/JCI88530.

Ramirez, Monica L.Gonzalez, and Guy S. Salvesen. 2018. “A Primer on Caspase Mechanisms.” *Seminars in Cell and Developmental Biology*. Elsevier Ltd. https://doi.org/10.1016/j.semcdb.2018.01.002.

Rasmussen, Line Jee Hartmann, Helene Steenkær Holm Müller, Bente Jørgensen, Stine Falsig Pedersen, and Else Kay Hoffmann. 2015. “Osmotic Shrinkage Elicits FAK- and Src Phosphorylation and Src-Dependent NKCC1 Activation in NIH3T3 Cells.” *American Journal of Physiology-Cell Physiology* 308 (2): C101–10. https://doi.org/10.1152/ajpcell.00070.2014.

Roos, Wynand P., and Bernd Kaina. 2006. “DNA Damage-Induced Cell Death by Apoptosis.” *Trends in Molecular Medicine*. Elsevier Current Trends. https://doi.org/10.1016/j.molmed.2006.07.007.

Rosenqvist, U., V. Licko, and J. H. Karam. 1976. “Evaluation of a ‘true’ Fractional Removal Rate of Glucose in Man by Bolus and Simulated Ramp Increase of Glucose.” *Diabetes* 25 (7): 580–85. https://doi.org/10.2337/diab.25.7.580.

Rossitto, Giacomo, Sheon Mary, Jun Yu Chen, Philipp Boder, Khai Syuen Chew, Karla B. Neves, Rheure L. Alves, et al. 2020. “Tissue Sodium Excess Is Not Hypertonic and Reflects Extracellular Volume Expansion.” *Nature Communications* 11 (1): 1–9. https://doi.org/10.1038/s41467-020-17820-2.

Roth, Isabelle, Valérie Leroy, H. Moo Kwon, Pierre Yves Martin, Eric Féraille, and Udo Hasler. 2010. “Osmoprotective Transcription Factor NFAT5/TonEBP Modulates Nuclear Factor-KB Activity.” *Molecular Biology of the Cell* 21 (19): 3459–74. https://doi.org/10.1091/mbc.E10-02-0133.

Rudolph, Alan S, and John H Crowe. 1985. “Membrane Stabilization during Freezing: The Role of Two Natural Cryoprotectants, Trehalose and Proline.” *Cryobiology* 22 (4): 367–77. https://doi.org/10.1016/0011-2240(85)90184-1.

Russo, M. A., G. D.V. van Rossum, and T. Galeotti. 1977. “Observations on the

Regulation of Cell Volume and Metabolic Control in Vitro; Changes in the Composition and Ultrastructure of Liver Slices under Conditions of Varying Metabolic and Transporting Activity." *The Journal of Membrane Biology* 31 (1): 267–99. https://doi.org/10.1007/BF01869409.

Saeys, Yvan, Sofie Van Gassen, and Bart N. Lambrecht. 2016. "Computational Flow Cytometry: Helping to Make Sense of High-Dimensional Immunology Data." *Nature Reviews Immunology* 16 (7): 449–62. https://doi.org/10.1038/nri.2016.56.

Sahu, Nisebita, Darlene Dela Cruz, Min Gao, Wendy Sandoval, Peter M. Haverty, Jinfeng Liu, Jean Philippe Stephan, et al. 2016. "Proline Starvation Induces Unresolved ER Stress and Hinders MTORC1-Dependent Tumorigenesis." *Cell Metabolism* 24 (5): 753–61. https://doi.org/10.1016/j.cmet.2016.08.008.

Saito, Haruo, and Francesc Posas. 2012. "Response to Hyperosmotic Stress." *Genetics* 192 (2): 289–318. https://doi.org/10.1534/genetics.112.140863.

Sano, Takanori, Kentaro Kawata, Satoshi Ohno, Katsuyuki Yugi, Hiroaki Kakuda, Hiroyuki Kubota, Shinsuke Uda, et al. 2016. "Selective Control of Up-Regulated and down-Regulated Genes by Temporal Patterns and Doses of Insulin." *Science Signaling* 9 (455): 1–12. https://doi.org/10.1126/scisignal.aaf3739.

Santos, Bento, Alejandro Chevalie, Marie-Josee Hebert, Jane Zagajeski, and R Gullans, Steven. 1998. "A Combination of NaCl and Urea Enhances Survival of IMCD Cells to Hyperosmolality." *American Journal of Renal Physiology*, 327–36. http://ajprenal.physiology.org/content/274/6/F1167.

Sasagawa, Satoru, Yu-ichi Ozaki, Kazuhiro Fujita, and Shinya Kuroda. 2005. "Prediction and Validation of the Distinct Dynamics of Transient and Sustained ERK Activation." *Nature Cell Biology* 7 (4): 365–73. https://doi.org/10.1038/ncb1233.

Schatz, Valentin, Patrick Neubert, Agnes Schröder, Katrina Binger, Matthias Gebhard, Dominik N Müller, Friedrich C Luft, Jens Titze, and Jonathan Jantsch. 2016. "Elementary Immunology: Na(+) as a Regulator of Immunity." *Pediatric Nephrology (Berlin, Germany)*, February. https://doi.org/10.1007/s00467-016-3349-x.

Scherer, Clemens, Larissa Pfisterer, Andreas H. Wagner, Maren Hödebeck, Marco Cattaruzza, Markus Hecker, and Thomas Korff. 2014. "Arterial Wall Stress Controls NFAT5 Activity in Vascular Smooth Muscle Cells." *Journal of the American Heart*

Association 3 (2). https://doi.org/10.1161/JAHA.113.000626.

Schmidt-Nielsen, B, B Graves, and J Roth. 1983. “Water Removal and Solute Additions Determining Increases in Renal Medullary Osmolality.” *The American Journal of Physiology* 244 (5): F472-82. papers2://publication/uuid/C67F11BB-243A-4581-89FC-5B4A283054F8.

Scrivo, Rossana, Laura Massaro, Cristiana Barbati, Marta Vomero, Fulvia Ceccarelli, Francesca Romana Spinelli, Valeria Riccieri, et al. 2017. “The Role of Dietary Sodium Intake on the Modulation of T Helper 17 Cells and Regulatory T Cells in Patients with Rheumatoid Arthritis and Systemic Lupus Erythematosus.” Edited by Masataka Kuwana. *PLOS ONE* 12 (9): e0184449. https://doi.org/10.1371/journal.pone.0184449.

Seniuk, Anika, Jonas L. Thiele, Andra Stubbe, Philipp Oser, Alva Rosendahl, Marlies Bode, Catherine Meyer-Schwesinger, Ulrich O. Wenzel, and Heimo Ehmke. 2020. “B6.Rag1 Knockout Mice Generated at the Jackson Laboratory in 2009 Show a Robust Wild-Type Hypertensive Phenotype in Response to Ang II (Angiotensin II).” *Hypertension* 75 (4): 1110–16. https://doi.org/10.1161/HYPERTENSIONAHA.119.13773.

Shapiro, L., and C. A. Dinarello. 1995. “Osmotic Regulation of Cytokine Synthesis in Vitro.” *Proceedings of the National Academy of Sciences* 92 (26): 12230–34. https://doi.org/10.1073/pnas.92.26.12230.

Shimizu, Thomas S, Yuhai Tu, and Howard C Berg. 2010. “A Modular Gradient-Sensing Network for Chemotaxis in Escherichia Coli Revealed by Responses to Time-Varying Stimuli.” *Molecular Systems Biology* 6 (June). https://doi.org/10.1038/msb.2010.37.

Shin, Yoojin, Sewoon Han, Jessie S Jeon, Kyoko Yamamoto, Ioannis K Zervantonakis, Ryo Sudo, Roger D Kamm, and Seok Chung. 2012. “Microfluidic Assay for Simultaneous Culture of Multiple Cell Types on Surfaces or within Hydrogels.” *Nature Protocols* 7 (7): 1247–59. https://doi.org/10.1038/nprot.2012.051.

Shoval, Oren, Lea Goentoro, Yuval Hart, Avi Mayo, Eduardo Sontag, and Uri Alon. 2010. “Fold-Change Detection and Scalar Symmetry of Sensory Input Fields.” *Proceedings of the National Academy of Sciences of the United States of America*

107 (36): 15995–0. https://doi.org/10.1073/pnas.1002352107.

Skånland, Sigrid S. 2018. “Phospho Flow Cytometry with Fluorescent Cell Barcoding for Single Cell Signaling Analysis and Biomarker Discovery.” *Journal of Visualized Experiments*, no. 140 (October): e58386–e58386. https://doi.org/10.3791/58386.

Slee, E. Cohen, G. 1996. “Benzyloxycarbonyl-Val-Ala-Asp (OMe) Fluoromethylketone (Z-VAD.FMK) Inhibits Apoptosis by Blocking the Processing of CPP32.” *Biochem. J.*

Slee, Elizabeth A., Mary T. Harte, Ruth M. Kluck, Beni B. Wolf, Carlos A. Casiano, Donald D. Newmeyer, Hong Gang Wang, et al. 1999. “Ordering the Cytochrome C-Initiated Caspase Cascade: Hierarchical Activation of Caspases-2,-3,-6,-7,-8, and -10 in a Caspase-9-Dependent Manner.” *Journal of Cell Biology* 144 (2): 281–92. https://doi.org/10.1083/jcb.144.2.281.

Soni, Sourabh, Prince Anand, and Yogendra S. Padwad. 2019. “MAPKAPK2: The Master Regulator of RNA-Binding Proteins Modulates Transcript Stability and Tumor Progression.” *Journal of Experimental & Clinical Cancer Research* 38 (1): 121. https://doi.org/10.1186/s13046-019-1115-1.

Sorre, Benoit, Aryeh Warmflash, Ali H. H. Brivanlou, and Eric D. D. Siggia. 2014. “Encoding of Temporal Signals by the TGF-β Pathway and Implications for Embryonic Patterning.” *Developmental Cell* 30 (3): 334–42. https://doi.org/10.1016/j.devcel.2014.05.022.

Spidlen, Josef, Karin Breuer, Chad Rosenberg, Nikesh Kotecha, and Ryan R. Brinkman. 2012. “FlowRepository: A Resource of Annotated Flow Cytometry Datasets Associated with Peer-Reviewed Publications.” *Cytometry Part A* 81A (9): 727–31. https://doi.org/10.1002/cyto.a.22106.

Spurgeon, B. E. J., A. Aburima, N. G. Oberprieler, K. Taskén, and K. M. Naseem. 2014. “Multiplexed Phosphospecific Flow Cytometry Enables Large-Scale Signaling Profiling and Drug Screening in Blood Platelets.” *Journal of Thrombosis and Haemostasis* 12 (10): 1733–43. https://doi.org/10.1111/jth.12670.

Stam, Jose, Wayel Abdulahad, Minke G. Huitema, Caroline Roozendaal, Pieter C. Limburg, Margriet van Stuijvenberg, and Elisabeth H. Schölvinck. 2011. “Fluorescent Cell Barcoding as a Tool to Assess the Age-Related Development of

Intracellular Cytokine Production in Small Amounts of Blood from Infants." Edited by Laurent Rénia. *PLoS ONE* 6 (10): e25690. https://doi.org/10.1371/journal.pone.0025690.

Steiner, Robert A., William J. Bremner, and Donald K. Clifton. 1982. "Regulation of Luteinizing Hormone Pulse Frequency and Amplitude by Testosterone in the Adult Male Rat*." *Endocrinology* 111 (6): 2055–61. https://doi.org/10.1210/endo-111-6-2055.

Stewart, Benjamin J, John R Ferdinand, Matthew D Young, Thomas J Mitchell, Kevin W Loudon, Alexandra M Riding, Nathan Richoz, et al. 2019. "Spatiotemporal Immune Zonation of the Human Kidney." *Science (New York, N.Y.)* 365 (6460): 1461–66. https://doi.org/10.1126/science.aat5031.

Stookey, Jodi, Carl Pieper, and Harvey Cohen. 2004. "Hypertonic Hyperglycemia Progresses to Diabetes Faster than Normotonic." *European Journal of Epidemiology* 19 (10): 935–44. https://doi.org/10.1007/s10654-004-5729-y.

Sulen, André, Stein-Erik Gullaksen, Lucius Bader, David W. McClymont, Jørn Skavland, Sonia Gavasso, and Bjørn T. Gjertsen. 2016. "Signaling Effects of Sodium Hydrosulfide in Healthy Donor Peripheral Blood Mononuclear Cells." *Pharmacological Research* 113: 216–27. https://doi.org/10.1016/j.phrs.2016.08.018.

Szabados, László, and Arnould Savouré. 2010. "Proline: A Multifunctional Amino Acid." *Trends in Plant Science* 15 (2): 89–97. https://doi.org/10.1016/J.TPLANTS.2009.11.009.

Takagi, Hiroshi. 2008. "Proline as a Stress Protectant in Yeast: Physiological Functions, Metabolic Regulations, and Biotechnological Applications." *Applied Microbiology and Biotechnology* 81 (2): 211–23. https://doi.org/10.1007/s00253-008-1698-5.

Takeda, Kohsuke, Takuya Noguchi, Isao Naguro, and Hidenori Ichijo. 2008. "Apoptosis Signal-Regulating Kinase 1 in Stress and Immune Response." *Annual Review of Pharmacology and Toxicology* 48 (1): 199–225. https://doi.org/10.1146/annurev.pharmtox.48.113006.094606.

Tanner, John J., Sarah Maria Fendt, and Donald F. Becker. 2018. "The Proline Cycle As a Potential Cancer Therapy Target." *Biochemistry* 57 (25): 3433–44.

https://doi.org/10.1021/acs.biochem.8b00215.

Thiemicke, Alexander, Hossein Jashnsaz, Guoliang Li, and Gregor Neuert. 2019. “Generating Kinetic Environments to Study Dynamic Cellular Processes in Single Cells.” *Scientific Reports* 9 (1): 10129. https://doi.org/10.1038/s41598-019-46438-8.

Thurley, Kevin, L F Wu, and Steven J Altschuler. 2017. “Behaviors of Cell-to-Cell Communication Network Motifs.” *Submitted*.

Titze, Jens, Holger Krause, Hermann Hecht, Peter Dietsch, Jörn Rittweger, Rainer Lang, Karl A. Kirsch, and Karl F. Hilgers. 2002. “Reduced Osmotically Inactive Na Storage Capacity and Hypertension in the Dahl Model.” *American Journal of Physiology - Renal Physiology* 283 (1 52-1). https://doi.org/10.1152/ajprenal.00323.2001.

Titze, Jens, Alain Maillet, Rainer Lang, Hanns Christian Gunga, Bernd Johannes, Guillemette Gauquelin-Koch, Emanuelle Kihm, Irina Larina, Claude Gharib, and Karl August Kirsch. 2002. “Long-Term Sodium Balance in Humans in a Terrestrial Space Station Simulation Study.” *American Journal of Kidney Diseases* 40 (3): 508–16. https://doi.org/10.1053/ajkd.2002.34908.

Trama, Jason, William Y. Go, and Steffan N. Ho. 2002. “The Osmoprotective Function of the NFAT5 Transcription Factor in T Cell Development and Activation.” *The Journal of Immunology* 169 (10): 5477–88. https://doi.org/10.4049/jimmunol.169.10.5477.

Trempolec, Natalia, Natalia Dave-Coll, and Angel R Nebreda. 2013. “SnapShot: P38 MAPK Substrates.” *Cell* 152 (4): 924-924.e1. https://doi.org/10.1016/j.cell.2013.01.047.

Tropini, Carolina, Eli Lin Moss, Bryan Douglas Merrill, Katharine Michelle Ng, Steven Kyle Higginbottom, Ellen Pun Casavant, Carlos Gutierrez Gonzalez, et al. 2018. “Transient Osmotic Perturbation Causes Long-Term Alteration to the Gut Microbiota.” *Cell* 173 (7): 1742-1754.e17. https://doi.org/10.1016/J.CELL.2018.05.008.

Tsai, Wanxia Li, Laura Vian, Valentina Giudice, Jacqueline Kieltyka, Christine Liu, Victoria Fonseca, Nathalia Gazaniga, et al. 2019. “High Throughput PSTAT Signaling Profiling by Fluorescent Cell Barcoding and Computational Analysis.”

Journal of Immunological Methods 477 (November): 112667. https://doi.org/10.1016/J.JIM.2019.112667.

Ullrich, K J, B Schmidt-Nielson, R O'Dell, G Pehling, C W Gottschalk, W E Lassiter, and M Mylle. 1963. "Micropuncture Study of Composition of Proximal and Distal Tubular Fluid in Rat Kidney." *The American Journal of Physiology* 204: 527–31.

Urban, J. P.G. 1994. "The Chondrocyte: A Cell under Pressure." *Rheumatology* 33 (10): 901–8. https://doi.org/10.1093/rheumatology/33.10.901.

Urban, J. P.G., A. C. Hall, and K. A. Gehl. 1993. "Regulation of Matrix Synthesis Rates by the Ionic and Osmotic Environment of Articular Chondrocytes." *Journal of Cellular Physiology* 154 (2): 262–70. https://doi.org/10.1002/jcp.1041540208.

Urban, J.P.G., and A. Maroudas. 1979. "The Measurement of Fixed Charged Density in the Intervertebral Disc." *Biochimica et Biophysica Acta (BBA) - General Subjects* 586 (1): 166–78. https://doi.org/10.1016/0304-4165(79)90415-X.

Ussing, Hans H. 1960. "The Alkali Metal Ions in Isolated Systems and Tissues." In *Handbuch Der Experimentellen Pharmakologie*.

Varani, James, Michael K. Dame, Laure Rittie, Suzanne E.G. Fligiel, Sewon Kang, Gary J. Fisher, and John J. Voorhees. 2006. "Decreased Collagen Production in Chronologically Aged Skin: Roles of Age-Dependent Alteration in Fibroblast Function and Defective Mechanical Stimulation." *American Journal of Pathology* 168 (6): 1861–68. https://doi.org/10.2353/ajpath.2006.051302.

Verbruggen, Nathalie, and Christian Hermans. 2008. "Proline Accumulation in Plants: A Review." *Amino Acids* 35 (4): 753–59. https://doi.org/10.1007/s00726-008-0061-6.

Voet, Donald, and Judith Voet. 2011. *Biochemistry*. 4th ed. Wiley.

Wagner, Erwin F, and Angel R Nebreda. 2009. "Signal Integration by JNK and P38 MAPK Pathways in Cancer Development." *Nature Reviews. Cancer* 9 (8): 537–49. https://doi.org/10.1038/nrc2694.

Wahiduzzaman, Md. Imtaiyaz Hassan, Asimul Islam, and Faizan Ahmad. 2019. "Urea Stress: Myo-Inositol's Efficacy to Counteract Destabilization of TIM-β-Globin Complex by Urea Is as Good as That of the Methylamine." *International Journal of Biological Macromolecules*, November. https://doi.org/10.1016/J.IJBIOMAC.2019.10.153.

Wang, Yu Bao, Valérie Leroy, Arvid B. Maunsbach, Alain Doucet, Udo Hasler, Eva Dizin, Thomas Ernandez, Sophie De Seigneux, Pierre Yves Martin, and Eric Féraille. 2014. “Sodium Transport Is Modulated by P38 Kinase-Dependent Cross-Talk between ENaC and Na,K-ATPase in Collecting Duct Principal Cells.” *Journal of the American Society of Nephrology* 25 (2): 250–59. https://doi.org/10.1681/ASN.2013040429.

Warburg, Otto. 1956. “On the Origin of Cancer Cells.” *Science* 123 (3191): 309–14. https://doi.org/10.1126/science.123.3191.309.

Weber, Ernst Heinrich. 1850. *Der Tastsinn Und Das Gemeingefühl.* http://psychologie.biphaps.uni-leipzig.de/wundt/opera/ehweber/tastsinn/Tastsinn.htm.

Weisheit, Christina K, Daniel R Engel, and Christian Kurts. 2015. “Dendritic Cells and Macrophages: Sentinels in the Kidney.” *Clinical Journal of the American Society of Nephrology : CJASN* 10 (10): 1841–51. https://doi.org/10.2215/CJN.07100714.

Wheaton, William W., and Navdeep S. Chandel. 2011. “Hypoxia. 2. Hypoxia Regulates Cellular Metabolism.” *American Journal of Physiology - Cell Physiology*. American Physiological Society. https://doi.org/10.1152/ajpcell.00485.2010.

White, F, and A Grollman. 1964. “Autoimmune Factors Associated with Infarction of the Kidney.” *Nephron* 1 (December): 93–102.

Wiig, Helge, Agnes Schröder, Wolfgang Neuhofer, Jonathan Jantsch, Christoph Kopp, Tine V. Karlsen, Michael Boschmann, et al. 2013. “Immune Cells Control Skin Lymphatic Electrolyte Homeostasis and Blood Pressure.” *Journal of Clinical Investigation* 123 (7): 2803–15. https://doi.org/10.1172/JCI60113.

Wilck, Nicola, András Balogh, Lajos Markó, Hendrik Bartolomaeus, and Dominik N. Müller. 2019. “The Role of Sodium in Modulating Immune Cell Function.” *Nature Reviews Nephrology* 15 (9). https://doi.org/10.1038/s41581-019-0167-y.

Winston Chang, Joe Cheng, JJ Allaire , Yihui Xie, Jonathan McPherson. 2020. “Shiny: Web Application Framework for R.” https://cran.r-project.org/web/packages/shiny/index.html.

Woo, Seung Kyoon, Sang Do Lee, Ki Young Na, Won Kun Park, and H Moo Kwon. 2002. “TonEBP/NFAT5 Stimulates Transcription of HSP70 in Response to

Hypertonicity." *Molecular and Cellular Biology* 22 (16): 5753–60. https://doi.org/10.1128/MCB.22.16.5753-5760.2002.

Wood, Janet M. 1999. "Osmosensing by Bacteria: Signals and Membrane-Based Sensors." *Microbiology and Molecular Biology Reviews* 63 (1): 230–62. https://doi.org/10.1128/mmbr.63.1.230-262.1999.

———. 2011. "Bacterial Osmoregulation: A Paradigm for the Study of Cellular Homeostasis." *Annual Review of Microbiology* 65 (September): 215–38. https://doi.org/10.1146/annurev-micro-090110-102815.

Wu, Chuan, Nir Yosef, Theresa Thalhamer, Chen Zhu, Sheng Xiao, Yasuhiro Kishi, Aviv Regev, and Vijay K. Kuchroo. 2013. "Induction of Pathogenic TH17 Cells by Inducible Salt-Sensing Kinase SGK1." *Nature* 496 (7446): 513–17. https://doi.org/10.1038/nature11984.

Yancey, Paul H. 2005. "Organic Osmolytes as Compatible, Metabolic and Counteracting Cytoprotectants in High Osmolarity and Other Stresses." *Journal of Experimental Biology* 208 (15): 2819–30. https://doi.org/10.1242/JEB.01730.

Yancey, Paul H., Mary E. Clark, Steven C. Hand, R. David Bowlus, and George N. Somero. 1982. "Living with Water Stress: Evolution of Osmolyte Systems." *Science* 217 (4566): 1214–22. https://doi.org/10.1126/science.7112124.

Yang, Ji, Huijie Zhang, Sujiao Sun, Xue Wang, Ying Guan, Qili Mi, Wanli Zeng, et al. 2020. "Autophagy and Hsp70 Activation Alleviate Oral Epithelial Cell Death Induced by Food-Derived Hypertonicity." *Cell Stress and Chaperones*, 1–12. https://doi.org/10.1007/s12192-020-01068-2.

Yarza, Ramon, Silvia Vela, Maite Solas, and Maria J Ramirez. 2015. "C-Jun N-Terminal Kinase (JNK) Signaling as a Therapeutic Target for Alzheimer's Disease." *Frontiers in Pharmacology* 6: 321. https://doi.org/10.3389/fphar.2015.00321.

Yi, Buqing, Jens Titze, Marina Rykova, Matthias Feuerecker, Galina Vassilieva, Igor Nichiporuk, Gustav Schelling, Boris Morukov, and Alexander Choukèr. 2015. "Effects of Dietary Salt Levels on Monocytic Cells and Immune Responses in Healthy Human Subjects: A Longitudinal Study." *Translational Research* 166 (1): 103–10. https://doi.org/10.1016/j.trsl.2014.11.007.

Young, J. W., J. C. W. Locke, and M. B. Elowitz. 2013. "Rate of Environmental Change

Determines Stress Response Specificity." *Proceedings of the National Academy of Sciences* 110 (10): 4140–45. https://doi.org/10.1073/pnas.1213060110.

Young, Jonathan W., James C. W. Locke, and Michael B. Elowitz. 2013. "Rate of Environmental Change Determines Stress Response Specificity" 110 (10). https://doi.org/10.1073/pnas.1213060110.

Young, Jonathan W, James C W Locke, and Michael B Elowitz. 2013. "Rate of Environmental Change Determines Stress Response Specificity." *Proceedings of the National Academy of Sciences of the United States of America* 110 (10): 4140–45. https://doi.org/10.1073/pnas.1213060110.

Zeng, Tengyue, Libing Zhu, Min Liao, Wenli Zhuo, Shunliang Yang, Weizhen Wu, and Dong Wang. 2017. "Knockdown of PYCR1 Inhibits Cell Proliferation and Colony Formation via Cell Cycle Arrest and Apoptosis in Prostate Cancer." *Medical Oncology* 34 (2): 1–9. https://doi.org/10.1007/s12032-016-0870-5.

Zhang, Ying, Yi-Ping Ho, Ya-Ling Chiu, Hon Fai Chan, Ben Chlebina, Tom Schuhmann, Lingchong You, and Kam W. Leong. 2013. "A Programmable Microenvironment for Cellular Studies via Microfluidics-Generated Double Emulsions." *Biomaterials* 34 (19): 4564–72. https://doi.org/10.1016/J.BIOMATERIALS.2013.03.002.

Zhang, Zheng, Natalia I Dmitrieva, Jong-Hwan Park, Rodney L Levine, and Maurice B Burg. 2004. "High Urea and NaCl Carbonylate Proteins in Renal Cells in Culture and in Vivo, and High Urea Causes 8-Oxoguanine Lesions in Their DNA." *Proceedings of the National Academy of Sciences of the United States of America* 101 (25): 9491–96. https://doi.org/10.1073/pnas.0402961101.

Zhou, Xiaoming. 2015. "Regulation of Tonicity-Dependent Activation of NFAT5 by Mitogen-Activated Protein Kinases." *Abdomen*. http://www.smartscitech.com/index.php/Abdomen/article/view/767.

Zhou, Xiaoming, Joan D. Ferraris, and Maurice B. Burg. 2006. "Mitochondrial Reactive Oxygen Species Contribute to High NaCl-Induced Activation of the Transcription Factor TonEBP/OREBP." *American Journal of Physiology - Renal Physiology* 290 (5). https://doi.org/10.1152/ajprenal.00378.2005.

Zhou, Xiaoming, Joan D. Ferraris, Natalia I. Dmitrieva, Yusen Liu, and Maurice B. Burg. 2008. "MKP-1 Inhibits High NaCl-Induced Activation of P38 but Does Not Inhibit the

Activation of TonEBP/OREBP: Opposite Roles of P38␣ and P38␦” 105 (14). http://www.ncbi.nlm.nih.gov/pubmed/18367666.

Zou, Ai Ping, Ningjun Li, and Allen W. Cowley. 2001. “Production and Actions of Superoxide in the Renal Medulla.” In *Hypertension*, 37:547–53. Lippincott Williams and Wilkins. https://doi.org/10.1161/01.hyp.37.2.547.

Zunder, Eli R., Rachel Finck, Gregory K. Behbehani, El Ad D. Amir, Smita Krishnaswamy, Veronica D. Gonzalez, Cynthia G. Lorang, et al. 2015. “Palladium-Based Mass Tag Cell Barcoding with a Doublet-Filtering Scheme and Single-Cell Deconvolution Algorithm.” *Nature Protocols* 10 (2): 316–33. https://doi.org/10.1038/nprot.2015.020.

APPENDIX

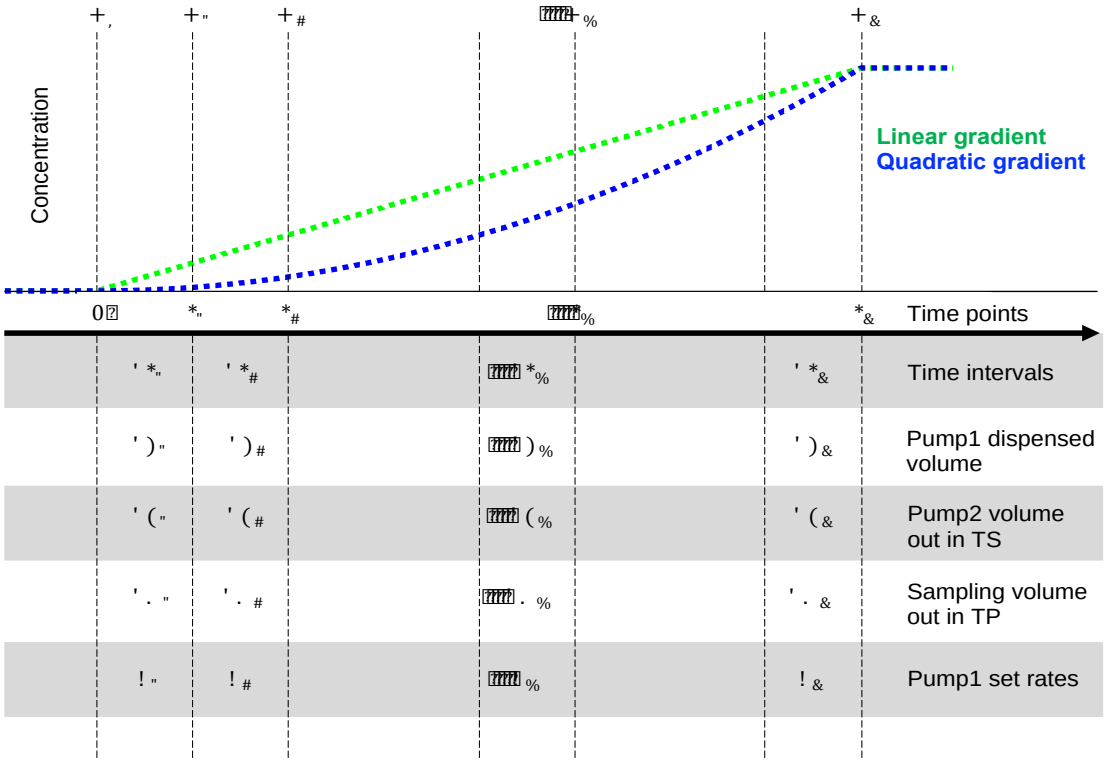

Figure A1: A diagram illustration of algorithm to compute the pump profiles.

We calculate the stimulus concentration for any profile over discrete time points set by programmable pump by combining several short segments with linear concentration profiles. During each interval, we increase (Figure A2) or decrease (Figure A3) the concentration linearly with a fixed rate to achieve increasing or decreasing kinetics of any shape over time. For linear gradient kinetics, the rates are fixed during all intervals ($k_1 = k_2 = \cdots k_N$). By changing the rate from one interval to the next, any arbitrary profile over the whole treatment time can be generated ($k_1 \neq k_2 \neq \cdots k_N$). During each interval (dt_i), stimulus is delivered continually over time by adding appropriate amount (dv_i) of concentrated stimulus. The profiles are corrected for the added (dv_i) and removal (du_i and dw_i) volumes therefore change in stimulus concentration.

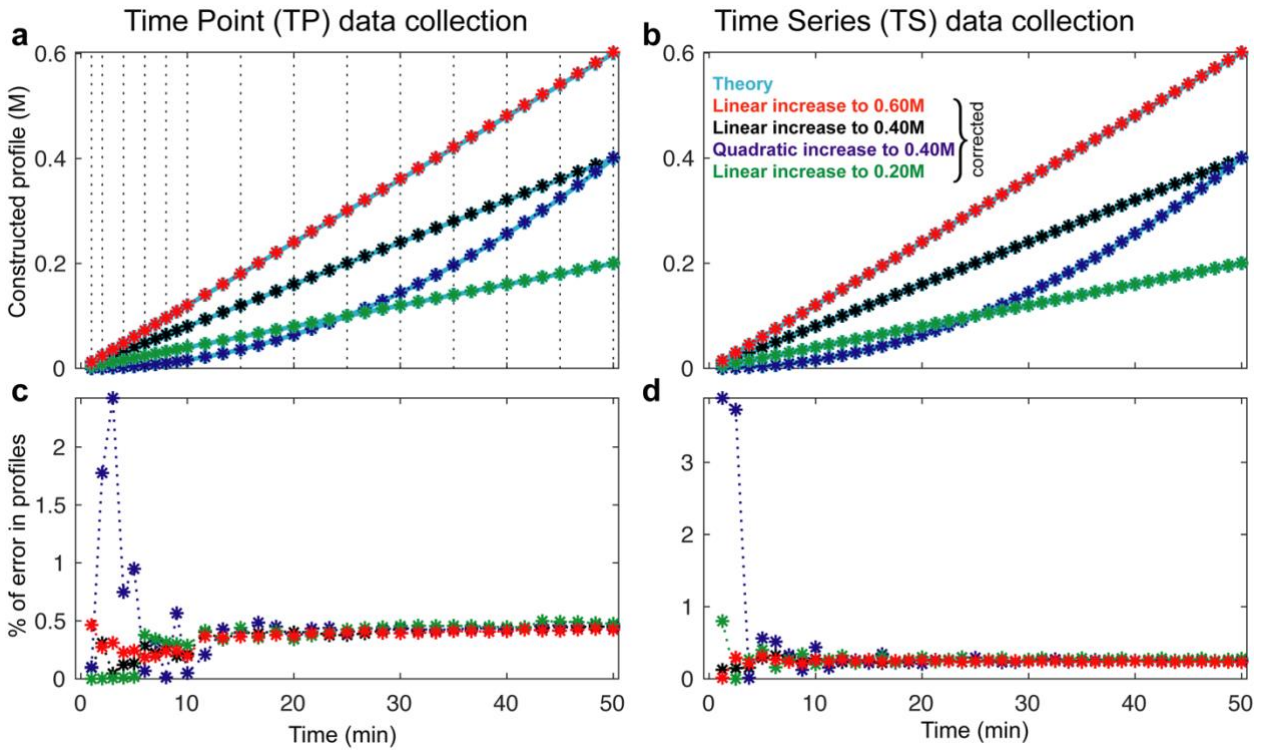

Figure A2: Calculated pump profiles for increasing linear and nonlinear gradient kinetics

(a-b) Calculation of pump profile generation for Time Point (TP, a) and Time series (TS, b) data collection. In both TP and TS experiments, computed pump profiles (corrected for volume removal and therefore change in stimulus concentration) are linear increasing gradient to 0.60M (red), linear increasing gradient to 0.40M (black), quadratic increasing gradient to 0.40M (blue), and linear increasing gradient to 0.20M (green), all compared to their theoretical values (cyan). (c-d) Error comparisons between computed pump profiles and their corresponding proposed concentration profiles for TP (c) and TS (d) experiments. The profiles are generated under the following conditions (the same conditions are used for Figure A3); the concentrated stimulus concentration $C_{max} = 4\ M$. *The total flask volume is set* $V_0 = 50\ mL$ *at* $t = 0$. *Pump 2 rate was set to* $\bar{k} = 0.1\ mL/min$ *for TS and* $\bar{k} = 0$ *for TP experiment. Samples are taken out at the fixed volumes of* $dw_i = 1\ mL$ *at the time points [1,2,4,6,8,10,15,20,25,30,35,40,45,50] minutes for TP (dotted lines in a), while no sampling is done for TS. Both TP and TS profiles are generated over 50 minutes. TS is computed in 40 intervals and TP profile in 34 intervals set optimally by* the programmable syringe pump.

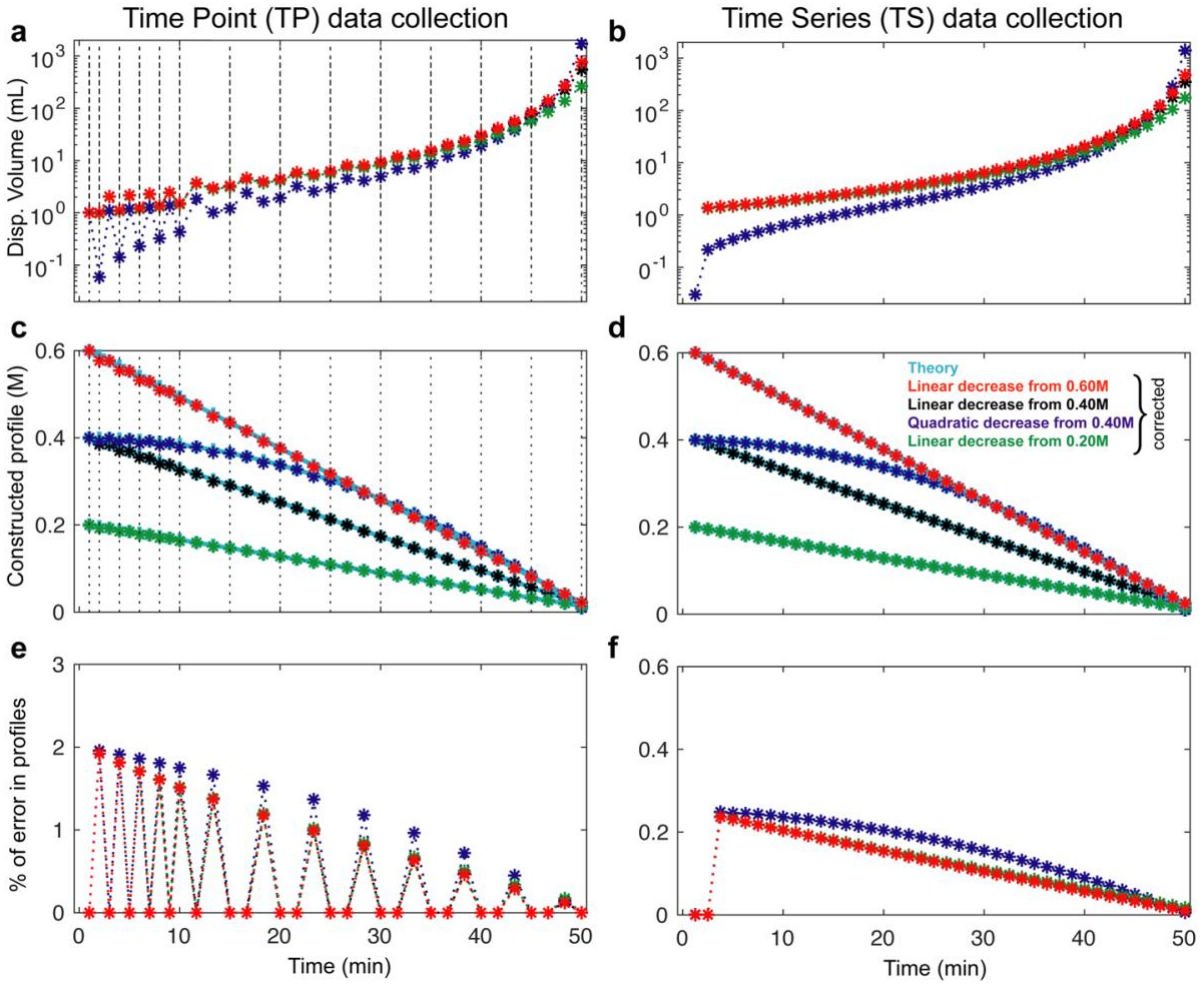

Figure A3: Calculated pump profiles for decreasing linear and nonlinear gradient kinetics

(***a-f***) *Calculation of decreasing pump profile generation for Time Point (TP,* ***a,c,e****) and Time series (TS,* ***b,d,f****) data collection. In both TP and TS experiments, computed pump profiles (corrected for volume removal and therefore change in stimulus concentration) are linear decreasing gradient from 0.60M (red), linear decreasing gradient from 0.40M (black), quadratic decreasing gradient from 0.40M (blue), and linear decreasing gradient from 0.20M (green), all to 0.01M and all compared to their theoretical values (cyan). (**a-b**) Computed and instrument adapted syringe dispense volume. (**c-d**) Computed concentration profiles over time. (**e-f**) Error comparisons between computed decreasing pump profiles and their corresponding proposed concentration profiles for TP (**e**) and TS (**f**) experiments.*

Interval	Time points (min)	Disp. Volume* (mL)	Cumulative Disp. Volume (mL)	Pump rate (µL /min)	Molarity* (M)	Error* % in molarity compared to theory
1	1.25	0.125	0.125	100	0.01	0
2	2.5	0.126	0.251	100.8	0.02	0
3	3.75	0.126	0.377	100.8	0.03	0
4	5	0.127	0.504	101.6	0.04	0
5	6.25	0.127	0.631	101.6	0.05	0
6	7.5	0.127	0.758	101.6	0.06	0
7	8.75	0.127	0.885	101.6	0.07	0
8	10	0.128	1.013	102.4	0.08	0
9	11.25	0.128	1.141	102.4	0.09	0
10	12.5	0.128	1.269	102.4	0.1	0
11	13.75	0.129	1.398	103.2	0.11	0
12	15	0.129	1.527	103.2	0.12	0
13	16.25	0.129	1.656	103.2	0.13	0
14	17.5	0.13	1.786	104	0.14	0
15	18.75	0.13	1.916	104	0.15	0
16	20	0.131	2.047	104.8	0.16	0
17	21.25	0.131	2.178	104.8	0.17	0
18	22.5	0.131	2.309	104.8	0.18	0
19	23.75	0.131	2.44	104.8	0.19	0

20	25	0.132	2.572	105.6	0.2	0
21	26.25	0.133	2.705	106.4	0.211	0.476
22	27.5	0.132	2.837	105.6	0.221	0.455
23	28.75	0.133	2.97	106.4	0.231	0.435
24	30	0.134	3.104	107.2	0.241	0.417
25	31.25	0.134	3.238	107.2	0.251	0.4
26	32.5	0.134	3.372	107.2	0.261	0.385
27	33.75	0.134	3.506	107.2	0.271	0.37
28	35	0.135	3.641	108	0.281	0.357
29	36.25	0.135	3.776	108	0.291	0.345
30	37.5	0.136	3.912	108.8	0.301	0.333
31	38.75	0.136	4.048	108.8	0.311	0.323
32	40	0.137	4.185	109.6	0.321	0.312
33	41.25	0.137	4.322	109.6	0.331	0.303
34	42.5	0.137	4.459	109.6	0.341	0.294
35	43.75	0.138	4.597	110.4	0.351	0.286
36	45	0.138	4.735	110.4	0.361	0.278
37	46.25	0.138	4.873	110.4	0.371	0.27
38	47.5	0.139	5.012	111.2	0.381	0.263
39	48.75	0.14	5.152	112	0.391	0.256
40	50	0.14	5.292	112	0.401	0.25

Table A1: Calculation results for TS experiment profile generation.

Interval	Time points (min)	Disp. Volume* (mL)	Cumulative Disp. Volume (mL)	Pump rate (µL/min)	Molarity* (M)	Error* % in molarity compared to theory
1	1	0.1	0.1	100	0.008	0
2	2	0.099	0.199	99	0.016	0
3	3	0.097	0.296	97	0.024	0
4	4	0.097	0.393	97	0.032	0
5	5	0.096	0.489	96	0.04	0
6	6	0.096	0.585	96	0.048	0
7	7	0.095	0.68	95	0.056	0
8	8	0.094	0.774	94	0.064	0
9	9	0.094	0.868	94	0.072	0
10	10	0.093	0.961	93	0.08	0
11	11.667	0.154	1.115	92.4	0.093	0.357
12	13.333	0.154	1.269	92.4	0.107	0.312
13	15	0.156	1.425	93.6	0.12	0
14	16.667	0.153	1.578	91.8	0.133	0.25
15	18.333	0.154	1.732	92.4	0.147	0.227
16	20	0.156	1.888	93.6	0.16	0
17	21.667	0.152	2.04	91.2	0.173	0.192
18	23.333	0.154	2.194	92.4	0.187	0.179
19	25	0.155	2.349	93	0.2	0
20	26.667	0.153	2.502	91.8	0.213	0.156
21	28.333	0.154	2.656	92.4	0.227	0.147

22	30	0.155	2.811	93	0.24	0
23	31.667	0.152	2.963	91.2	0.253	0.132
24	33.333	0.153	3.116	91.8	0.267	0.125
25	35	0.155	3.271	93	0.28	0
26	36.667	0.152	3.423	91.2	0.293	0.114
27	38.333	0.153	3.576	91.8	0.307	0.109
28	40	0.154	3.73	92.4	0.32	0
29	41.667	0.152	3.882	91.2	0.333	0.1
30	43.333	0.153	4.035	91.8	0.347	0.096
31	45	0.154	4.189	92.4	0.36	0
32	46.667	0.151	4.34	90.6	0.373	0.089
33	48.333	0.153	4.493	91.8	0.387	0.086
34	50	0.154	4.647	92.4	0.4	0

Table A2. Calculation results for TP experiment profile generation.

*Note on rounding the values: We round the calculated values of dv_i (in mL) to 3 decimal places, which is required by the software of the syringe pump. The resulting calculated pump rates for k_i (in µL /min) are within the range of recommended minimum to maximum pump rate of the syringe pump. The reconstructed molarities and their errors are plotted without rounding in Figure 3.3 and **Figures A2-A3**, while in Tables A1 and A2 we round them to 3 decimal places for illustration purposes.